Zeitschrift: IABSE reports = Rapports AIPC = IVBH Berichte
Band: 79 (1998)

Rubrik: Working session: Innovative design of bridges. Papers and Posters

Working Session

Innovative Design of Bridges

Papers and Posters

Leere Seite
Blank page
Page vide

A New Solution Proposal for a Long-Span Bridge

Victor POPA
Expert Bridge Designer
Iptana-Search Co.
Bucharest, Romania

Victor Popa, born 1942, received his civil eng. degree from Techn. Constr. Univ. of Bucharest in 1966. He is currently Head of the Bridge Design Department at Iptana-Search Co. and assoc. professor at TCUB.

Michael M. STANCIU
Bridge Eng.
Iptana-Search Co.
Bucharest, Romania

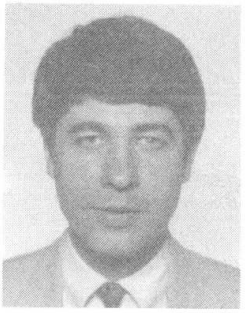

Michaela M. Stanciu, born 1957, received his civil eng. degree from the Univ. of Oklahoma in 1983 and his Master of Science in 1987. He is president of Iptana-Search, an American-Romanian civil eng. company, located in Bucharest, Romania

Summary

The paper presents a proposal with a solution for a long-span bridge, which can be applied over the large rivers like the Danube river in Romania or similar. The bridge can be a highway, a railway or a combination of highway and railway bridge. The bridge in this solution consists in a cable-stayed bridge, which has an arch type Nielsen or Langer in the middle area of the main span. This arch strengthens the deck and allows to decrease the height of the pylon. The arch also improves the general stability of the structure by inclination of the arches towards the axis of the bridge and therefore by increasing the torsion rigidity.

1. Introduction

It is a known fact that the bridges having the longest spans are cable-stayed or suspension bridges. Up to now remarkable bridges have been constructed or are under construction. Main spans reach incredible sizes, such as in the cable-stayed bridges Normandie (France, 1994, with a main span of 856 m) and Tatara (Japan, to be finished in 1999, with a main span of 890 m), as well as the suspension bridges Humber (UK, 1981, with a main span of 1410 m), Grand Belt (DK, 1998, with a main span of 1624 m) and Akashi-Kaikyo (Japan, 1998, with its world's longest main span of 1990 m).
The purpose of achieving such impresive constructions is not just to set up world records, but to satisfy real society needs and at the same time with the minimize the negative impact on the environment. Such record constructions require creative design, construction methods and also maintenance procedures. One main task of the structural engineers is to make things simpler, especially construction methods and maintenance procedures. The authors of the present paper are proposing a new solution for a long-span bridge, which can supply a series of technical-economical advantages.

2. Brief commentary regarding the conception of cable-stayed bridges

The cable-stayed bridges generally have two pylons and three spans (Fig. 1), but sometimes can only have one pylon with two symmetrical or unsymmetrical spans (Fig. 2). For the well balanced cable-stayed bridges with three spans, the optimum ratio $\mathbf{l_1/l}$ is about **0.4** and the optimum ratio **h/L** is about **0.2**, where **"l_1"** is the lateral span length, **"l"** is the main span length and **"h"** is height of the pylon, above the carriageway level (Fig. 1 and Fig. 2).

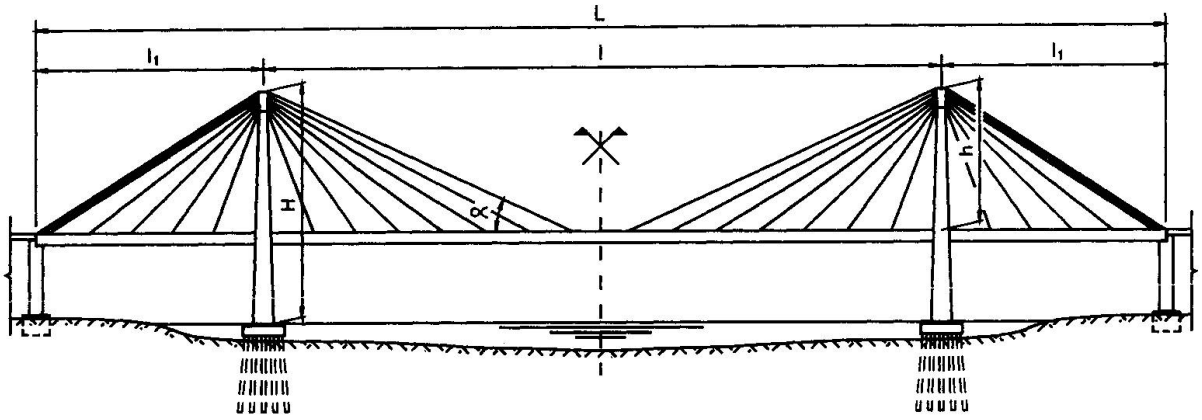

Fig. 1 Cable-stayed bridge having two pylons and three spans

Examining the cable-stayed bridges described in references [1] and [2], we can notice that the ratio l_1/l is varying in general between 0.33 and 0.45 and the ratio h/l is varying between 0.17 and 0.33 for most of the bridges. Averaging these values, we obtain the optimum ratio values presented above.

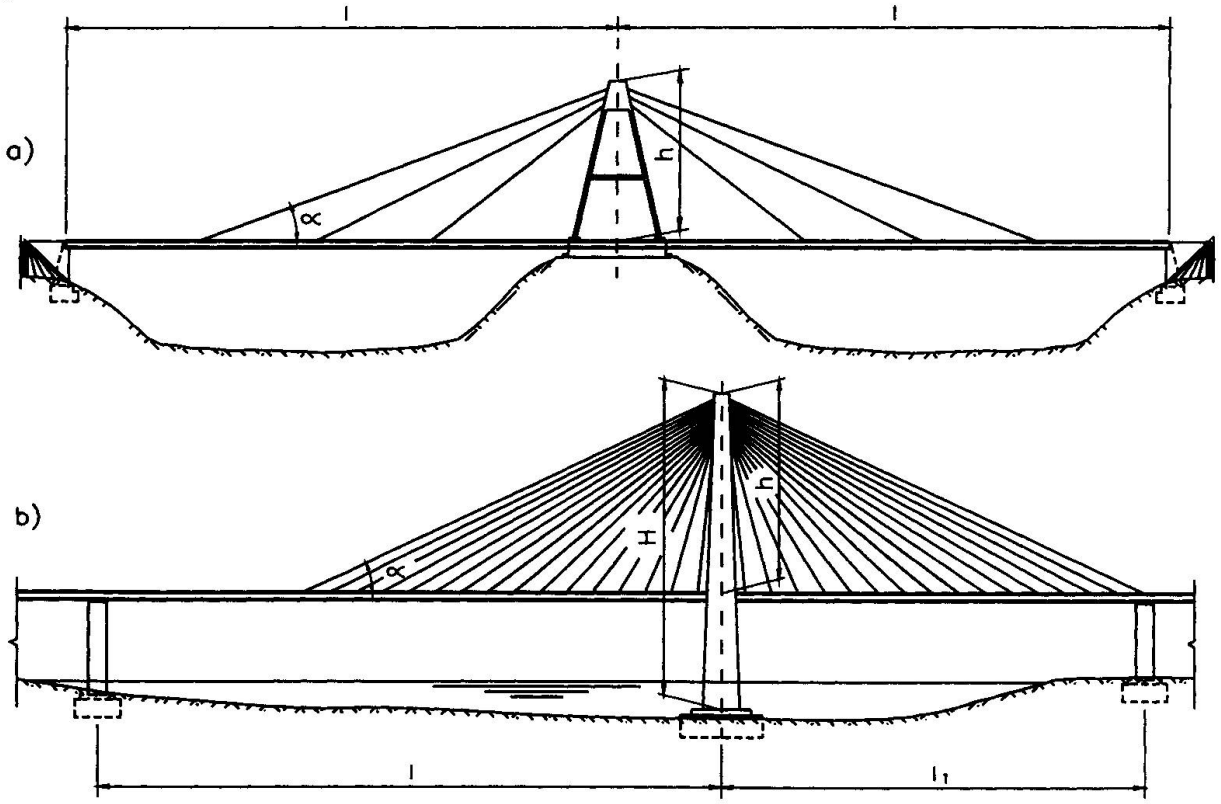

Fig.2 Cable-stayed bridge having one pylon and two spans.
a) symmetrical bridge; b) unsymmetrical bridge

The ratio $l_1/l = 0.4$ is required by the necessity of a good stress distribution on the deck in both the side and main spans. When the l_1/l ratio is too small, the stresses increase in the main span, but when the l_1/l ratio is too big, the stresses increase in the side spans. The l_1/l ratio can be decreased if heavier construction materials are used for side spans, and lighter for the main span. For instance, lower l_1/l ratio could be obtained if the concrete or composite type structures are used for the deck in the side spans and metal structures in the main span. Such structures are used more and more in bridge engineering. A suggestive example is the Normandie bridge, which has reinforced concrete side spans and metal structure central span. The decreased l_1/l ratio allows the pylons to be closer to the riverbanks, thus diminishing the construction difficulties, reducing the investment cost, as well as the execution time period.

The $h/l = 0.2$ ratio is required by the need to have the α angle - between the most inclined cable axis and the average level of the supported deck (see Fig. 1 and 2) – less than 25°. Even though, theoretically, it is recommended that this angle be larger than 30°, the practice shows that this condition is difficult to be respected. Sometimes the α angle is smaller, having values of 25° and even 20°. A small α angle leads to an inefficient cable and big axial stresses in the deck. A large α angle leads to a high pylon. The pylon height is therefore determined by the h/l ratio. We can notice that for the optimum ratio $h/l = 0.2$ the pylon height is big enough to lead to construction difficulties and large investment costs. Considering that the total pylon height "H" is much bigger, because it also includes the height under the superstructure, we conclude that pylon units play a significant point in the investment cost. It is often said that the sum of the total height of the two pylons, including the foundation depth, equals or exceeds the main span length. This observation highlights the pylon importance as part of the cable-stayed bridge structure, as well as an important part of the total investment cost. Analyzing the pylon cost – height diagram, we can see that the investment cost does not increase proportionally with the height, but quicker, (Fig. 3).

A solution for diminishing the pylon height, respectively the h/l ratio and also the l_1/l ratio is presented below. This solution was elaborated for a combined highway and railway bridge over the Danube river in Romania, but it can be adopted anywhere else, under similar conditions.

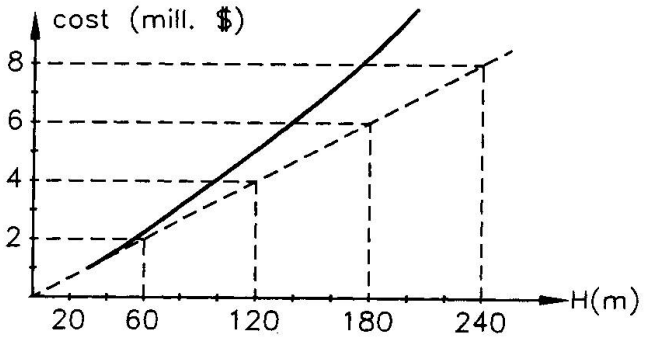

Fig. 3 Pylon cost-height diagram

3. Structural Concept

A new bridge could be placed over the Danube river in areas where the river bed is approximately 1000m wide.
A solution for an efficient crossing is a bridge with a large main span, and pylons placed as close to the riverbanks as possible.
Thus two important requirements are accomplished as follows:

- navigation on the Danube can be open at all times;
- pylon foundation construction can be done from the riverbanks;

The accomplisment of the second requirement leads to the following benefic effects:

- decrease of the investment cost by lowering the cost of the pylons;
- opportunity of a better foundation execution under a better control than in the case of the execution from "the water".

The proposed solution for a bridge carrying two railroad tracks and four highway lanes is a cable-stayed bridge having two pylons and a truss deck stiffened in the middle area of the main span by means of a Nielsen type arch having inclined hangers, or Langer type having vertical hangers (Fig. 4).

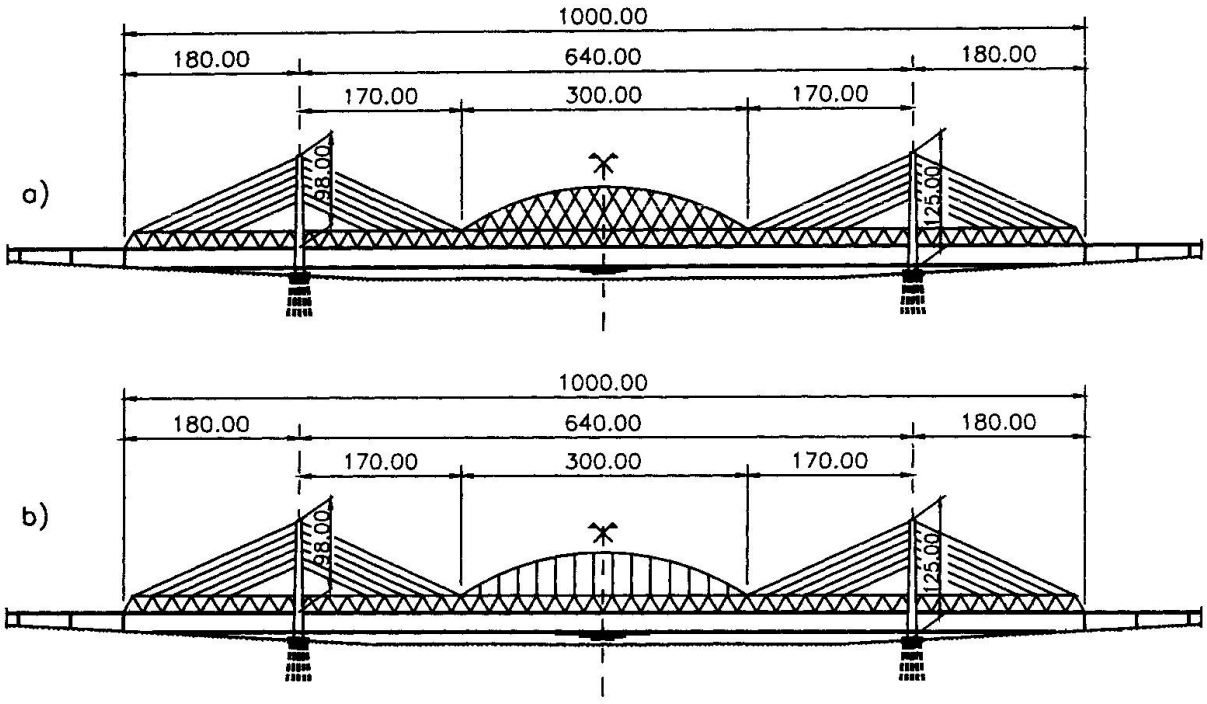

Fig. 4 Cable-stayde bridge stiffened by means of a middle arch. Elevation
a) arch type Nielsen; b) arch type Langer

In this way it is created a strengthened spatial structure, well balanced, having a good transverse stiffness, able to support all loads. The two railroad tracks are placed between the two stiffening arches and the four carriageways are placed on the side cantilevers (Fig. 5).
The bridge infrastructure is made of reinforced concrete, but the towers can be made out of steel. The bridge superstructure is metallic, but for the side spans it is recommended to have a heavier composite structure, in order to balance better the stresses in the three spans.
Comparatively examining the bridge in the proposed solution with a classical cable-stayed bridge having the same length (Fig. 6) we can observe the following:

- l_1/l ratio is reduced to a value of 180 / 640 = 0.28, compared to the ratio of l_1/l = 220 / 560 = 0.39 for the classical solution;
- h/l ratio is reduced to a value of 98 / 640 = 0.15, compared to the ratio of h/l = 116 / 560 = 0.2 for the classical solution;
- the pylons are shorter with approximately 18 m each and are closer to the riverbanks with 40 m.

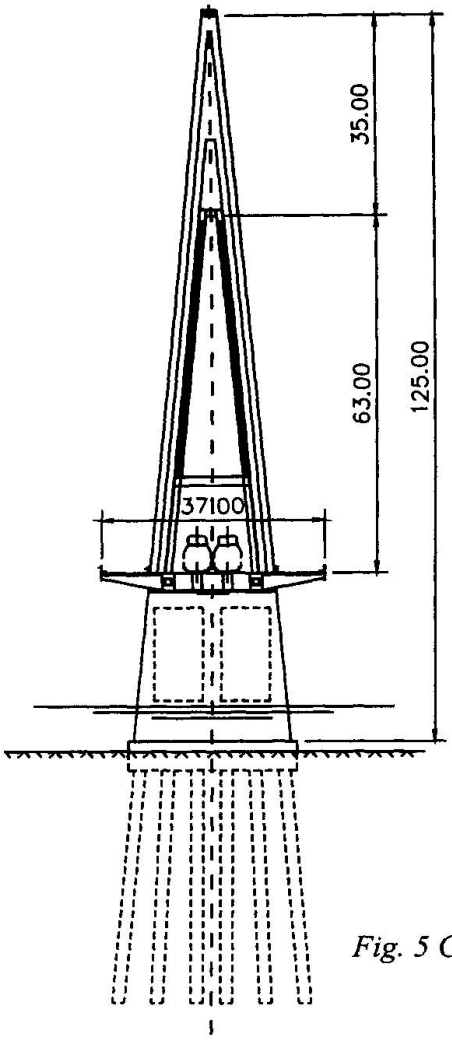

All these changes produce the following technical and economical advantages:
- simpler construction methods for the pylon, especially for the heavy foundations placed in the river bed water;
- decreases the bridge construction time, by lowering the pylon height as well as ensuring the possibility of constructing the arch span and the side spans simultaneously;
- lower investment;
- the bridge estetics are pleasant and appealing.

The construction phasing for the bridge is schematically shown in Figure 7 and includes the following stages:
1. infrastructure construction using the well known classical methods (see Fig. 7a);
2. simultaneous construction of the side spans by mounting into the cantilevers of the deck units and the structure type Nielsen by assembling on the riverbanks (see Fig. 7b);
3. mounting of the central structure type Nielsen by launching it on the water and then by lifting it up to the final position by means of hydraulic jacks and steel bands (see Fig. 7c);
4. carriageway construction and final operations.

Fig. 5 Cable-stayed bridge in the proposed solution. Cross section

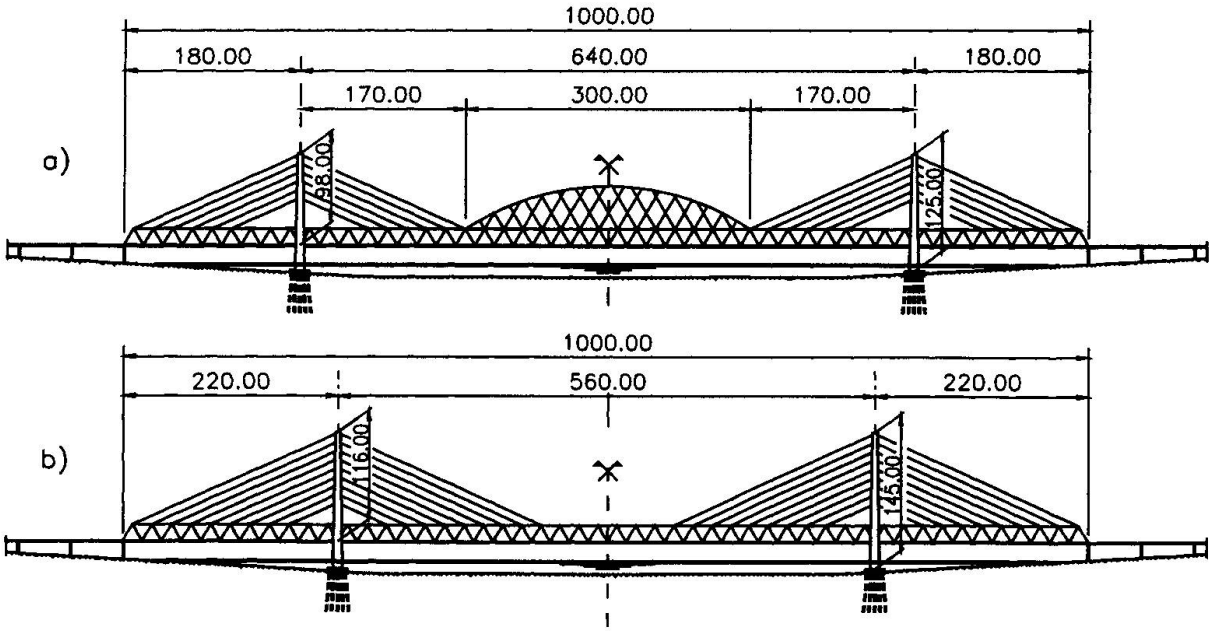

Fig. 6 Comparative cable-stayed bridge solutions
a) Proposed solution; b) Classical solution

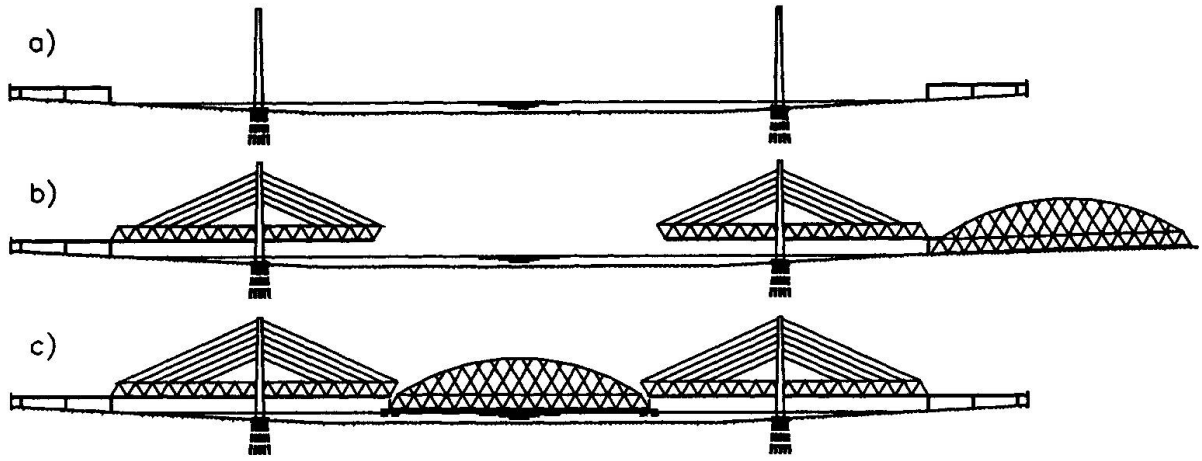

Fig. 7 Schematized technology for the bridge in the proposed solution
a) infrastructure construction; b) side structure execution; c) structure type Nielsen mounting

4. Conclusions

The idea of additional strengthening of the long-span superstructures in the middle area of the main span is rather old and it's been used in different ways. Even Leonardo da Vinci has among his sketches a type of cable-stayed bridge, consolidated in the middle area with similar arches type Nielsen [1]. Another bridge that it's known is a transbording bridge in Marseille von Arnodin, having a span of 140 m and similar structure to the one we are proposing – cable-stayed structure consolidated in the central area with a truss girder having parabolic upper side flanges [1]. We can mention other works similar to the presented one, such as: The Firth of Forth bridge in Scotland (1883 – 1890) by Baxer and J.Fowler [3], [5], footbridge at Oberschöneweide in Berlin [5], the Quebec bridge (1917) [4].

The bridge solution proposed in this paper transposes the idea in the long-span modern bridge area. It is obvious that thorough studies are still needed for the practical use of the solution and maybe the most important topic would be the testing of the structure on a model in the aerodynamic tunnel. The authors consider their solution as a modest and maybe useful contribution to the diversified multitude of new and daring ideas in the field of the long-span bridges.

References:

[1] Roik, K., Albrecht, G., Weyer, U.: Schrägseilbrücken. Ernst & Sohn. Verlag für Architektur und technische Wissenschaften, Berlin 1986;
[2] Walter, R., Houriet, B., Isler, W., Moïa, P.: Cable-stayed bridges. Thomas Telford Ltd., London 1988
[3] Wittfoht, H.: Building, Bridges. History, Technology, Construction. Beton – Verlag. Düsseldorf 1984;
[4] Toncović, K.: Oblikovanje mostova. Tehnika knjiga. Zagreb 1983.
[5] Jurecka, Ch..: Brücken Historische Entwicklung-Faszination der Technik. Verlag Anton Schroll & Co. Wien und München, 1979;

Applicability of Dischinger-Type to Ultra-Long Span Bridges

Nobuyuki NARITA
Prof.
Tokyo Metropolitan Univ.
Hachiouji, Japan

Hitoshi NAKAMURA
Res. Associate
Tokyo Metropolitan Univ.
Hachiouji, Japan

Ken-ichi MAEDA
Prof.
Tokyo Metropolitan Univ.
Hachiouji, Japan

Kunikatsu NOMURA
Res. Eng.
Kawada Industries Inc.
Tokyo, Japan

Summary

In this study, trial designs of Dischinger-type cable-stayed suspension bridges with a center span of 2,500 m, in which ratios of suspended parts were used as variable, were performed. Three types of cable-stayed suspension bridge models and the suspension bridge model were constructed. On comparing the weight of steel of superstructures from the results of trial designs, cable-stayed suspension bridges were superior to the suspension bridge considering the scale of substructures. In addition, buckling stability analyses and coupled flutter analyses for all types were carried out. From the results, it was found that cable-stayed suspension bridges were stable enough in buckling problems, and had the critical wind velocity higher than the suspension bridge. Therefore, the authors confirmed that Dischinger-type cable-stayed suspension bridges were competitive with suspension bridges as ultra-long span bridges.

1. Introduction

Realization of ultra-long span bridges with a span length ranging from 2,000 m to 3,000 m is influenced by their aerodynamic stability. Accordingly, for the construction of next- generation bridges following the Akashi-Kaikyo Bridge, research on new cable-supported bridges with high economic efficiency and high torsional rigidity is attracting much attention. We have already proposed a Dischinger-type cable-stayed suspension bridge as a long-span bridge, which replaces a cable-stayed bridge whose maximum possible span length is assumed to be 1,500 m [1], and predicted that it is feasible to apply for ultra-long span bridges [2]. The torsional rigidity in the cable-stayed suspension bridge is increased due to a combination of a streamlined stiffening box-girder suspension bridge and a cable-stayed bridge. In this study, we executed a trial design of this bridge by setting the center span length at 2,500 m and varying the length of the suspended parts. In addition, focusing on the buckling and aerodynamic stabilities of the bridges, we investigated its applicability and feasibility as an ultra-long span bridge.

2. Design concept and trial design

2.1 Analysis model and trial design

Using models with a center span length of 2,500 m for a rough investigation, we executed trial designs of three types of cable-stayed suspension bridges with different ratios of suspended part length to stayed part length, as well as a suspension bridge, as shown in *Figure 1*, with the aim of highlighting their structural characteristics with varying suspended part length. The suspended part lengths of the center span were 960, 1,280 and 1,600 m in Type-1, Type-2 and Type-3 models, respectively. The suspension bridge model is the Type-4 model. The height of the main tower was varied in accordance with stayed part lengths. *Table 1* shows cross-

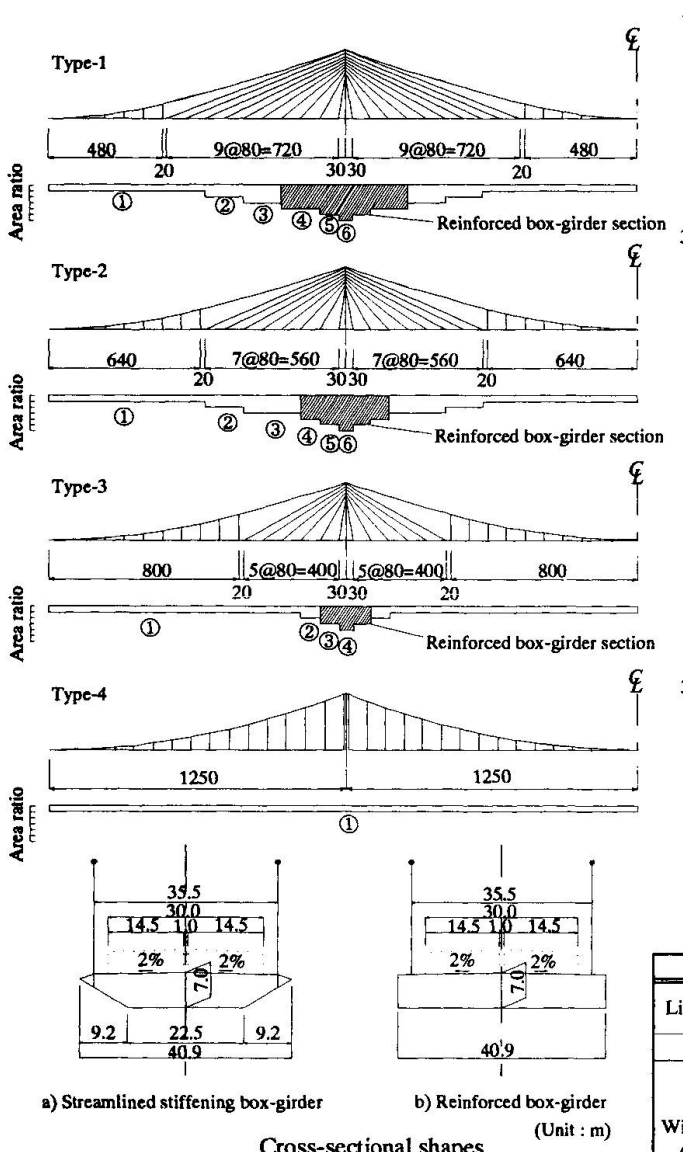

Cross-sectional shapes

Fig. 1 Analysis models

Table 1 Cross-sectional properties

Type-1

	①	②	③	④	⑤	⑥
$A_G(m^2)$	1.614	2.191	2.828	3.141	3.418	3.695
$I_{G,in}(m^4)$	13.304	18.304	23.667	30.061	31.088	32.11
$I_{G,out}(m^4)$	230.576	322.523	410.358	573.465	689.233	805.001
$J_G(m^4)$	26.923	37.284	51.388	70.565	73.161	74.365
$A_{mc}(m^2)$	side span : 0.418			center span : 0.405		
$A_{ac}(m^2)$	0.01861~0.05585					

Type-2

	①	②	③	④	⑤	⑥
$A_G(m^2)$	1.614	1.645	2.191	2.408	2.553	2.685
$I_{G,in}(m^4)$	13.304	13.366	18.304	23.656	24.181	24.659
$I_{G,out}(m^4)$	230.576	240.353	322.523	438.702	499.342	554.469
$J_G(m^4)$	26.923	27.172	37.284	50.843	52.571	53.415
$A_{mc}(m^2)$	side span : 0.584			center span : 0.575		
$A_{ac}(m^2)$	0.01577~0.04851					

Type-3

	①	②	③	④
$A_G(m^2)$	1.614	1.733	1.992	2.058
$I_{G,in}(m^4)$	13.304	14.307	18.943	19.182
$I_{G,out}(m^4)$	230.576	253.457	381.682	409.246
$J_G(m^4)$	26.923	29.932	41.663	42.296
$A_{mc}(m^2)$	side span : 0.739		center span : 0.731	
$A_{ac}(m^2)$	0.01366~0.03861			

Type-4

	①
$A_G(m^2)$	1.614
$I_{G,in}(m^4)$	13.304
$I_{G,out}(m^4)$	230.576
$J_G(m^4)$	26.923
$A_{mc}(m^2)$	0.870

Main tower

	/column
$A_T(m^2)$	3.000~5.796
$I_{T,in}(m^4)$	22.6~45.9
$I_{T,out}(m^4)$	42.3~131.0
$J_T(m^4)$	33.0~46.0

Table 2 Load conditions

		Type-1	Type-2	Type-3	Type-4
Live load	Concentrated(tf)	167.365			
	Distributed(tf/m)	3.906			
Temperature(℃)		±30			
Wind load (tf/m)	Girder	3.233			
	Tower	19.133	18.733	18.451	18.451
	Main Cable	0.658	0.777	0.876	1.043
	Stay Cable	0.133 ~0.206	0.124 ~0.185	0.163 ~0.116	——

sectional properties in each model. In all models, the cross-sectional depth of the main girder was 7 m. A static calculation was performed on the basis of the basic cross section of 12-mm upper flange thickness and 10-mm lower flange thickness. The cross sections that exceeded allowable stress were treated by an increase in the plate thickness. In the calculations, design and load conditions were in accordance with design specifications of Honshu-Shikoku Authority [3]. For the cable-stayed suspension bridges, a linearized finite displacement analysis was applied for the influence line in-plane analysis, and a finite displacement analysis was applied for the out-of-plane wind load analysis. For the suspension bridge, a deflection theory analysis expressed as stiffness matrix formula and Moisseiff's lateral load analysis were applied for the respective analyses.

Figure 2 shows member-end forces and deformations of the above four models, when dead loads, live loads and thermal forces were applied, and when wind loads with a design basic wind speed U_{10} of 50 m/s was applied. *Table 2* shows load conditions in these analyses.

Results of the trial design showed that the member-end force generated at the main girder of the suspension bridge was a fairly small; the maximum stress generated on the basic cross section due to in-plane bending moment and out-of-plane bending moment was 400 kgf/cm^2 and 1,300 kgf/cm^2, respectively.

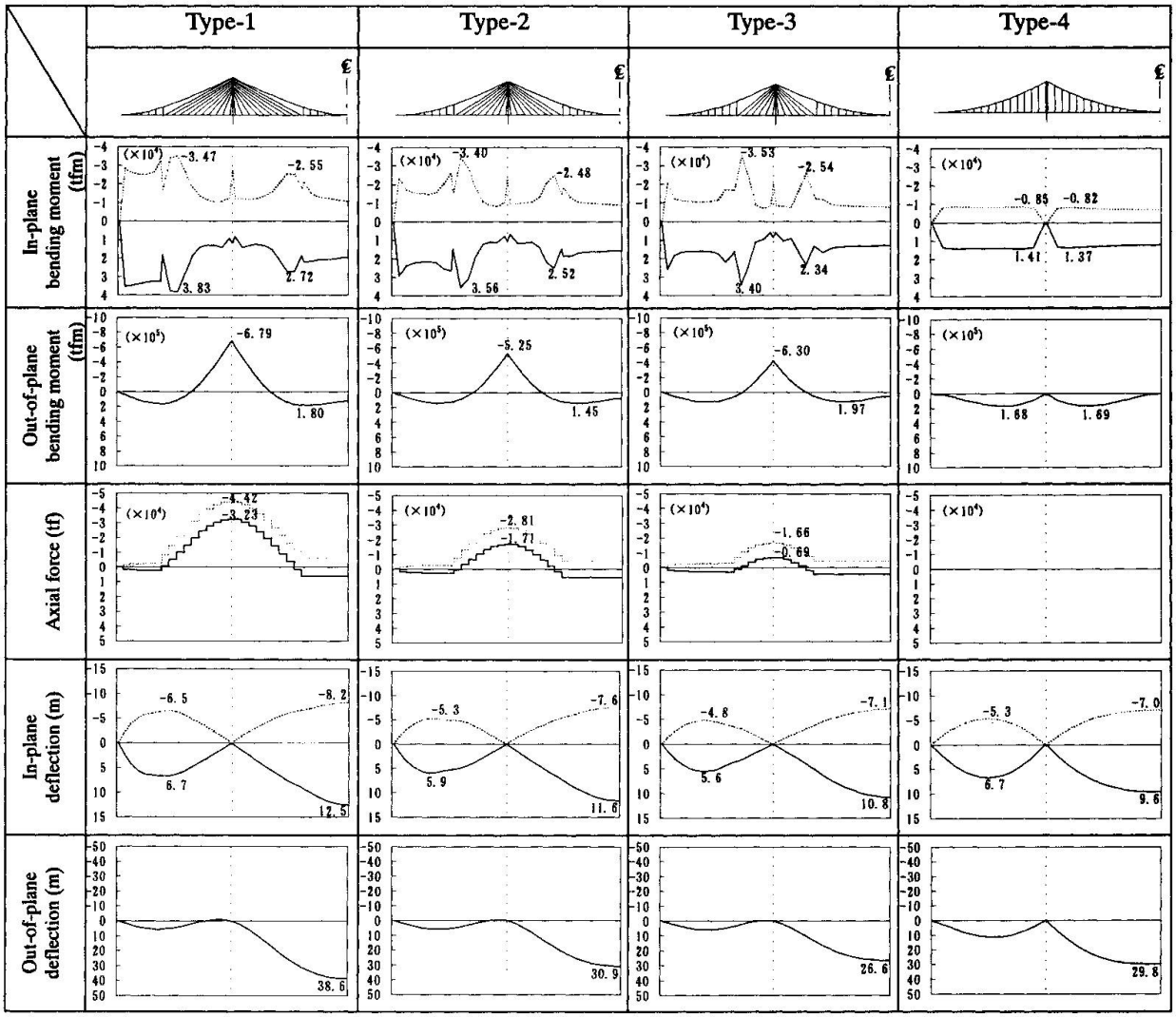

Fig. 2 Member-end forces and deformations of main girders

In the cable-stayed suspension bridges, basic cross sections of the suspended part did not exhibit any problems in terms of stress. However, at the stayed parts, since the out-of-plane bending moment due to axial force and wind load increases, it was necessary to use the reinforced box-girder as shown in *Figure 1 b)*, in addition to increasing the plate thickness near the main tower of the main girder.

In-plane deflection in the cable-stayed suspension bridges was larger than that in the suspension bridge. The deflection tended to increase with increasing suspended part length. With respect to out-of-plane deflection, the amount of deformation was the largest in Type-1, and the smallest in Type-3. The amounts of out-of-plane deflection in Type-2 and Type-4 were similar.

2.2 Comparison of weight of steel

Figure 3 shows the results of the calculation of steel weight. The ratio of weight of main girder and main tower to total steel weight was the largest for Type-1 among the 4 models, and the total steel weight for Type-1 was the largest, weighing approximately 250,000 tf. In contrast, although the weight of the main girder and main tower of the Type-2 cable-stayed suspension bridge is higher than that of Type-4, total steel weight of Type-2 was almost the same as that of Type-4 since the weight of the cable is lower in Type-2; the total steel weight of Type-2 was approximately 230,000tf. The calculated results showed that the total steel weight of Type-3 was the lowest. In the Type-4 suspension bridge, the weight of the main cable, which involves a fairly high cost of construction, was the highest. Accordingly, the economic efficiency of the Type-4 suspension bridge is lower than that of Type-2 when the cost of the

superstructure is taken into account. Considering the total cost including those of the superstructure and the substructure, the difference in the construction cost between the two types of bridges is predicted to increase. Thus, cable-stayed suspension bridges can be sufficiently competitive with suspension bridges in terms of economic efficiency, when an appropriate suspended part length is set, as observed in the case of Type-2.

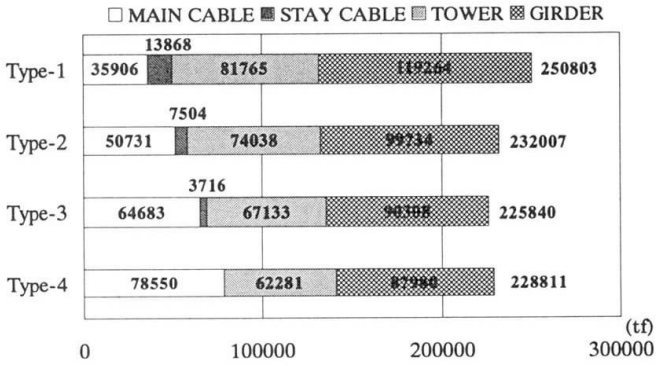

Fig. 3 Comparison of weight of steel

3. Stability check

In cable-stayed suspension bridges, axial force of the main girder becomes dominant with an increase in the stayed part length, which leads to a problem in buckling stability. Therefore, we conducted a stability check related to the main girder cross section, at the position of the main tower where the main girder axial force is maximum, using the following equation of stability check based on the specifications for highway bridges [4].

$$\frac{\sigma_c}{\sigma_{ca}} + \frac{\sigma_{bc}}{\sigma_{bao}\left(1-\sigma_c/\sigma_{ea}\right)} \le 1 \quad , \quad \sigma_{ca} = \sigma_{cag} \cdot \sigma_{cal} / \sigma_{cao} \quad , \quad \ell_e = \pi\sqrt{\frac{EI}{\lambda N}}$$

where :
- σ_c : Compressive stress due to axial force acting on the sections were stress is checked
- σ_{bc} : Flexural compressive stress due to bending moment acting around minor axis
- σ_{bao} : Upper limit of allowable flexural compressive stress without consideration of local buckling
- σ_{ea} : Allowable Euler buckling stress around minor axis
- σ_{cag} : Allowable axial compressive stress without consideration of local buckling
- σ_{cal} : Allowable stress for local buckling
- σ_{cao} : Upper limit of allowable axial compressive stress without consideration of local buckling
- ℓ_e : Effective buckling length specified in each division (m)

(Unit: kgf/cm^2)

Here, the load condition was set to be equal to the live loads so as to maximize the main girder axial force at the main tower position, which was determined on the basis of results of the influence line analysis conducted separately. In addition, we obtained buckling eigenvalues using a linearized buckling eigenvalue analysis, under the application of the severest live load described above. In this stability check, the properties of assumed cross section was used.

Table 3 shows results of the stability check. λ in the table represents the minimum buckling eigenvalue which provides the in-plane buckling of the main girder. These results show that even Type-1, in which the stayed part length is the largest and the buckling stability is assumed to be the smallest, satisfies the equation of the stability check. The total length of the stayed parts of the center span in Type-1 was approximately 1,400 m, which does not exceed the critical span length of the cable-stayed bridges.

Table 3 Stability check

	Type-1	Type-2	Type-3
N_G(tf)	40052	24411	13103
$M_{G,in}$(tfm)	13093	11255	10443
$I_{G,in}$(m^4)	22.191	17.373	13.637
A_G(m^2)	2.469	1.913	1.516
ℓ_e(m)	138	125	114
λ	6.012	9.506	16.663
Grade of material	SM570	SM490Y	SM400
(kgf/cm^2)	2600	2100	1400
Stability check	0.93	0.89	0.91

4. Characteristics of coupled flutter

4.1 Natural vibration characteristics

Prior to the coupled flutter analysis, we conducted a natural vibration analysis. As a part of the results of the analysis, *Figure 4* shows diagrams and vibration frequencies of the most dominant basic modes (1st symmetric deflection mode and 1st symmetric torsion mode). The deflection frequency increases with increasing suspended part length, whereas torsional frequency tends to decrease. Judging from the results using these two modes, the frequency ratio increases as the bridge type approaches that of a suspension bridge.

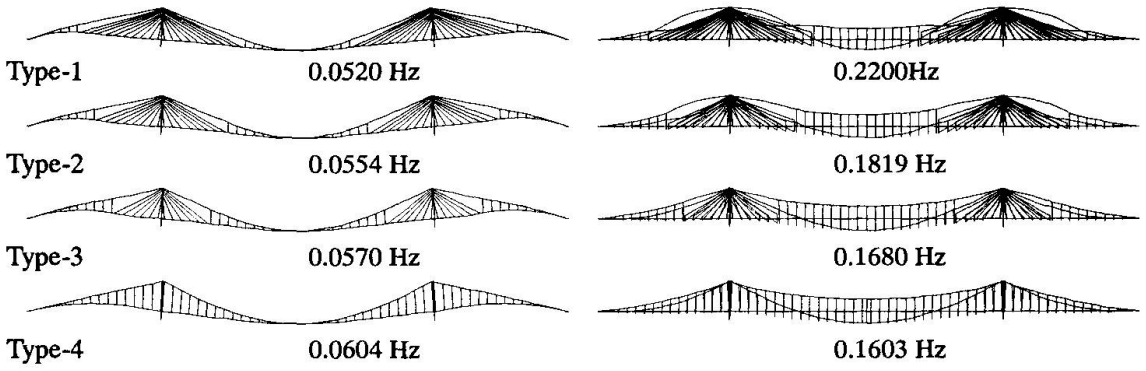

a) 1st symmetric deflection mode b) 1st symmetric torsion mode

Fig. 4 Basic modes by natural vibration analysis

4.2 Estimation of critical wind velocity

We estimated the critical wind velocity of flutter using a coupled flutter analysis based on the modal analysis, by applying the unsteady aerodynamic force based on the plate-wing theory and considering the natural vibration mode up to the 40th mode [5].

Figure 5 shows a relationship between critical wind velocity and weight of steel. The results show that the critical wind velocities were 76, 71, 65 and 63 m/s for cable-stayed suspension bridges Type-1, Type-2, Type-3 and the Type-4 suspension bridge, respectively, indicating that aerodynamic stability of the cable-stayed suspension bridges is superior compared to that of the suspension bridge. The results also show that in cable-stayed suspension bridges, critical wind velocity increases with increasing stayed part length. This is because the increased stayed part length leads to an increase in the rigidity of the entire structure.

For Type-2 and Type-4 bridges, the cross sections of the main girder were changed to twice and then four times of the original value, and the critical wind velocity was calculated. The relationship between the calculated critical wind velocity and total steel weight is also shown in *Figure 5*. If we attempt to ensure the same critical wind velocity for both Type-2 and Type-4, then the Type-4 suspension bridge must have a fairly large value of steel weight. If we attempt to ensure a critical wind velocity of 80 m/s only by an increase in the cross sectional area of the main girder, then the total steel weight of Type-2 cable-stayed suspension bridge should be approximately 300,000 tf, and that of Type-4 suspension bridge should be approximately 360,000 tf as shown in *Figure 5*. Thus, the increase in the total steel weight required for Type-2 is approximately 30% relative to the original weight. In the actual design, the aerodynamic stability of the bridges cannot be ensured using such a simple method; however, in cases of ultra-long span bridges, we can predict that cable-stayed suspension bridges are advantageous over suspension bridges.

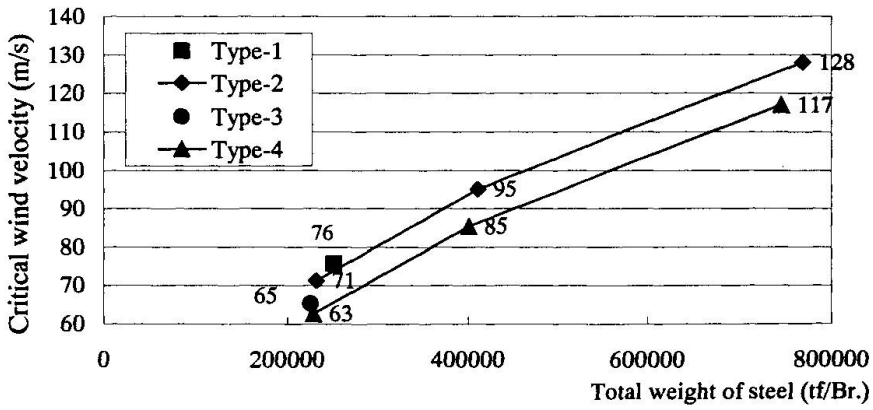

Fig. 5 Relationship between critical wind velocity and weight of steel

5. Applicability of cable-stayed suspension bridges to ultra-long span bridges

The characteristics of the cable-stayed suspension bridges are summarized based on the results of the above investigations, and their applicability to ultra-long span bridges is discussed.

(1) Variety of design and feasibility of the side-span ratio can be improved by appropriately setting lengths of suspended and stayed parts. This implies that different structural systems can be selected in accordance with various conditions such as the side-span ratio and span length, and amount of the axial force and the bending moment of the main girder can be controlled. In addition, since earth-anchored stayed cables are used as the main cables of the side span, characteristics of the earth-anchored cable-stayed bridges can be utilized.

(2) Since a stayed part and a suspended part can be constructed simultaneously in the construction of the main girder, the construction period can be shortened. Furthermore, the main girder of the stayed part can be constructed using a cantilever erection method, following the completion of the main tower.

(3) Regarding the aerodynamic stability, the rigidity of the entire bridge can be increased by setting appropriate stayed part lengths. Thus, superior aerodynamic stability can be obtained as compared to the suspension bridges. In addition, various measures for ensuring the aerodynamic stability can be adopted, taking advantage of the large degree of structural freedom.

(4) In ultra-long span suspension bridges, the weight of the main cables, which account for a large portion of the construction cost, becomes significantly high. Therefore, in most cases, cable-stayed suspension bridges with low cable weight can be economically advantageous over suspension bridges.

Thus, the cable-stayed suspension bridges can be sufficiently competitive, compared to suspension bridges, in terms of ultra-long span bridges, as they make use of the advantages of both the suspension bridge and the cable-stayed bridge, while compensating for their disadvantages at the same time.

6. Conclusions

To investigate the applicability of cable-stayed suspension bridges as ultra-long span bridges, we executed trial designs of three types of the cable-stayed suspension bridges with different suspended part lengths, and confirmed that the cable-stayed suspension bridges can be sufficiently competitive, compared with suspension bridges, in terms of economic efficiency. In the cable-stayed suspension bridges, aerodynamic stability, which significantly influences the feasibility of ultra-long span bridges, can be improved while maintaining economic efficiency comparable to suspension bridges. In terms of buckling stability, which also influences the feasibility of ultra-long span bridges, no problem was found in the safety checking of the cable-stayed suspension bridges; namely, the total length of the stayed parts does not exceed critical span length of the cable-stayed bridge. Furthermore, the construction period can be shortened.

As shown, cable-stayed suspension bridges can be effectively used as ultra-long span bridges with a span length of over 2,000m and can be highly economical and practical as compared to the suspension bridges.

References

[1] K.Nomura, S.Nakazaki, N.Narita, K.Maeda, H.Nakamura: "Structural characteristic and economy of cable supported bridges with long span", Journal of Structural Engineering, Vol.41A, 1995. (in Japanese)
[2] N.Narita, K.Maeda, K.Nomura, S.Nakazaki, H.Nakamura: "Feasibility study on Dischinger-type cable-stayed suspension bridges as a type of ultra-long span bridges", Journal of Constructional Steel, Vol.4, 1996. (in Japanese)
[3] Honshu-Shikoku Authority: Specifications on Superstructure Design, 1989. (in Japanese)
[4] Japan Road Association: Specifications for Highway Bridges, 1996. (in Japanese)
[5] M.Iwamoto: Prediction of aerodynamic behavior of cable supported bridges, Ph.D. thesis, University of Tokyo, 1995. (in Japanese)

Beyond the Limits of Erection Activities

Michel PETREQUIN
Engineering Mgr
Gec Alsthom
Grenoble, France

Michel Petrequin, born in 1960, obtained his degree in 1983 at the Arts et Metiers School of Eng. in Paris. He has worked with large French groups as an engineering mgr on important projects, gaining experience in design, manufacturing and erection of structural equipment. With Gec Alsthom, he was Eng. Mgr for the Storebaelt Project. At present he works as a private consultant.

Mario De MIRANDA
Consulting Eng.
DMA-Studio De Miranda
Milan, Italy

Mario de Miranda, born in 1954, obtained a degree in eng. in 1979 at the Politecnico di Milano. He is a partner of DMA, founded by professor Fabrizio de Miranda, and has worked on large projects on many aspects of design and analysis of bridges and in construction methods and equipment. Consultant for Gec Alsthom for erection of the Storebaelt Bridge.

Summary

The Storebaelt East Bridge has a total length of 6.8 km and includes a major suspension bridge with a 1,624 m. long central span.
While representing an exciting challenge for all the workers, technicians and engineers involved, its erection, which was recently completed, also required an approach which bordered upon the current limits in erection of large bridges using innovative solutions.
This paper illustrates some aspects and figures involved in erection of the bridge and discusses some of these limits and how they may be overcome.

1. Introduction

The Storebaelt Bridge Project appears in a book dated March 9, 1936. At that time, a bridge with a 400 m. long central span was planned. 62 years later, the bridge exists and is a 1,624 m. suspension bridge, the longest box girder suspension bridge in the world.
When its construction was started, no longer spans had ever been built and its erection called for going beyond the present limits.

The East Bridge is about 6.8 km long, running from Halsskov, on the Zealand side, to the small island of Sprogo, located at the centre of the Great Baelt channel and linked to Funen by the West Bridge, the concrete viaduct that completes the Storebaelt link.

The East Bridge includes the 2.7 km long suspension bridge and two approach viaducts with lengths of 2.54 km and 1.54 km respectively, each one formed by 193 m. spans, with continuous box girder superstructures. Details of the bridge are given in [1] to [6].

The erection of all the superstructure, including the intermediate phase of cable spinning, started in January, 1995, and was completed 34 months later, in December, 1997.

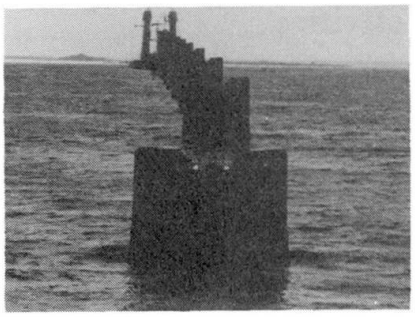

Fig. 1 - 2 - Before and after the erection work

The bridge was designed by a Joint Venture between COWIconsult, B. Hojlund Rasmussen and Ramboll & Hannemann (DK) for the final Client STOREBAELT A.S. [1].
STOREBAELT, split the East bridge contract between two main contractors: GBC (DK) for the civil works and COINFRA (I) for the steel structures [2], [3]. GEC ALSTHOM (F) obtained the contract for erection of the bridge from COINFRA. This included erection of the approach spans and of the suspended bridge that consisted in manufacturing the main cables and its hangers and deck erection. GEC ALSTHOM gained previous experience in building bridges with the erection of the Normandy Bridge (that was the longest cable-stayed bridge in the world) and therefore has skills in temporary works and welding activity. In order to face the challenge represented by erection of the Storebaelt Bridge, GEC ALSTHOM subcontracted work lots in order to obtain the complementary skills of other operators.
•SMIT MARITIM CONTRACTORS (NL) was in charge of transporting the girders by barge from Aalborg to the Halsskov site and of lifting the approach span sections and the two specific sections of the suspended deck at the anchor blocks using heavy crane barges.
•GIBSON (GB) was in charge of lifting the deck sections using the gantry lifting systems already used for the Tsing Ma bridge in Hong Kong.
•BM Contracting (DK) and GEC ALSTHOM Entreprise (F) were responsible for structural welding.
•COMAG (F), owing to its experience working in mountain conditions, was responsible for all activities connected to manufacturing of the main cables.
The company GEC ALSTHOM performed all engineering on erection methods, design and manufacturing of temporary equipment and chose DE MIRANDA Associati (I) as the structural engineering consultant, in order to have a good approach to the numerous technical problems involved.

2. Erecting the Storebaelt East Bridge

The approach spans

Girders were of the box section type, 6.7 m. deep, with two side slanting webs and a central vertical web. The structural weight of the standard 193 m long girders is about 2,400 t.
The continuous girder deck was built in the following basic phases [4]:
_Loading of full-length girders onto a barge and transportation from Aalborg to the site, 300 km by sea.
_Positioning and mooring of the barge and of an auxiliary floating crane, and lifting of the girder by means of a fixed crane installed on the previously erected girder and of the floating crane.
_Placement of the girder on temporary bearings: the rear end section remained suspended from the fixed crane aligned to the previous section, while the front section was placed on a 4.5 m. high bearing structure, in order to give the necessary angle between adjacent girders before welding.
_After section length cutting to fit with the pier axis distance, the section was finally matched by jacking and welded.
_Lowering of girder on the front support, thereby applying a negative bending moment to the section at the preceding pier which, when combined with the bending moments of all successive construction steps, provided the necessary final bending moment at the pier.
Instead of the usual progressive step-by-step lowering with jacks and shims, a more drastic system was chosen: the use of a floating crane to hold the girder end temporarily, lift it to free the support structure, slide it forward by means of cantilever guides and lower the girder onto supports.

The suspension bridge

The box girder had a flat trapezoidal shape with sharp edges, with a total width of 31.20 m. and a total depth of 4.34 m. Each standard girder section is 48 m. long and is formed of three 16 m. long welded segments.The structural weight of a standard section is about 530 t.
The girder is vertically supported over the entire length by hangers. No vertical supports are present at the pylon; only transversal restraints.
In order to optimise distribution of the bending moment, the designer provided moment adjustment at the pylon sections and near the anchor blocks, to be achieved by girder pre-stressing during erection.

After all cable work was completed, girder erection could take place, in the following basic phases:
_Installation of four special gantry cranes on the main cables, capable of running on the cables, to accurately position and lift the sections, with a lifting capacity of 600 t. each. Two cranes and four lifting points were provided for each segment. After the load out and the transport of two sections simultaneously, the barge is moored by anchoring for a section lifting.
_Picking up the section using two spreader beams and special anchoring devices, and its lifting from the barge up to the final elevation.
_Bringing the lifted section close to the adjacent one, and precise positioning to match them at deck level.
_Joining the sections by means of temporary connections.
_Installing the hanger sockets in their anchor blocks and then transferring the section load from the gantry crane to the final hangers.
_Welding of section when joints closed the rotational gap, which had remained open up to that stage.
_Applying pre-stressing moments, where required, by de-shimming some hanger sockets, thereby allowing the deck to shift along the hanger up to the final anchor position. The deck at these hanger locations was previously installed at an elevated position by means of proper shims.
All erection phases were analyzed by extensive progressive computer analysis able to define both the evolution of structure forces and the sections displacements in order to allow the correct matching of sections. This last task required a special effort mainly to compute the exact shimming heights when considering that bridge deflections were of the order of meters during the evolution of the erection phases while the precision required to match the sections to be butt welded was of the order of few millimetres.

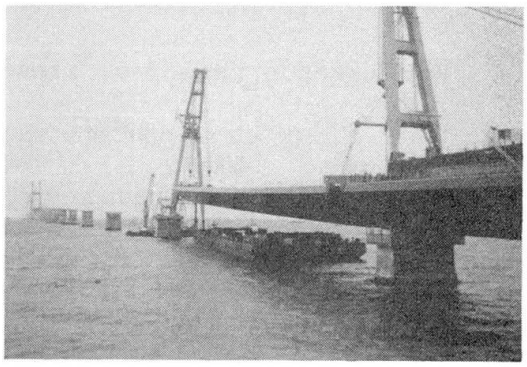

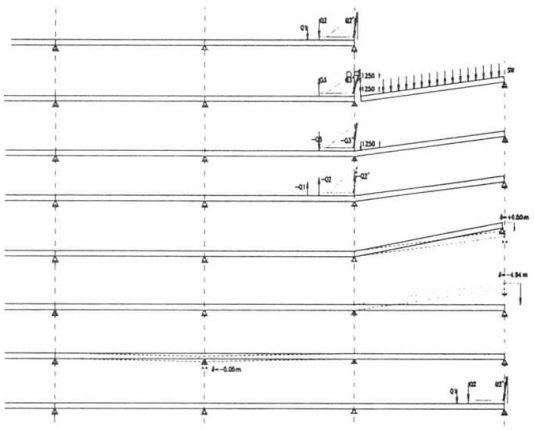

Fig. 3 - 4 - Approach spans: Lifting, front end lowering, typical span erection phases

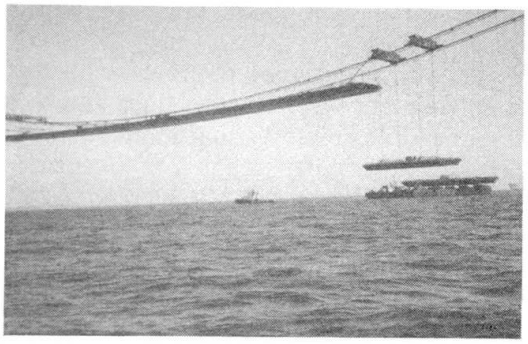

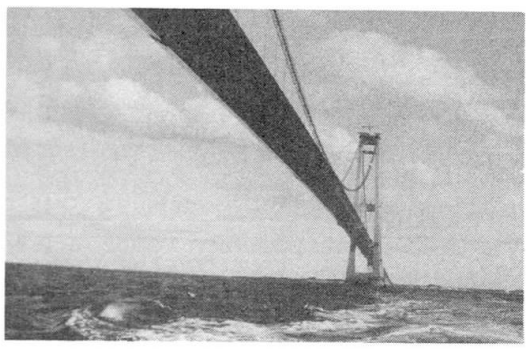

Fig. 5 - 6 - Installing suspension bridge sections

3. Wind, waves and thermal influence

Vortex shedding at approach spans

Wind effects played an important role in erection activities.
Vortex shedding soon appeared to be a possibly decisive load condition, since the structural frequencies at various stages of construction were close to the critical frequencies related to the design wind speed for erection conditions. A vibration damping system was therefore studied.
Wind tunnel tests on both sectional models and on the full bridge model were available and gave useful data on structural response and consequent actions.
However, certain results of the wind tunnel tests were contradicted by observation of the vibrations which actually occurred in the first spans, when the damping system had not been yet installed, at a different wind speed to the one predicted by the wind tunnel results.
Discrepancies were mainly attributed to the large difference in the Reynolds number between the tested model and the actual full-scale section [5], [6].

A vibration damping system was then designed on the basis of the field data and proved to be effective, since no more vibrations occurred.
This system was mainly based on the frequency tuning concept, i.e. increasing the natural frequency of the system to increase the critical wind speed accordingly.
This was achieved by means of steel cables, with proper cross section, stretching force and position, anchored to weight tuned concrete blocks dropped onto the seabed.
The system was designed to increase the critical speed beyond frequent wind speed values and to reduce the maximum forces and bending moments applied to the girder structure when resonance occurred at higher wind speeds and concrete blocks tended to lift. In this condition, the non-linearity of the system proved to be effective in significantly reducing the maximum response on the first two advancing, and more stressed, girders.

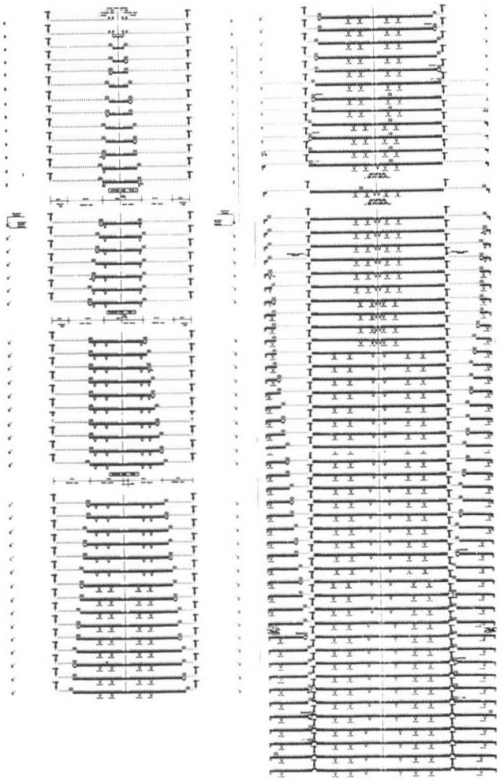

Fig. 7 - Diagram of analysis phases of the suspension bridge

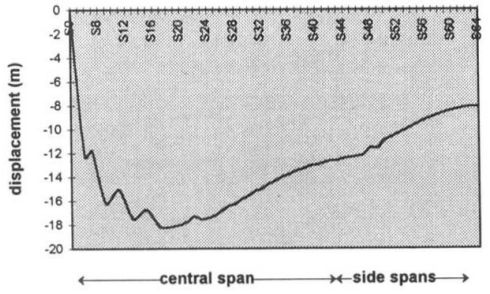

Fig. 8 - Vertical displacements of cables at midspan during erection steps

The influence of the wind on the erection sequence of the suspension bridge

The erection sequence adopted consisted of starting from the mid-span of the central span and going towards the pylons; then starting from the anchor blocks and completing the deck toward the pylons.
Different sequences were actually possible, but wind stability considerations governed the decision. It was, in fact, only possible to guarantee a critical flutter speed higher than the design wind speed considered for erection activities by starting from the mid-span.
During deck erection, the critical speed is generally lower than that occurring for the completed deck, dropping to only 40% of the speed for the completed deck when about 20% of the deck is erected, then rising to near the final value, depending on the actual torsional stiffness of the deck.
To achieve the required flutter speeds, the torsional stiffness of the deck when only temporary connections were installed was extensively studied and temporary connections were designed which

fulfilled torsional-flutter requirements, but also remained functional and efficient according to the erector's needs.

The influence of the wind and waves on lifting

The maximum lifted weight was the central section, weighting about 900 t.
Standard sections were installed at an average rate of about one section per day, with cases of two sections per day when favourable conditions allowed it.
Static and dynamic loads are applied to the gantry crane and all lifting equipment during lifting.
The main dynamic load occurs when lifting starts, when the section is still on the barge and is subject to the actions of the waves moving together with the barge.
If the barge and its load drop in a wave at this point, when the section has almost been taken off the barge, large dynamic effects occur.
The dynamic amplification factor related to this effect was studied through dynamic analysis of large, non-linear displacements for the design wave conditions.
Data was also obtained to examine the problem of possible re-contact between the section and the barge due to the combined effect of slow lifting speed and wave motion.
Von Karman Vortex and buffeting effects were found to be of minor importance in lifting operations, giving lower DAFs and allowable response.

Buffeting and flutter requirements on temporary joint connections

While flutter conditions required sufficient torsional stiffness of the temporary connections between installed sections, wind buffeting governed their capacity to transmit longitudinal forces.
The average wind action gives low bending moments for all stages in which the deck is simply suspended to the cables, without transverse restraints at the pylons.
When transverse restraints are used, a significant increase in bending moments occurs. The deck is therefore kept unrestrained until the welding of joints has been completed.
However, turbulent wind action and its dynamic effects on the deck are the main source of horizontal bending moments during the construction stages. The innovative temporary connections were designed to fulfil the dual needs of keeping sections in position while allowing significant rotation on the vertical plane and allowing simple section connection.
They also had to be able to transmit longitudinal forces related to horizontal bending moment and shear due to dynamic wind action, vertical shear force given by erection loads and torsional moments still due to buffeting action. Torsional stiffness, as said, was a further condition.
Various types of finite element analysis were carried out to support and address the design of temporary connections, as well as of all temporary equipment and structures, including local stress analysis, dynamic analysis for wind buffeting action and step-by-step analysis of the progressively erected structure.

The need for good weather windows

Generally speaking, mechanical erection activities are not heavily dependent on weather conditions.
Work is not stopped until the wind speed reaches 20 to 25 m/s. The influence of windy, rainy or icy conditions on work progress and efficiency may lie more in the fact that working comfort is lower. This fact can be partially compensated when designing the equipment by considering ergonomics.
Maritime activities, on the other hand, are closely linked to weather conditions, so criteria were defined during the study phase to analyse feasibility of the activity.
These criteria (wind, current speed and direction, wave height and period) are used to analyse barge movement when the sections are being transported or lifted off the barge. If local weather statistics are known, it is possible to construct an activity program and to check that all the technical solutions envisaged are correct.
On the actual day of activity, it is the responsibility of the crane barge captain alone to decide whether or not to commence activity. The non-rational aspect of his decision may sometimes cause dismay, but serves as a useful reminder that a certain degree of forbearance is required on this type of project.

4. Concluding Remarks

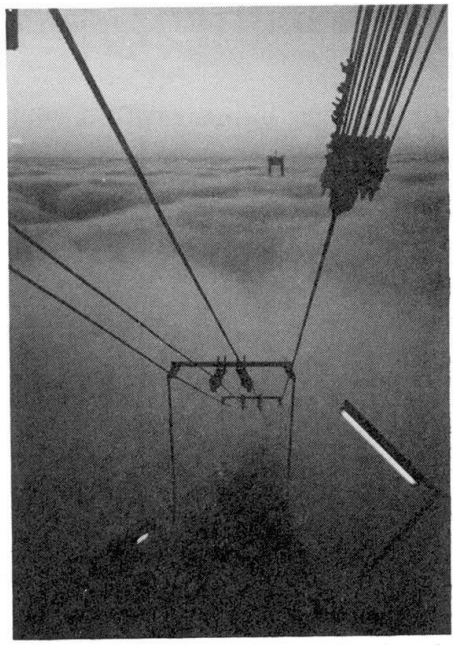

Fig. 9 - Good weather at top level

The erection of the approach spans brought to light the particular problems involved in transporting, lifting and matching 200 m. long sections.
These problems quickly increase with span length, but seem to be mainly limited to the capacity and availability of transporting and lifting equipment.
Wind must be taken into account, but is not a critical factor in this case.

Erection of the suspension bridge demonstrated and confirmed that both sea conditions and wind effects, together with thermal effects, can constrain and severely limit erection activities.
The present uncertainties in predicting wind effects, together with the short amount of time available for some activities, also place certain limits on activity.
As stated, certain welding activities require very quick action, so it could be difficult to join very large sections in the amount of time available, even if not too large problems should arise in transporting and lifting sections weighing more than 1,000 t.
Critical flutter speed during the first phases of erection are well below the speed for the bridge in service.
Taking into account the fact that the critical flutter speed decreases when the span length increases, and that the accuracy of the theoretical prediction of wind effects can be reduced on very large-scale structures, new solutions should be used to erect longer spans safely:
- Although active mechanical and aerodynamic control devices [7], [8] have not yet been tested on actual large structures, they will undoubtedly help to achieve these aims. A system which increases flutter speed would also allow the erector to chose the best procedure from a logistic point of view.
- Another option is to erect faster. This should be possible by lifting larger elements, like two sections already assembled. For this the lifting devices should have an active system of load control and section structure and attachments should be designed consequently.

In any case it appears essential that the most detailed definition and analysis of erection methods be carried out at the same time and as part of the bridge design.

6. References:

[1] Ch. Tolstrup, A.S. Jacobsen - *Suspension bridge over the Eastern Channel of the Great Belt* - IABSE Symposium 1991 - Leningrad.

[2] A. Caramelli, G. Vannacci - *The construction of the Storebaelt East Bridge* - Costruzioni Metalliche - n. 1 - 1994.

[3] E. Rolla - U. Sparatore, A. Testa - *The construction of the Storebaelt East Bridge* - EACWE Conference- Genova - 1997.

[4] M. de Miranda, M. Petrequin - *Some aspects of the erection of the Storebaelt East Bridge* - C.T.A. Conference Oct. 1997.

[5] DMA - *Control of vortex induced vibrations* - Sdem Internal Report n. 15 - may 1995 -

[6] G. Schewe, A. Larsen - *Reynolds Number Effects in the flow around a bluff bridge deck cross section* - EACWE Conference - Genova 1997.

[7] A. Carotti, M. de Miranda - *An active protection system for wind induced vibrations of pipeline suspension bridges* - Proc. of 2nd International Symposium on Structural Control, Univ. of Waterloo, Ontario, Can. 1985.

[8] K.M. Ostenfeld, A. Larsen - *Bridge engineering and aerodynamics* - DMI Symposium - Copenhagen - 1992.

Long-Span Composite Cable-Stayed Bridge with New Hybrid Girder

Masayuki OKIMOTO
Chief Res.
Nippon Steel Corp., Steel Struct. Dev. Center
Tokyo, Japan

Yoshihiro HISHIKI
Mgr
Kajima Corp.
Tokyo, Japan

Tomonori TOMINAGA
Researcher
Nippon Steel Corp., Steel Struct. Dev.
CenterTokyo, Japan

Kousuke FURUICHI
Senior Res. Eng.
Kajima Corp.
Tokyo, Japan

Summary

In this paper, the possibility to construct a 3-span continuous composite cable-stayed bridge with main span of 890m was studied. In the objective bridge, the new composite 2 girder structure, which uses steel-pipe structure filled with concrete as main girder together with prestressed concrete deck slab, was adopted in part of central span, and prestressed concrete girder was used in other parts. Through the study, it was confirmed that the static behavior of the objective composite bridge was almost the same as that of the basic model (prestressed concrete cable-stay bridge), and the dynamic behavior was also satisfactory, and the possibility to construct the objective composite bridge was verified. In addition, it was clarified that the construction of the objective composite bridge could be performed with easier procedure at lower cost.

1. Introduction

Recently, the opportunity to adopt the composite structure in large cable-stayed bridge has increased. In this paper, the design of a 3-span continuous composite cable-stayed bridge with main span of 890m was conducted. In the objective bridge, the new composite 2 girder structure, which uses steel-pipe structure filled with concrete as main girder together with prestressed concrete(hereafter called PC) deck slab, was adopted in part of central span, and PC girder was used in other parts. Before the design of the composite cable-stayed bridge, as the basic model which demonstrates the possibility of realization, the design of a 3-span continuous PC cable-stayed bridge was performed. The static behavior, dynamic behavior and structure detail of design were investigated.

2. Basic structure

2.1 Objective bridge

The 3-span continuous PC cable-stayed bridge as shown in Fig.1, the design of which was already conducted in separate study, was selected as the basic model (hereafter called allPC model), and the objective composite bridge was determined by changing part of central span of the basic model to composite section as shown in Fig.2 (hereafter called composite model). As for the composite section, the steel-pipe structure filled with concrete was used as main girder, and PC slab was adopted.

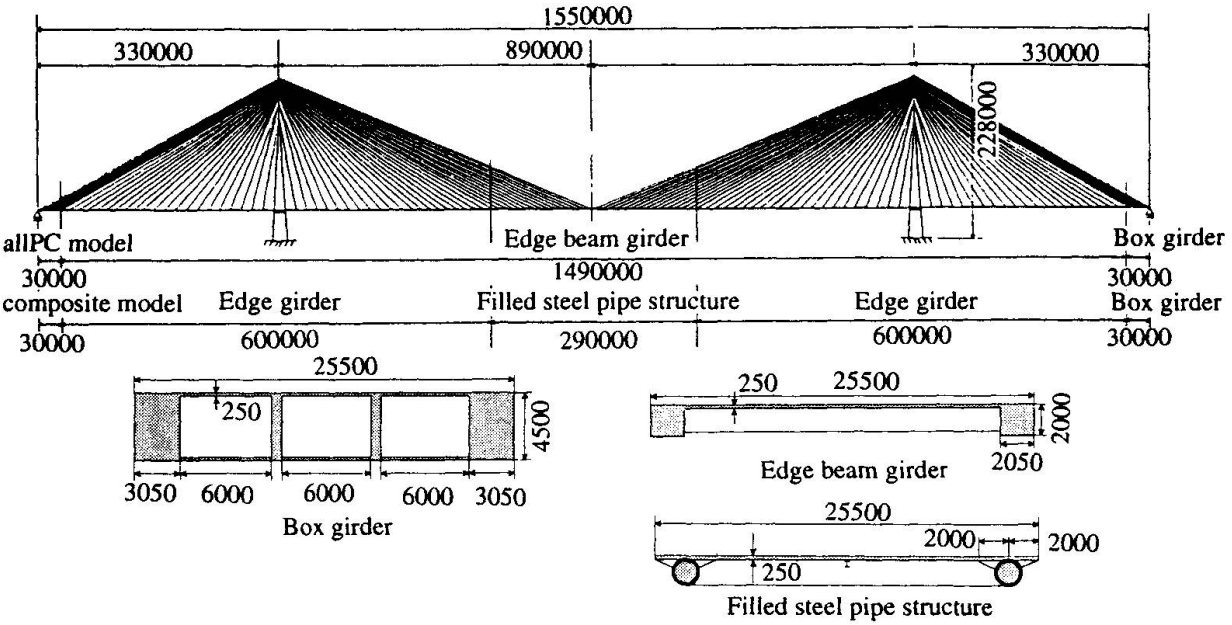

Fig.1 Model for study

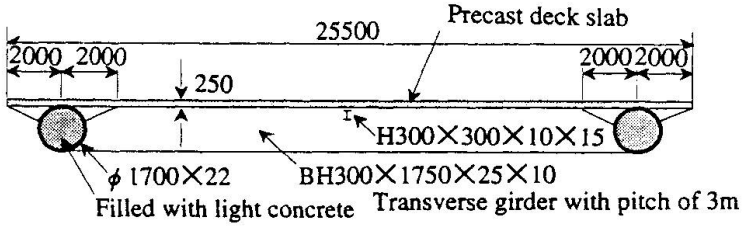

Fig.2 Filled steel pipe girder

2.2 Determination of section of composite main girder

Table.1 Type and features of main girder section

Type	Structural features	Cost	Capacity	Field joint	General evaluation
A	I beam	1.0	△	○	○
B	steel-pipe	0.8	○	○	◎
C	angle steel pipe	1.0	△	△	△
D	welded box section	1.2	◎	○	△
E	welded π section	1.0	△	○	△
F	moulded π section	0.8	○	△	△

As composite main girder, following 6 types of girders were studied and compared: (A) I section, (B) steel-pipe, (C)angle steel pipe, (D)welded box section, (E) welded π section, and (F) moulded π section. Table1 represents the study cases.Considering the construction cost, the capacity and the construction procedure, (B)steel-pipe was finally adopted as main girder.

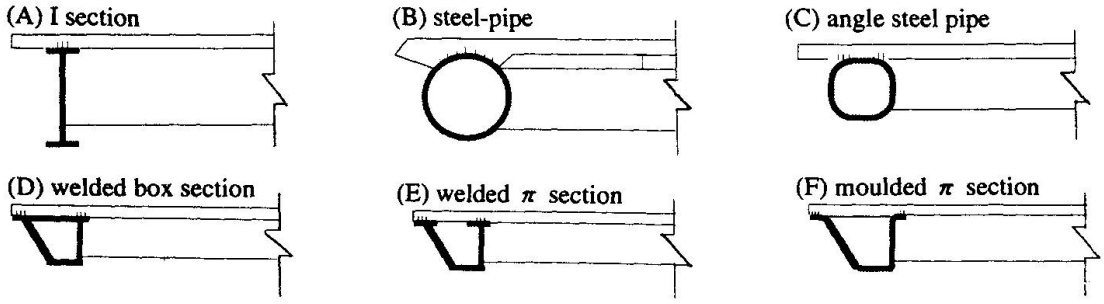

2.3 Structure features of new composite main girder

The new type structure has following three features: (1) 2 girder structure using steel-pipe; (2) steel-pipe main girder filled with concrete; and (3) composite structure consisting of PC slab and steel-pipe main girder. The details of the features are described as following.

(1) 2 girder structure using steel-pipe
Compressive force and bending moment are acting on the main girder of cable-stayed bridge at the same time. Compared with plate girder, the steel-pipe is more difficult to buckle locally, and has higher capacity against compressive loading. In addition, compared with girder with I section, the steel-pipe section has larger torsional stiffness and smaller drag coefficient, and thus has better performance when being used in cable-stayed bridge.

(2) Steel-pipe main girder filled with concrete
In order to increase the capacity to resist compressive force, the steel-pipe was filled with concrete. As light concrete was used, the weight was reduced by 5tf/m. Therefore, in composite model, the whole dead load and the weight of cables were reduced by 5% and 7%, respectively, compared with allPC model.

(3) Composite structure consisting of PC deck slab and steel-pipe main girder
To increase the capacity to resist the combined loading of compressive axial force and positive bending moment, and to improve the wind-resistant performance, not the torsional stiffness, the combination of PC deck slab and steel-pipe main girder was adopted. Figure3 indicates the function of PC deck slab in the stress analysis of section and the process of producing the filled concrete.

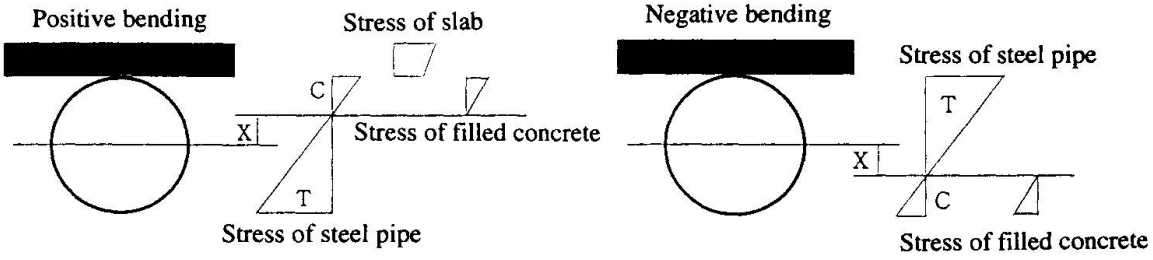

Fig.3 Distribution of stress

3. Study on static behavior

In this section, the computed section forces and reaction forces in allPC model and composite model, which were computed through static plane frame analysis, are compared, and the effects of creep and drying shrinkage are described. The analysis model of plane frame is shown in Fig.4.

(1) Characteristics of section forces
The bending moments of main girder due to dead loads and prestress in cables are shown in Fig.5, and the axial forces are indicated in Fig.6. By adjusting the forces in cables based on allPC model, the bending moments and axial forces in composite model could be almost the same as those in allPC model. The reaction forces at bearing points are represented in Table 2. It can be seen that, in composite model, no negative reaction force could occur either when dead load was applied to bearing point P1, or when bending moment due to live loads reached the maximum and minimum value.

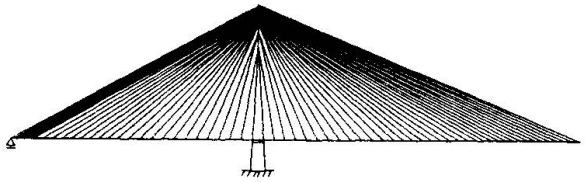

Fig.4 Plane frame analysis model

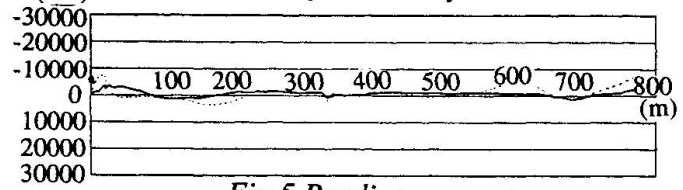

Fig.5 Bending moment

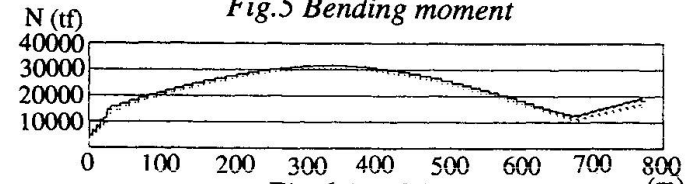

Fig.6 Axial force

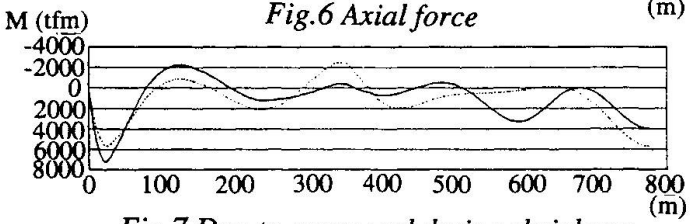

Fig.7 Due to creep and drying shrinkage

(2) Effect of creep and drying shrinkage
The variation of bending moment due to creep and drying shrinkage is indicated in Fig.7. In addition, the relationship between the section force at composite steel-pipe part after creep, and the allowable section force is shown in Fig.8.
From the figure, it can be confirmed that the section force generated after creep was smaller than the allowable section force.

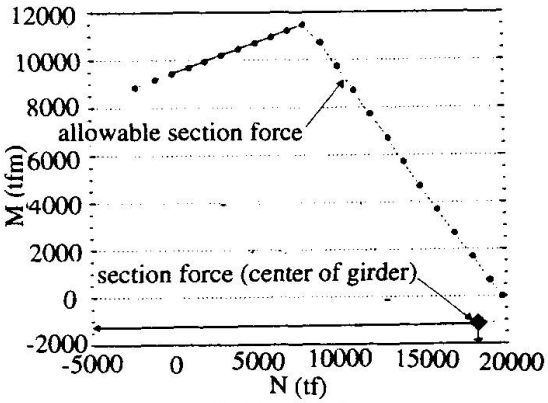

Fig.8 Check of stress

	Permanent load	When maximum bending moment occurred	When minimum bending moment occurred
Before creep	1556tf	2283tf	384tf
After creep	2573tf	3299tf	1400tf

Table.2 Reaction force at bearing point

4. Study on dynamic behavior

The mode analysis of the bridges using allPC model and composite model was carried out to investigate the fundamental behavior. And then, earthquake response analysis was conducted using acceleration response spectrum method. Three dimensional frame model was employed, and elastic spring (4000tf/m) was set at the top of column as damper. The acceleration response spectrum shown in Fig.9 was adopted. The mode shapes in the case of composite model are represented in Fig.10. The computed horizontal displacement at center of girder was 0.66m. In addition, it was confirmed that the section forces of main girder and tower were smaller than the allowable values. As for aerodynamic stability, the investigation using Selberg formulation was conducted, and the fundamental response behavior was studied. The more detailed investigations are planned to be conducted through wind-tunnel test.

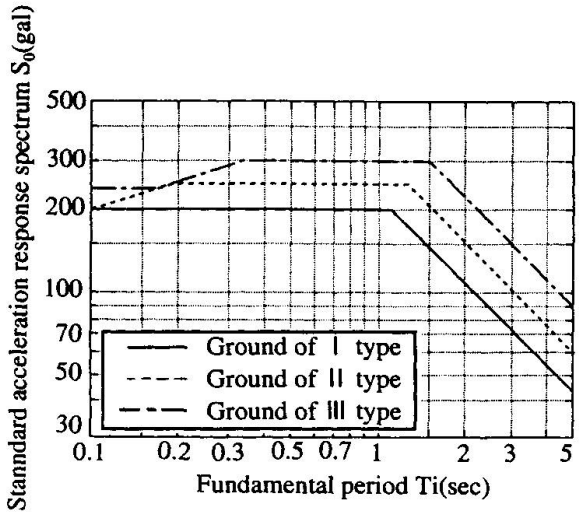

Fig.9 Acceleration response spectrum

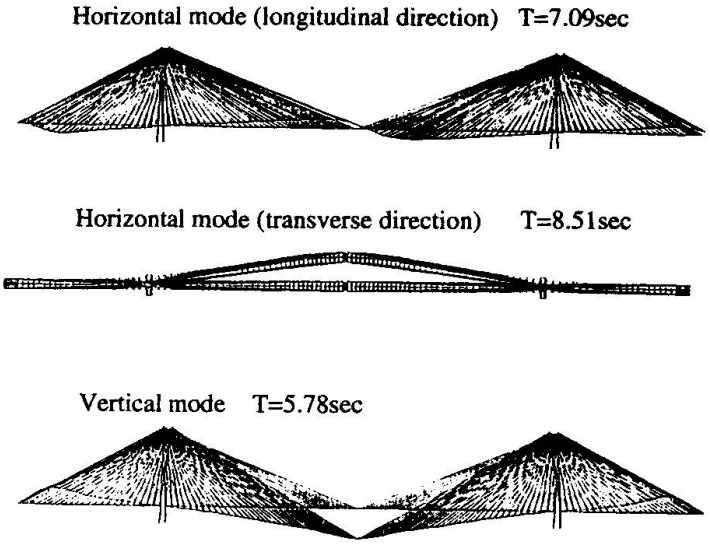

Fig.10 Vibration mode shapes

5. Structural details

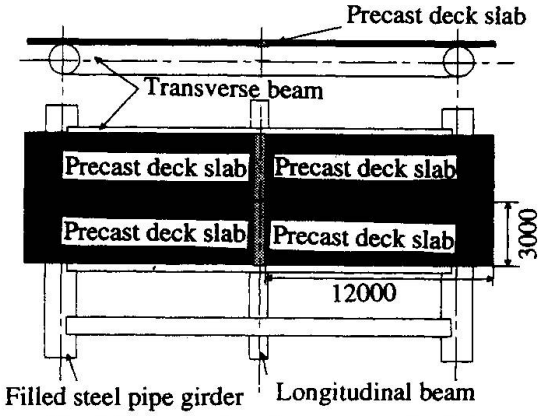

Fig.11 Example of precast sdeck lab

(1) Deck slab and frame structure
Figure 11 shows an example of precast PC deck slab. As the deck slab used for 2 main girder section, RC deck slab, PC deck slab and composite steel slab may also be adopted. However, precast PC deck slab is the most appropriate choice because the construction term could be shortened and the effects of creep and drying shrinkage are small.

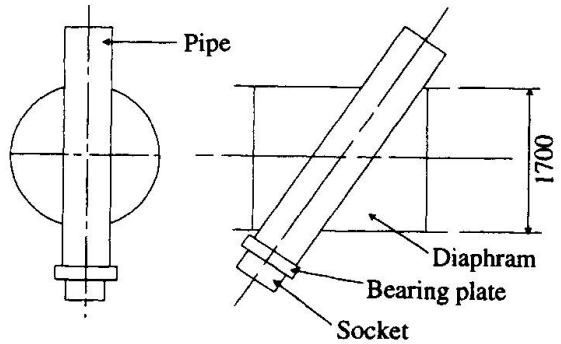

Fig.12 Anchor part for cables

(2)Anchor structure
As indicated in Fig.12, the steel pipe used for anchor part, which passes through the steel-pipe main girder, is separately made, and the cables could be connected successively. In addition, by using the method, the construction could be performed at low cost. As the tensile force of cables is applied at the center of steel-pipe girder, it could be smoothly transferred to the main girder and slab through diaphragm.

8. Conclusions

In this paper, the design of a composite cable-stayed bridge with main span of 890m was conducted. In part of central span, composite steel-pipe 2 girder was adopted. It was confirmed that it is possible to construct the presented composite bridge as well as allPC bridge. In addition, compared with allPC model, in the case of composite model, the weight could be reduced, and the construction could be performed with easier procedure at lower cost by appropriately designing the structural details. It is hoped that the results of this study could be helpful to the future research, design and construction of large composite cable-stayed bridge.

Reference

(1) Nakamura, Okimoto & Takeda: Structural characteristics of large composite cable-stayed bridge with steel-pipe as main girder, Steel Construction Engineering, No.17,1998.

A New Movable Floating Bridge Project in Osaka City

Eiichi WATANABE
Prof.
Kyoto Univ.
Kyoto, Japan

Tadaaki MARUYAMA
Sen. Eng.
Osaka Municipal Government
Osaka, Japan

Yukio KAWAMURA
Staff Officer
Osaka Municipal Government
Osaka, Japan

Hiroshi TANAKA
Bridge Eng.
Hitachi Zosen Co.
Osaka, Japan

Summary

The world's first swing and floating bridge is under construction in the Port of Osaka. It will be completed in the year of 2000 to connect two reclaimed islands. The bridge rests on two hollow steel pontoons and is supported horizontally by rubber fenders and dolphins. Investigated herein are many impotant engineering problems such as the dynamic response to the wave, wind, earthquake and vehicle loads. The bridge can be regarded as a high-tech bridge based on the advanced technology opening vistas onto the 21st century.

1. Introduction

A new movable floating bridge is under construction in the Port of Osaka. The main function of the bridge is to connect two reclaimed islands(i.e., Maishima and Yumeshima) across a waterway for the development of these islands. Though Yumeshima island is presently being reclaimed, it will serve as a residential and commercial area. The width of the waterway between the two islands is about 400m. This sub-waterway called "Noth waterway" will replace the main waterway of the Port of Osaka nearby in the case of the occurrence of some unforeseen accidents or events there. On such an occasion, large-sized vessels will need to pass the sub-waterway. In addition, the soil foundation of the reclaimed islands does not seem to have enough rigidity to resist the horizontal movement in case of the conventional bridge. Therefore a movable floating bridge with two pontoon foundations and at the same time swing type has been conceived for its functional and economical reasons. In addition, the construction period is short because the erection is done in a dock by the temporary supproting method and the nearly completed bridge will be towed to the erection site by the tugboats.
Presented herein is a brief summary of planning and experiments conducted.

2. Characteristics of Bridge

The ordinary fixed bridges or movable bridges with foundations fixed to seabed, such as swing bridge, bascule bridge, rolling bridge or transporter bridge have been investigated and assessed. It is concluded from the comparative study that those ordinary bridges will be difficult or economically infeasible; in stead, a bridge with two pontoon foundations of the swing type(Fig.1) is proposed to be adopted as the first of this kind in the world.

The new bridge has been temporally named "Yumeshima-Maiahima Bridge" after the name of the reclaimed islands near the site (Fig.2). It has the total length of 940m and the width of 38.4m with 6 lanes as shown in Fig.3. The floating part has the length of 410m and the main span length of 280m with double-arch rib construction standing on two steel hollow pontoons. The transitional bridges are installed at the both ends of the floating bridge to connect the approach bridges supported on the grounds and the floating bridge following the change of sea surface due to tidal change.

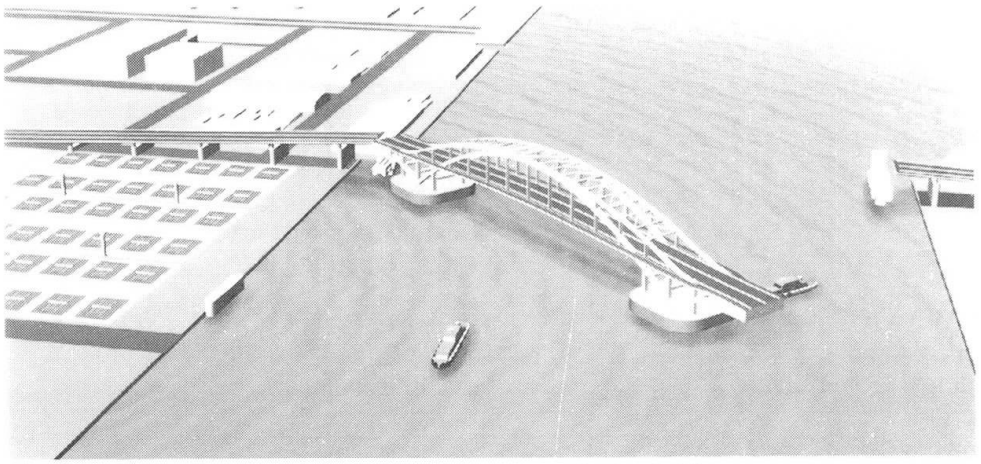

Fig. 1 The Yumeshima-Maishima Bridge and North Waterway

From the view point of the use of lands, only relatively small ships are usually allowed to pass the waterway under the bridge. However in the case of occurrences of some unforeseeable accidents or official events there, this waterway is to replace the main waterway nearby. The bridge will swing about the axis near the end of the floating part at Maishima side and the width of 200m in sub-waterway will be secured to pass large-sized vessels on such occasion.

The bridge is usually held securely by the clamped walls through the rubber fenders provided on the webs of the girders(Fig.4). The design specifications and dimensions are shown in Table 1.

The dynamic responses to the waves, winds and strong earthquake

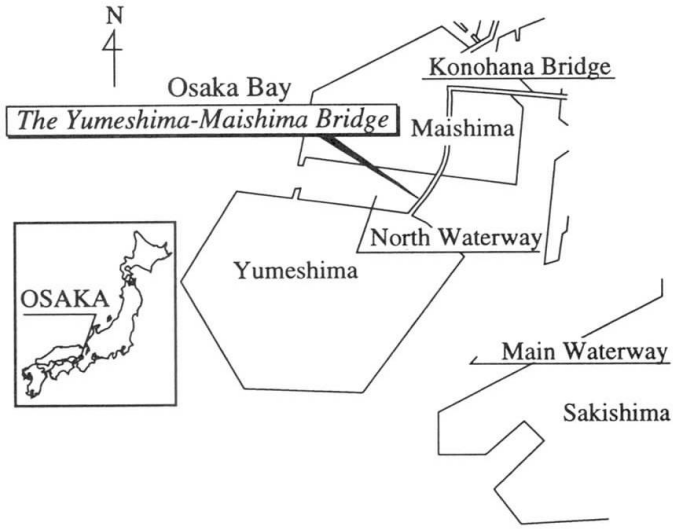

Fig. 2 Reclaimed Islands of Maishima and Yumeshima

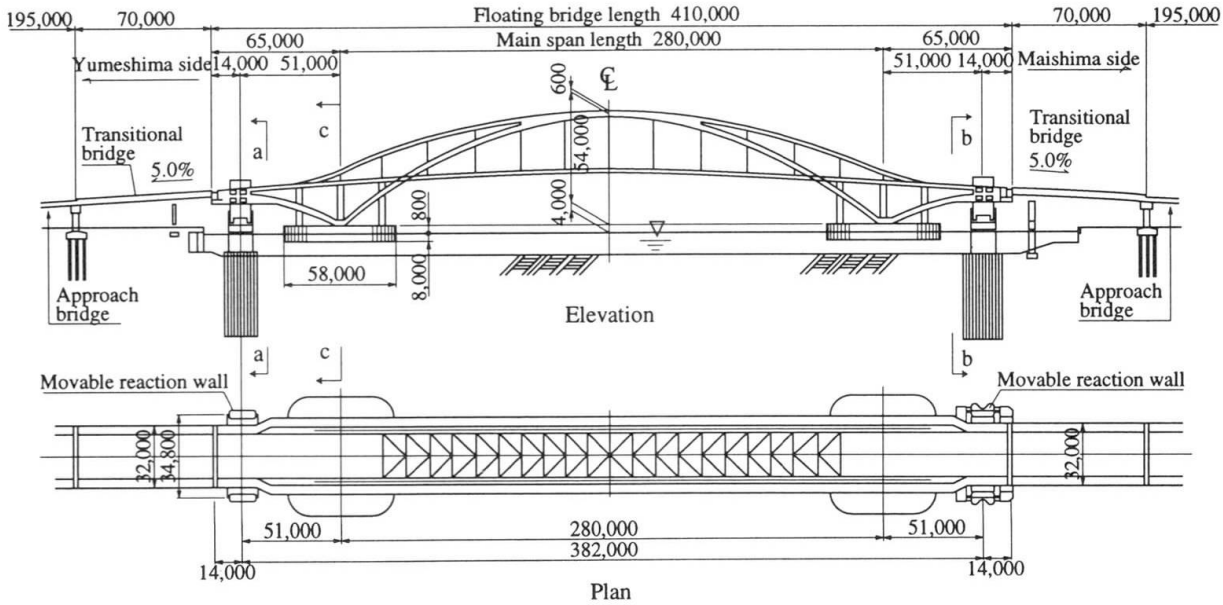

Fig. 3 The General View of The Yumeshima-Maishima Bridge

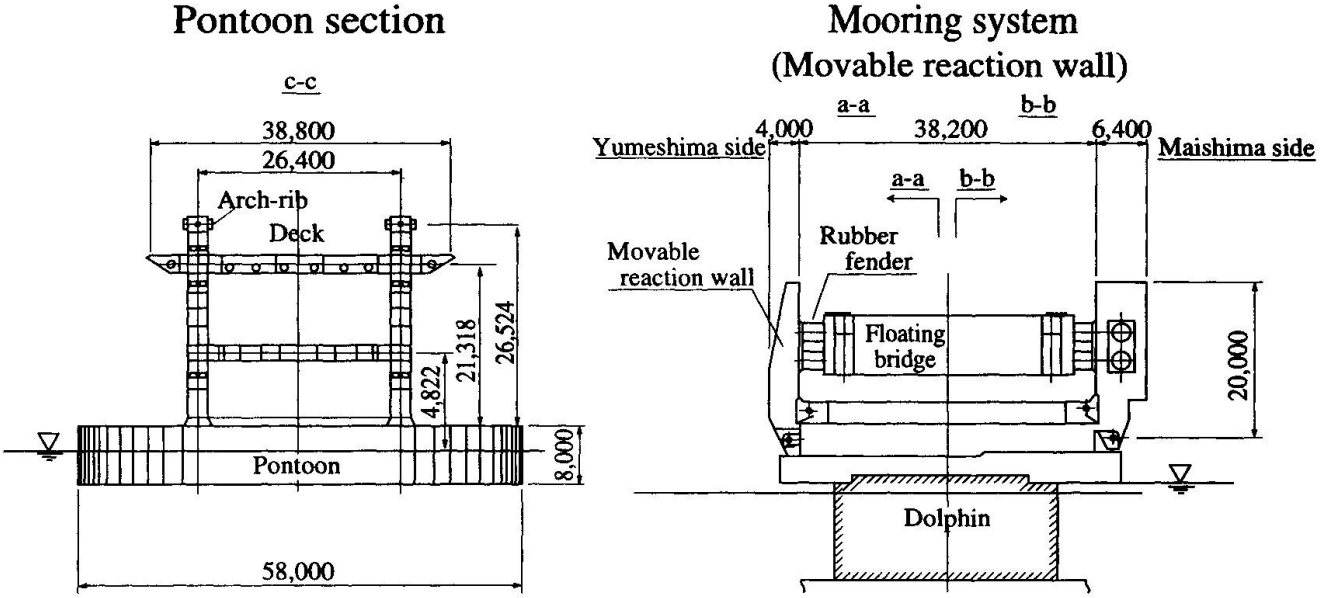

Fig. 4 Pontoon & Mooring System

Table 1. Design specifications and approximate steel weight

Bridge type	Movable swing floating bridge			
Road standard	Grade 4, Type 1			
Live load	B live load	Wind load	V_{10}=42 m/s	
		Waves	$H_{1/3}$=1.4 m, $T_{1/3}$=5.7~7.7s	
Bridge length	410m			
Effective width	31.2m (6-lanes roadway with 2-side walks)			
Length between supports	65.7m+280.0m+65.7m			
Lane width	When closed	135.0m	When open	200.0m
Under clearance		DL+26.0m		——
Super elevation	2% straight line			
Longitudinal gradient	5% both grades (V.C.L140m)			
Pavement thickness	Roadway/80mm Walkway/40mm			
Earthquake load	Level I	Bridge axis direction/Kh=0.05 Direction perpendicular to bridge axis/Kh=0.13		
	Level II	Bridge axis direction/Kh=0.11 Direction perpendicular to bridge axis/Kh=0.36		
Approximate steel weight (Unit in tons)	Pontoon	6,800		
	Floating bridge	19,400		
	Mooring structure	7,800		
	Total	34,000		

are one of the prime concerns. Besides, the dynamic responses are also studied when the heavy traffic vehicles run from the transitional bridge to the floating bridge over the expansion joins to connect them. The following numerical simulation methods have been developed to solve them.

1) The ordinary simulation method (i.e.,OSM) which incorporates the non-linear characteristics of the rubber fender mooring system gives time-domain responses of 6-degree-of-freedom motion due to waves and winds using the rigid model[2]. This method is extended to deal with the responses during the swinging procedure.

2) The hybrid simulation method (i.e.,HSM) which is composed of a computer, a tri-axial compression equipment and the models of the rubber fenders has been developed[3]. HSM deals only with the two dimensional dynamic motions and was used to verify the results of OSM.

3) A multi-degree-of-freedom analysis using the elastic model in water waves has been developed. The method is based upon spectrum method then uses the linearized model of the rubber fenders. It has cleared up the effect of flexibility of the bridge[4].

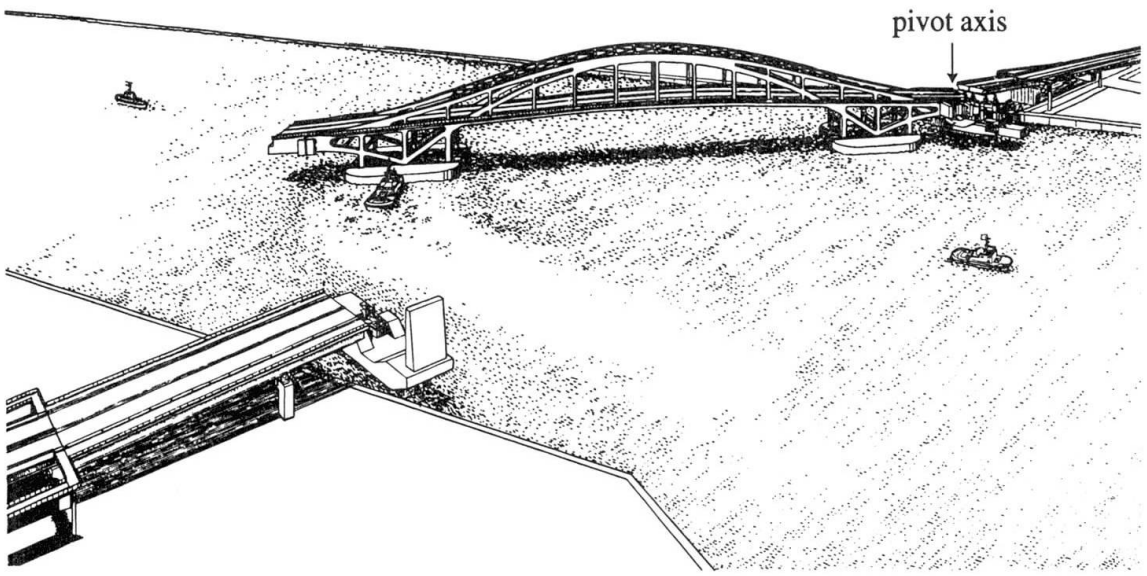

Fig. 5 Swinging Procedure

3. Swinging Procedure

The swing system is prepared to let large-sized vessels pass the sub-way in an emergency as mentioned previously. The swinging procedure is as follows:

A pivot axis is inserted and the transitional girders are lifted up by jack-up units. Then the reaction walls which are usually in the standing-position to moor the bridge are released and rotated, thereby completing preparation for swinging.

The bridge is swung about the pivot axis by tugboats(Fig.5).

After the swinging is completed, the bridge is temporarily moored and the opening operation of the bridge is finished. Then large ships can navigate the sub-waterway freely.

The procedure of the bridge closing is the reverse of the one just described.

4. Erection

The following erection method has been chosen in a dock yard(Fig.6):
The super structure with pontoons is assembled in a dock.
After the completion, the deck is filled with water and the bridge is towed to the erection site by tugboats.
The bridge is installed immediately to the mooring system by tug winch operation.
The superstructure and the substructure can be constructed at different places simultaneously. In this way, the construction period is remarkably reduced.

5. Experimental Study

Many experiments have been performed to ensure the safety and serviceability of this bridge.
Main items of the experiments are as follows:

(1) The rigid-body motions of the floating bridge model(scale:1/80) against water waves and winds were examined in a large-scaled water tank to compare with the OMS(Photo.1).
(2) The swinging and temporary mooring operation were ensured by using the above-mentioned rigid model(Photo.2).

(STEP 1) Erection is done in a dock by the temporary supporting method, using two 120t suspension jib cranes.

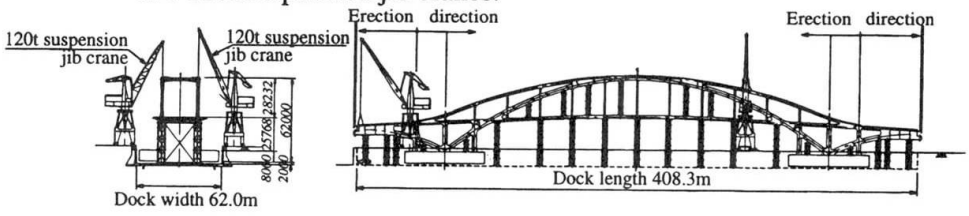

(STEP 2) The bridge is towed to the installation position by a formation of 8 tugboats in the 3,600 horsepower class.

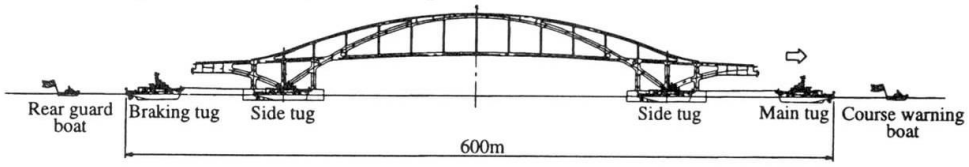

(STEP 3) The floating bridge is connected to the mooring equipment via tug winch operation.

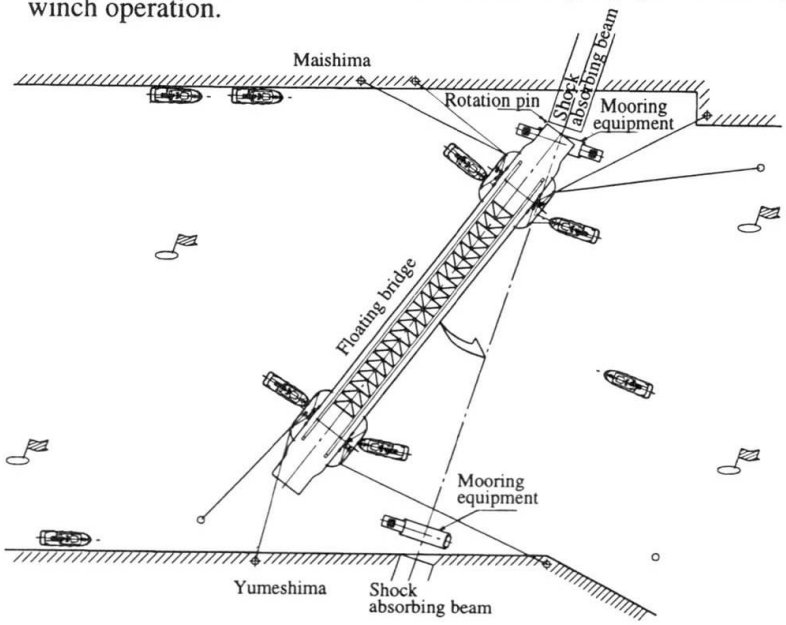

Fig. 6 Erection Steps

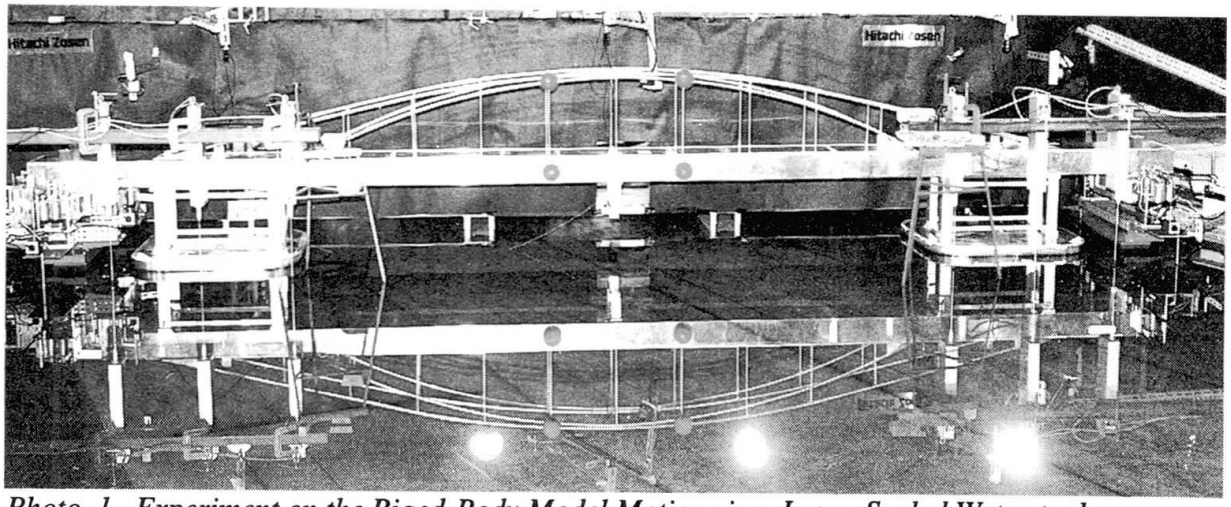

Photo. 1 Experiment on the Riged-Body Model Motions in a Large-Scaled Water-tank

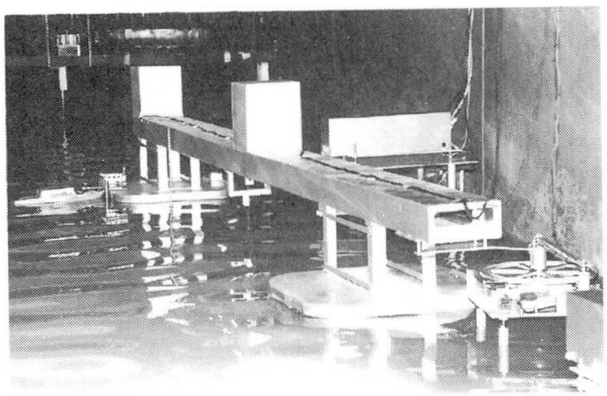

Photo. 2 Swinging and temporary mooring experiment (Scale: 1/80)

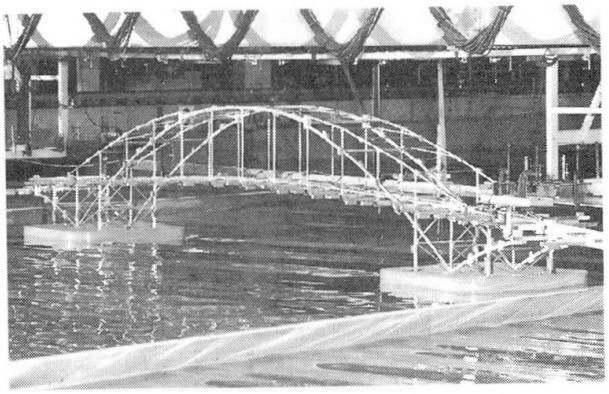

Photo. 3 In-wave elastic model experiment (Scale: 1/40)

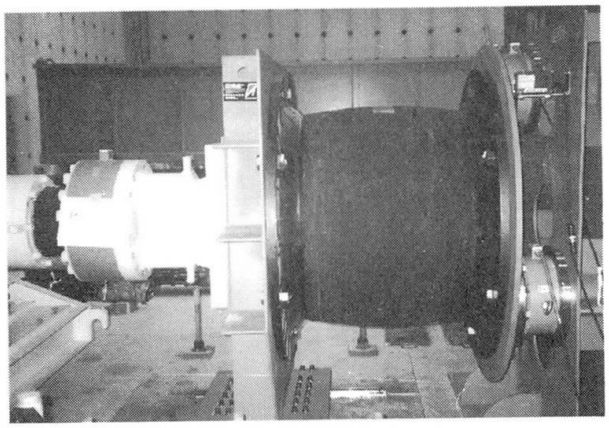

Photo. 4 Mooring fender characteristic test

(3) The effect of the flexibility as compared with the rigid body of the floating structure against wave loads was examined by using the elastic model(scale:1/40) and the effect was proved to be very small(Photo.3)
(4) The characteristics of the mooring rubber fender were clarified(Photo.4).
(5) The six static coefficients were measured by the wind tunnel tests and the wind drag force was reduced by changing the configuration of the girder.

6. Conclusions

The world's first floating and swing bridge is under construction in the Port of Osaka, Japan. This movable floating bridge is an all-steel bridge with two pontoons to connect two man-made islands of Maishima and Yumeshima. To suport the pioneering bridge work, many field observations are being planned both during and after construction for future constructions of similar floating bridges.

The authors wish to express sincere appreciation to the members of the Committee of the Movable Floating Bridge (chairman : Prof.Eiichi Watanabe of Kyoto University).

References

[1] Maruyama, T., E. Watanabe, T. Utsunomiya and H. Tanaka, "A New Movable Floating Arch Bridge in Osaka Harbor," *The sixth Asia-Pacific Conference on Structural Engineering & Construction*, pp.429-434, Jan.1998, Taiwan
[2] Ueda, S., "Analytical Method of Wave- and Wind-Induced Motions of Ship Moored at Quay-Walls and Its Applications," *Tech. Note of the Port and Harbor Research Institute,* No.504 (in Japanese)
[3] Oda, K., T. Maruyama, H. Tanaka, S. Nagata and S. Yamase, "Hybrid Simulation for A New Movable Floating Bridge," *The sixth Asia-Pacific Conference on Structural Engineering & Construction*, pp.435-440, Jan.1998,Taiwan
[4] Ueda, S., H. Seto, N. Kumamoto, K. Inoue and O. Oka, "Behavior of Floating Bridge under Wind and Wave Action," *International Workshop on Very Large Floating Structures*, pp.257-264, Nov.1996, Hayama, Japan

New Control Method for Flutter Suppression of Long-Span Bridges

Yozo FUJINO
Prof.
Univ. of Tokyo
Tokyo, Japan

Krzysztof WILDE
Assist. Prof.
Univ. of Tokyo
Tokyo, Japan

Toshinobu KAWAKAMI
Graduate Student
Univ. of Tokyo
Tokyo, Japan

Summary

In this paper a passive aerodynamic control of flutter of long-span bridge is proposed. The system consists of additional surfaces attached to the bridge deck and an additional pendulum. Rotation of control surfaces is used to generate stabilizing aerodynamic forces. The FEM analysis performed on multimode model of the bridge showed that the flutter critical wind speed can be increased to the required level when the bridge is equipped with the control surfaces of the length of 13% of the total length of the bride deck. It was found that the design of control action of the surfaces must incorporate control of oscillating flutter modes as well as divergent type of instability.

1. Introduction

Remarkable progress has been made over the last twenty years in research on using passive, active and hybrid systems as a means of structural protection against wind, earthquakes and other hazards[1,2]. The first full-scale application of active control to a building[3] was accomplished in 1989. The first application of active control to bridges[4] appeared in 1991. Now 14 bridge towers have employed active systems during erection. The full-scale active control systems that have been installed in bridges, aim mainly at reduction of vortex-induced vibration of towers during erection and are limited only to a relatively small amplitude range. There have been no applications of active control to the wind-induced flutter oscillations of girders of long-span bridges.

Traditionally "passive methods", such as an increase in the structural stiffness of bridge girders, have been used for flutter suppression. A deep truss section with high torsional stiffness was selected for the Akashi suspension bridge (main span of 1990 m) in Japan. Improvement in aerodynamic stability can also be obtained by streamlining the bridge deck. Nevertheless, for suspension bridges with a main span of several kilometers active methods provide new design alternatives. Murata and Ito[5] conducted analytical and experimental study with an active gyro installed on the bridge deck. The motion of the gyroscope was coupled with torsional motion of the deck and the moment of gyration was used for prevention of onset of flutter. The application of the Active Mass Driver (AMD) was studied by Dung et all.[6] The numerical simulations showed good improvement of the flutter wind speed.

The active flutter suppression methods, discussed above, aim at modification of the dynamic properties of the bridge structure itself. Modification of the flow around the bridge deck or generation of stabilizing aerodynamic forces from the flow is another approach to the flutter problem. Active aerodynamic methods can be defined as the prevention of flutter by using

aerodynamic control surfaces controlled by signals through an appropriate feedback control law. In this control methods stabilizing forces, generated on the control surfaces, increase proportionally to the wind speed squared, and thus proportionally to the forces acting on the bridge deck. Furthermore, the stabilizing forces are not generated directly by the actuators, but are drawn form the air flow, thus, the energy required for control is much smaller since it is used only for rotation of the control surfaces. The application of such methods for control of bridge vibration was proposed by Ostenfeld and Larsen[7]. Experimental study of the active aerodynamic control method with control surfaces attached to the bridge deck through the pylons was conducted by Kobayashi and Nagaoka[8], and obtained improvement of critical flutter wind speed, when compared to the deck without any devices, was of a factor of 2. However, the control algorithm in the experiment was selected intuitively and further improvement could be obtained by careful design of control law. Wilde and Fujino[9] proposed a variable-gain control law based on the optimal control theory. The analytical study showed that proper design of the amplitude and phase of the control surface motion can provide stability for any wind speed, even for very flexible bridge.

2. Passive aerodynamic control of flutter of bridge section

The active aerodynamic control of flutter of bridge decks gives the designer freedom in shaping the dynamics of a closed loop system. However, the control system requires actuators, sensors, a computer to execute the control law, and an external power supply. Furthermore, this method requires two or three parallel control systems to safeguard reliability, since the failure of the controller would most likely result in a collapse of the bridge. Thus, there is strong interest in developing a passive system which, though it might not be able to solve the flutter problem for any velocity of oncoming wind, could due to its simplicity and reliability, be easily accepted by bridge engineers.

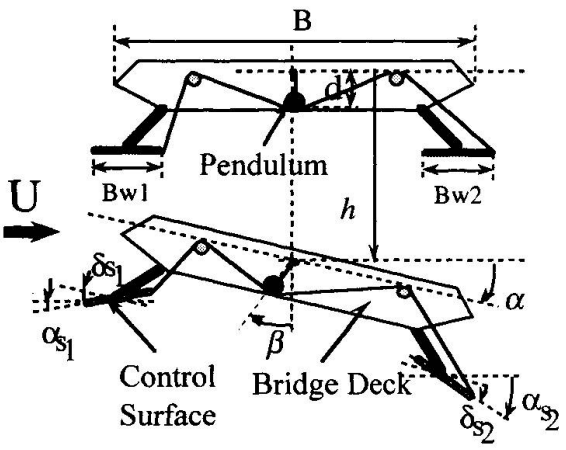

Fig. 1 Cross-section of the deck with passive aerodynamic control system.

A proposed passive system consists of two control surfaces attached to both edges of the deck and a pendulum placed inside the deck (Fig. 1). The pendulum is attached at the center of gravity of the deck. The mass of the pendulum is connected to the control surfaces, such that a torsional displacement of the deck and displacement of the pendulum, result in the appropriate motion of the leading and trailing surface.

2.1 Equation of motion

A mathematical description of the self-exciting aerodynamic forces acting on the bridge deck due to harmonic motion was suggested by Scanlan and Tomko[10]. In his formulation the wind-induced forces are functions of spatial coordinates, their first derivatives and so-called flutter derivatives. The flutter derivatives are the frequency dependent functions, which are determined for each type of bridge deck through specially designed wind tunnel tests. Estimation of the flutter wind speed is performed by an iterative search through the possible flutter frequencies. Wilde et all.[11] suggested the use of rational function approximation, similar to that widely used in

aerospace engineering, to represent the unsteady aerodynamics for arbitrary motion. Although, the equation of motion with approximated wind forces, is augmented by additional degrees of freedom, it can be formulated in the form of a set of frequency independent constant coefficient differential equations.

The equation of motion of the section of bridge deck of width B with aerodynamic control with pendulum has three structural degrees of freedom: heaving, h, pitching, α, and displacement of pendulum β. The equation of motion is

$$\mathbf{M}\ddot{\mathbf{q}}(t)+\mathbf{C}\dot{\mathbf{q}}(t)+\mathbf{K}\mathbf{q}(t)=\mathbf{B}_d\mathbf{F}_{ae}^{deck}(t)+\mathbf{B}_{s_1}\mathbf{F}_{ae}^{s_1}(t)+\mathbf{B}_{s_2}\mathbf{F}_{ae}^{s_2}(t), \tag{1}$$

where **M, C, K** are mass, damping and stiffness matrices and $\mathbf{q}(t)^T=\left[h/B, \alpha, \beta\right]$. In this equation, $\mathbf{F}_{ae}^{deck}(t)$, $\mathbf{F}_{ae}^{s_1}(t)$ and $\mathbf{F}_{ae}^{s_2}(t)$ are aerodynamic forces acting on the deck and leading and trailing control surface, respectively. The time domain formulation of aerodynamic forces, $\mathbf{F}_{ae}(t)$, is obtained through the rational function approximation[11] as

$$\begin{aligned}\mathbf{F}_{ae}(t)&=\mathbf{V}_f\mathbf{A}_0\mathbf{q}(t)+(B/U)\mathbf{V}_f\mathbf{A}_1\dot{\mathbf{q}}(t)+\mathbf{V}_f\mathbf{D}\mathbf{x}_a(t),\\ \dot{\mathbf{x}}_a(t)&=(U/B)\mathbf{V}_f\mathbf{R}\mathbf{x}_a(t)+(U/B)\mathbf{V}_f\mathbf{E}\mathbf{q}(t),\end{aligned} \tag{2}$$

where $\mathbf{V}_f=diag(-0.5\rho U^2B, 0.5\rho U^2B^2)$, U is a mean velocity of oncoming wind and ρ is the air density. The newly introduced variables $\mathbf{x}_a(t)$, called *aerodynamic states,* model the flow structure interaction. The coefficient matrices $\mathbf{A}_0$, $\mathbf{A}_1$, **D**, **E** and **R** are computed from the unsteady aerodynamic data obtained from experimentally determined flutter derivatives or theoretically determined flutter derivatives for a flat plate.

Two control patterns of coupling between rotation of control surfaces and torsional displacement of the deck are assumed in this paper. In Pattern 1 the direction of rotation of the leading, δ_{s_1}, and trailing, δ_{s_2}, surfaces are the same. In Pattern 2 the torsional displacement of the leading surface is opposite to the rotation of the deck, α, and the rotation of the trailing surface, is in the same direction as rotation of the deck. For both patterns the rotational ratio, g, of the leading and trailing surfaces are assumed to be the same. The mathematical formulas for both patters are:

Control Pattern 1	Control Pattern 2
$\delta_{s_1}=g(-\alpha+\beta),$	$\delta_{s_1}=g(-\alpha+\beta),$
$\delta_{s_2}=g(-\alpha+\beta),$	$\delta_{s_2}=g(\alpha-\beta).$

(3)

2.2 Numerical simulations

The bridge deck, used in the simulation, has a flat box section considered for use in the Akashi bridge[12], with a width of 30 m. The undamped natural frequencies of torsional and heaving mode are T_α = 7.48 s and T_h = 23.27 s, and the logarithmic decrements of both modes are δ_α= 0.005 and δ_h= 0.005, respectively. The width of the control surfaces is selected as 10% of the deck width and the surfaces' hinge lines coincide with the edges of the deck.

The root locus of eigenvalues with respect to wind speed of the bridge deck without control system is shown in Fig. 2. The flutter wind speed is found to be 38.8 m/s. Instability occurs due to the negative damping of the torsional dominant mode which is denoted on the graph as mode 2.

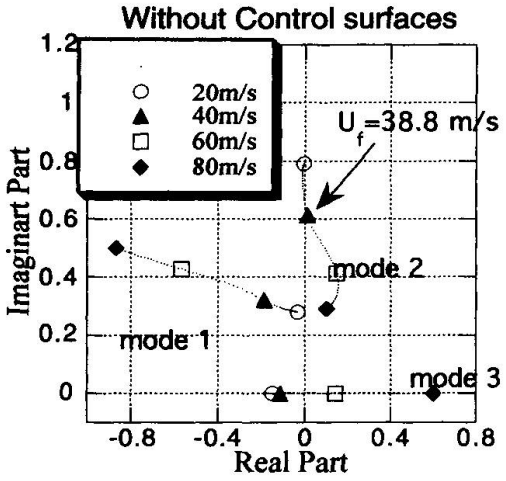

Fig. 2 Root locus of eigenvalues with respect to wind speed of bridge deck without control.

Damping in the heaving dominant mode (mode 1) is significantly increased as the pole moves away form the imaginary axis with increasing wind speed.

The maximum critical wind speeds for controlled system with pattern 1 and 2 with $\beta = 0$ are 51.6 m/s and 48.8 m/s, respectively. Increase of rotational ratio, g, above 11 for the system with control pattern 1, and above 6 for control with pattern 2, results in fast decrease of critical wind speed. Fig. 3 shows root locus for bridge controlled by both control patterns for g=6. The antisymmetric motion of the surfaces, pattern 1, adds considerable damping to torsional and heaving modes. However, aerodynamic mode (mode 3) becomes unstable. Instability of this real mode can be interpreted as divergence. The system with control pattern 2 becomes unstable due to negative damping of torsional dominant mode (mode 2). With this control the aerodynamic modes have large damping up to wind speed of 80 m/s.

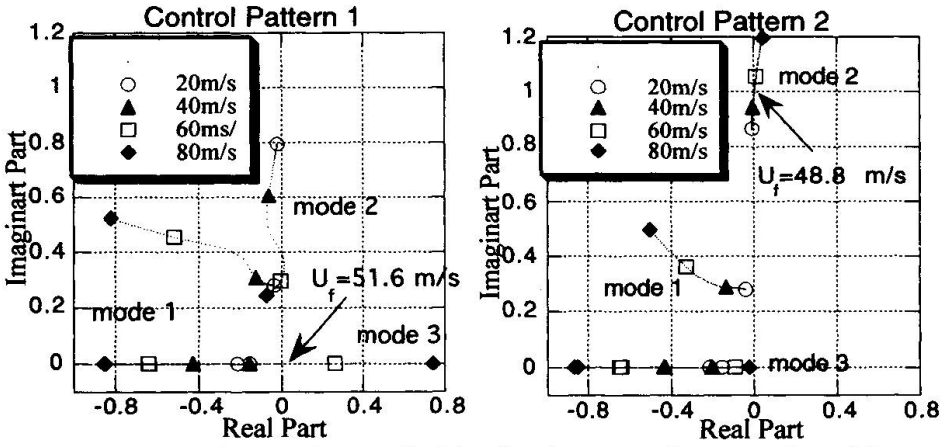

Fig. 3 Root locus of controlled bridge for control pattern 1 and 2.

Numerical simulations which include the motion of the pendulum shows that a long period pendulum is necessary to satisfy the condition of $\beta = 0$. For control pattern 1, g=6 and mass ratio of the pendulum of 1% the pendulum period must be larger than 200 s. However, for the mass ratio of 10% the sufficient period of pendulum is 24 s. The control with pattern 2 requires pendulum of period 100 s and 14 s for 1% and 10% mass ratio, respectively.

3. Design of passive aerodynamic control on multimode model of a bridge

A suspension bridge of a main span of 2500 m and side spans of 1000 m is shown in Fig. 4. Since the primary interest in flutter analysis is the coupling of torsional and vertical motion of the deck, the dynamics of the cables and towers are neglected in this study. The bridge is modeled by a three span continues simply supported beam. Standard beam elements are used to derive mass, stiffness and damping element matrices of the system. Each node has two structural degrees of freedom, namely, torsion and vertical displacement, and two degrees of freedom corresponding to aerodynamic states (Eq.2).

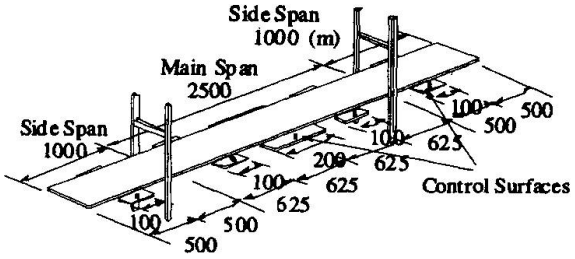

Fig. 4 Model of the bridge with position of control surfaces.

The properties of the bridge are selected such that the frequencies and damping of the first bending and torsional modes are consistent with the frequencies of sectional model of the bridge. The critical wind speed of the uncontrolled bridge is found to be 38 m/s. The instability occurs due to first torsional mode. The divergent type of instability occurs at the wind speed of 49 m/s. The root locus and mode shape of uncontrolled bridge at flutter wind speed are shown in Fig. 5.

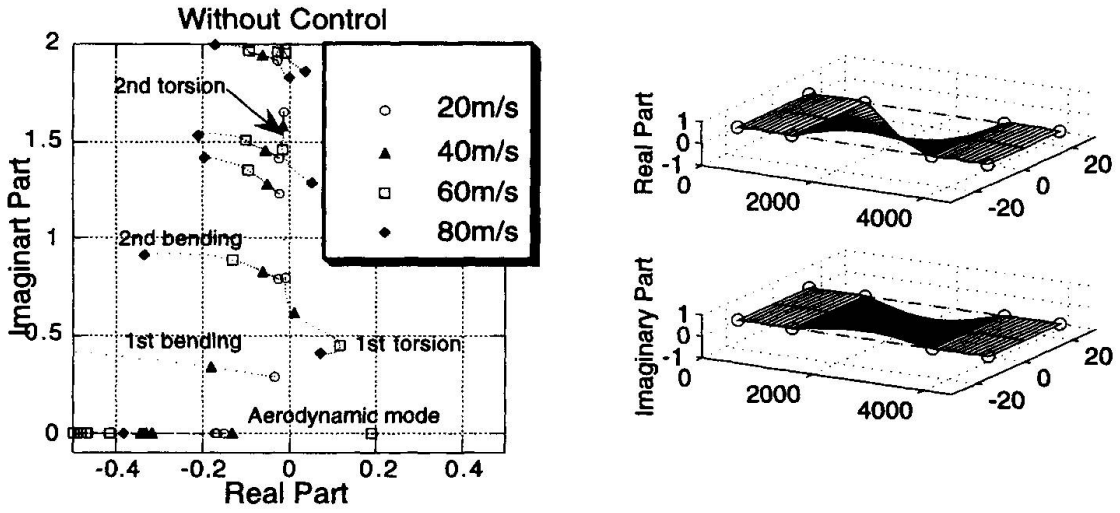

Fig. 5 Root locus of uncontrolled bridge and flutter mode shapes.

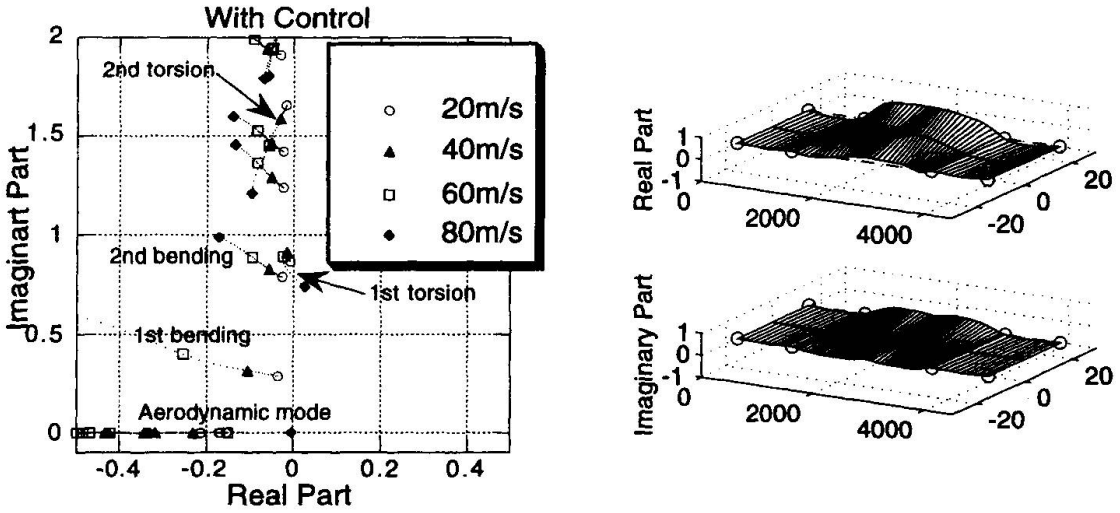

Fig. 6 Root locus of controlled bridge and flutter mode shapes.

Flutter control is performed by 5 additional control units consisting of leading and trailing surfaces. The sizes and positions of control surfaces as well as the rotational ratios and control patterns are optimized such that the critical wind speed of 75 m/s is obtained. The positions and sizes of the surfaces are shown in Fig. 4. The total length of the control surfaces is 13% of the total length of the bridge. The rotational ratio for the control units of side spans are found to be 10, while the rotational ratio for control units located on the main span are 15. The control unit located in the middle of the main span is controlled by control pattern 2. This control is mainly oriented towards the improvement of divergence . All other

10, while the rotational ratio for control units located on the main span are 15. The control unit located in the middle of the main span is controlled by control pattern 2. This control is mainly oriented towards the improvement of divergence . All other control units are controlled by pattern 1 and their main action is directed toward modification of the oscillatory modes of the system. The dynamics of the pendulums of the units is neglected in this study. The root locus of the controlled system is presented in Fig. 6. The instability occurs due to the first torsional mode at wind speed of 75 m/s. The divergent mode is stable up to the wind speed of 79 m/s. The flutter mode of the controlled bridge has large contribution of vertical displacement.

4. Concluding remarks

In this paper the design of passive aerodynamic control of bridge flutter on multimode model of a suspension bridge is presented. The design of the control on multimode model gives larger possibilities of selection of control actions. It was found that the control unit located in the middle of the main span should be concentrated mainly on suppression of divergence while the other units are modifying the flutter oscillatory modes. The flutter wind speed was improved to the required value with the use of the control surfaces which total length was 13 % of the length of the bridge.

5. References

1. Fujino, Y. Soong, T.T. and Spencer, B. F. Jr., 1996, "Structural Control: Basic Concepts and Applications," *Proceedings of the ASCE Structures Congress XIII*, Chicago, Illinois, April 15-18, 1277-1287.
2. Soong, T.T., 1990, *Active Structural Control: Theory and Practice*, Longman Scientific and Technical, Essex, England.
3. Sakamoto, M., Kobori, T. et al., 1994a, "Practical Applications of Active and Hybrid Response Control Systems and Their Verifications by Earthquake and Strong Wind Observations." *Proc. 1st World Conf. on Struct. Control"*, Pasadena, USA, WP2:90–99.
4. Tanida, K., Koike Y., Mutaguchi K., Uno N., 1991, "Development of Hybrid Active-Passive Damper," PVP–Vol. 211, ASME, 21–26.
5. Murata M., Ito M., 1971, " Suppression of Wind Induced Vibration of a Suspension Bridge by Means of a Gyroscope", *Wind Effects on Buildings and Structures*, Vol. 4, 40, pp. 1-10.
6. Dung N. N., Miyata T., Yamada H., 1996, "Application of Robust Control to the Flutter in Long-Span Bridges", *Journal of Structural Engineering JSCE* , Vol. 42A, pp. 847-853.
7. Ostenfeld K. and Larsen A., 1992, "Bridge Engineering and Aerodynamics", *Aerodynamics of Large Bridges*, (Larsen A. ed.), Copenhagen, A.A. Balkema, Rotterdam., pp. 3-22.
8. Kobayashi H. and Nagaoka H., 1992, "Active Control of Flutter of a Suspension Bridge", *Journal of Wind Engineering and Industrial Aerodynamics*, 41-44, pp. 143-151.
9. Wilde K., Fujino Y., 1996, "Variable Gain Control Applied to Aerodynamic Control of Bridge Deck Flutter", *Proceedings of the 35th IEEE CDC*, Kobe, Japan, Vol. 1, WM08, pp. 682-687.
10. Scanlan R., Tomko J., 1971, "Airfoil and Bridge Deck Flutter Derivatives", *J. Eng. Mech. Div., ASCE*, **97**, No. EM6, pp. 1717-1737.
11. Wilde K., Fujino Y., Masukawa J., 1996, "Time Domain Modeling of Bridge Deck Flutter" *Journal of Structural Engineering, JSCE*, Vol. 13, pp. 93s-104s.
12. Fujino Y., Iwamoto M., Ito M., Hikami Y., 1992, "Wind Tunnel Experiments Using 3D Models and Response Prediction for a Long-Span Suspension Bridges", *J. Wind Engineering and Industrial Aerodynamics*, vol. 41-44, pp. 1333-1344.

Aseismic Design of the Akashi Kaikyo Bridge

Hirokazu IEMURA
Prof.
Kyoto Univ.
Kyoto, Japan

Zenon AGUILAR
Graduate Student.
Kyoto Univ.
Kyoto, Japan

Akira IGARASHI
Assoc. Prof.
Kyoto Univ.
Kyoto, Japan

Masahiko YASUDA
Civil Eng.
Honshu-Shikoku Bridge Authority
Kobe, Japan

Summary

A four-station array observation system has been used to monitor the long-period seismic activity around the Akashi Kaikyo Bridge construction site. Since its installation in 1990, more than one hundred earthquake records, including aftershocks of the Hyogoken-Nanbu Earthquake, have been obtained. These records are used to synthesize long-period ground motions due to hypothetical huge earthquakes, using empirical methods. Seismogenic sources along the Median Tectonic Line of southwest Japan, and the Nankaido Trough are considered as possible sources of large earthquakes. The synthesized signals show peak displacement values of about 50 cm, although most of their acceleration response spectra show lower or equal level compared with the design spectra for the Akashi Kaikyo Bridge.

1. Introduction

The Akashi Kaikyo Bridge, the world's longest suspension bridge, has a center span of 1990 m and its fundamental vibration period is about 20 seconds. There have been few studies to verify the design earthquake load in such a long-period range; therefore, in 1990 an array observation system consisting of four stations was placed around the bridge construction site (Fig. 1), to monitor the long-period seismic activity in this area. The installed pick-ups are reliable from 0.0025 to 70 Hz, having a resolution of 0.00005 kine. More than a hundred of earthquake records have been obtained so far by this array. Long-period ground motions were observed for far-field large earthquakes, which present peak displacement values of about 7 mm and dominant periods from 8 to 20 sec. Short-period ground motions of near-field small earthquakes were also observed, most of them corresponding to aftershocks of the Hyogoken-Nanbu Earthquake. These events show different features reflecting the effect of local soil conditions.

In the present study, records obtained by this array observation system are used as empirical Green's functions for estimating long-period ground motions around the bridge construction site, induced by hypothetical huge earthquakes. Seismogenic sources along the Median Tectonic Line of southwest Japan, and the Nankaido Trough are assumed as sources of large earthquakes, for which, synthetic ground motion are obtained to verify the design spectra for the Akashi Kaikyo bridge. The empirical Green's function simulation technique and source mechanisms of several past large earthquakes are used to synthesize these long-period ground motions.

2. Observed Earthquake Ground Motion

During the observation period, a total of 156 earthquake ground motions were recorded by this array, almost half of them being aftershocks of the 1995 Hyogo-ken Nanbu Earthquake. The number of observed records varies among the station, since they were triggered independently one another. A great variety of earthquake ground motion signals have been recorded from near-field small earthquakes to far-field large earthquakes with magnitude larger than M 7.0 and hypocentral distance longer than 1500 km.

The far-field earthquake records present peak displacements less than 7 mm, and dominant periods ranging from 8 to 20 sec, similar to the fundamental vibration periods of the Akashi Kaikyo Bridge. Some of these earthquake records are shown in Fig. 2, which are used in this study as empirical Green's function to synthesize long-period ground motions.

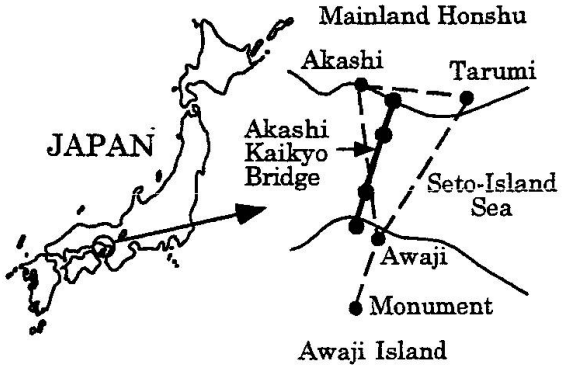

Fig. 1 Location of the Akashi Kaikyo Bridge along with location of the array observation system

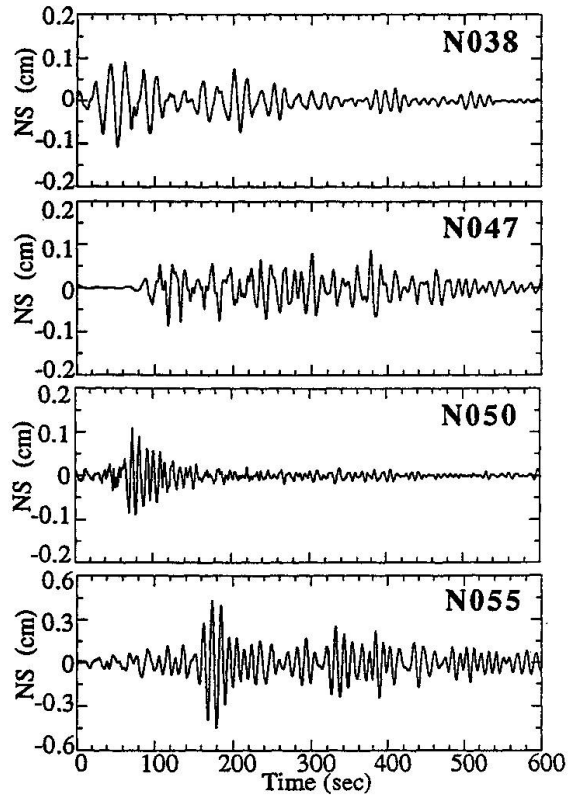

Fig. 2 Displacement time histories of events used as EGF, recorded at Akashi Station.

3. Synthetic Long-period Ground Motion Induced by a Huge Earthquake

The main concern of this study is to analyze the possible sources of huge earthquakes, that could generate long-period strong ground motion in the Akashi Kaikyo Bridge construction site. In this sense, two geological structures were identified, one being the Median Tectonic Line of southwest Japan (hereafter MTL), and another the Nankaido Trough, both of them south from the site of interest. Thus, hypothetical huge earthquake are assumed to be generated by these two seismogenic sources and, using the empirical Green's function method, synthetic ground motions are obtained at the array stations, which are compared with the design spectra for the bridge.

Simulation Method

The synthesizing procedure used in this study is the empirical Green's function method (hereafter EGF). The basis for this method is to estimate the ground motion due to a large earthquake as a sum of small-event records. The method proposed by Irikura (1986) is adopted here, in which the synthetic strong ground motion $U(t)$ is given by

$$U(t)=\sum_{i=1}^{N}\sum_{j=1}^{N}\left(\frac{r}{r_{ij}}\right)F\left(t-t_{ij}\right)*u_{ij}(t) \qquad (1)$$

where, $u_{ij}(t)$ is the small event used as EGF and r its hypocentral distance, r_{ij} the distance from the (i,j) sub-element to the observation site, i and j the specifying number of small event when the fault plane of the large earthquake is divided into NxN sub-elements, the notation * represents convolution. $F(t)$ and t_{ij} are defined as

EGF	Date	Mag.	Epicent. Dist.(km)	Depth (km)	Azimuth (°)
N038	92.07.30	7.0	932.0	0.0	237.9
N047	93.01.15	7.8	1132.0	120.0	225.8
N050	93.02.07	6.6	395.0	25.0	210.7
N055	93.07.12	7.8	964.8	27.0	202.5

Table 1 Parameters of the recorded signals used as Green's Functions

Fault Parameter	Fault 1	Fault 2
Length (km)	60.0	45.0
Width (km)	20.0	20.0
Strike (°)	263.0	257.3
Dip (°)	82.5	75.0
Slip (°)	180.0	180.0
Seismic moment	2.2×10^{27}	1.4×10^{27}

Table 2: Parameters of the two-fault-plane source mechanism along the MTL

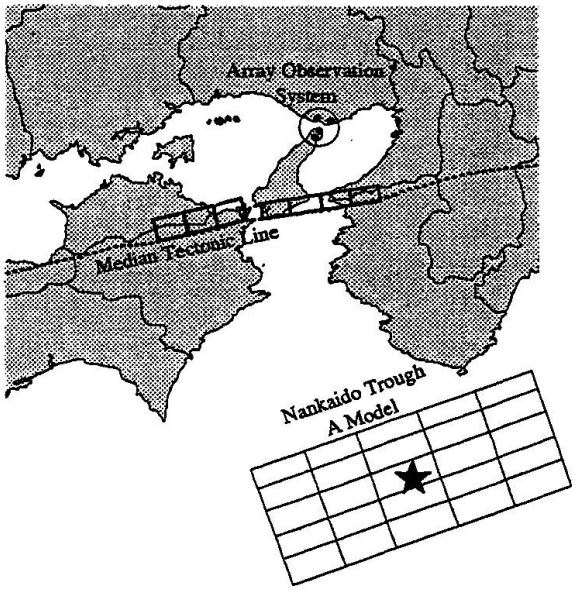

Fig. 3 Assumed two-fault-plane source mechanism on the MTL, along with the A model source mechanism on the Nankaido Trough.

$$F(t)=\delta(t)+\frac{1}{n'}\sum_{k=1}^{(N-1)n'}\delta\left[t-(k-1)\frac{\tau}{(N-1)n'}\right] \quad (2)$$

and

$$t_{ij}=\frac{r_{ij}-r_0}{V_S}+\frac{\xi_{ij}}{V_r} \quad (3)$$

where, r_o is the distance from the rupture starting point to the site, ξ_{ij} the distance from the rupture starting point to each sub-element *(i,j)*. V_s and V_r are the S wave and rupture propagation velocities, τ the target event's rise time, and n' an integer number to shift to a higher frequency range the spurious high frequency that appear due to regular duplication of the small event slip function. N is given by the ratio of seismic moments of the large and small earthquakes.

In order to include irregularities to the rupture-front propagation, to avoid spatial aliasing, the rupture propagation velocity V_r is changed randomly as follows:

$$t_{ij}=\frac{r_{ij}-r_0}{V_S}+\frac{\xi_{ij}}{V_r}+t_{rmd} \quad (4)$$

where t_{rmd} varies randomly from $-0.1\xi_{ij}/V_r$ to $0.2\xi_{ij}/V_r$ (Takeo and Kanamori, 1997).

Green's Functions

Simulation of long-period strong ground motions using EGF method requires that small events used as Green's function must have a good signal-to-noise ratio at long periods. Since most of the near-field earthquake records obtained by the Akashi Kaikyo array observation do not present this characteristic, we opted for using records of large far-field earthquakes, which inherently present long-period waveforms.

Four events recorded at Akashi station are used as Green's functions, namely: The M7.0 Sanriku Haruka Oki earthquake (N038), the M7.8 Kushiro Oki earthquake (N047), the M6.6 Notohanto Oki earthquake (N050), and the M7.8 Hokaido Nansei Oki earthquake. These events' parameters are listed in Table 1.

Fig. 2 shows the displacement time history of these four events recorded at Akashi station. These records were band-pass filtered in the range [0.05 - 0.5] Hz, which is the frequency range of interest for this study. Peak displacements ranging from 0.1 to about 0.5 cm are observed, and their dominant periods ranges from 8 to 20 sec.

Seismogenic Source on the Median Tectonic Line

After the 1995 Hyogo ken Nanbu Earthquake, the potential hazard that the MTL represents to the Akashi Kaikyo Bridge is investigated. Despite the recently high seismic activity observed along this geological structure, historical records for about 1000 years show that no destructive

earthquake have occurred directly related with it. However, studies on seismicity of the MTL state that earthquakes with magnitudes as large as M 8.0 could occur owing to faulting along its active segment (Shiono, K., 1980).

Since long-period (2 to 20 sec) ground motions generated by huge earthquakes are of primary concern, a magnitude M 8.0 earthquake is assumed to be generated by this geological structure in this study. Thus, after the MTL's segmentation given by Kanaori et al (1994), two fault planes with a total length of 105 km, extending from eastern Shikoku to western Kii Peninsula, are assumed as its source mechanism (Fig. 3). The seismic moment for the larger fault plane is assumed to be 2.24×10^{27} dyne-cm, and 1.4×10^{27} dyne-cm for the smaller one, which all together are equivalent to that of an intraplate M 8.0 earthquake. The parameters of this source mechanism are listed in Table 2.

To analyze the effects of S wave and rupture propagation velocities, and of rupture starting point location on the synthetic signals, two parametric analyses are done. In the first one, for a given position of the rupture starting point, four sets of S wave and rupture propagation velocities, varying from 2.5 to 4.0 km/sec and from 2.0 to 3.2 km/sec respectively, are analyzed. Waveform and response spectra of the synthetic signals show similar characteristics in all the cases, reflecting little influence by these parameters.

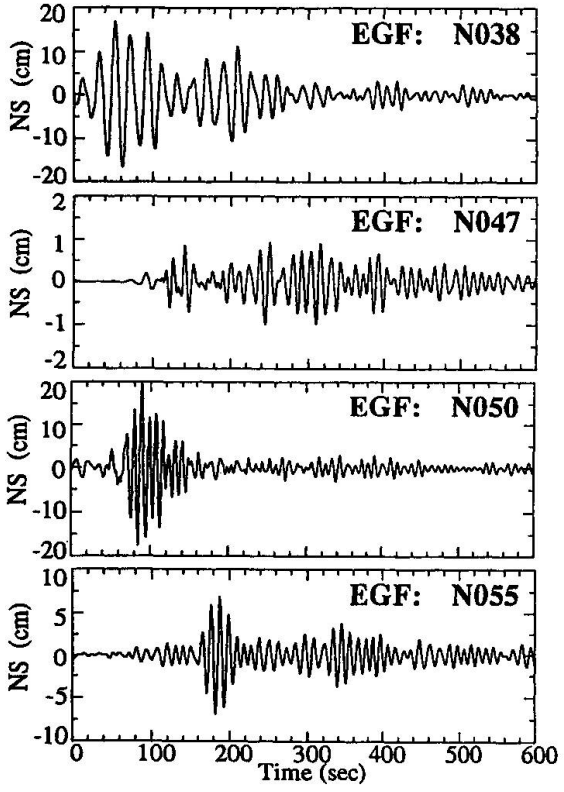

Fig. 4 Synthetic displacement time histories at Akashi Station induced by the MTL two fault plane source mechanism.

The second parametric analysis is done locating the rupture starting point in each sub-element of the fault planes. The S wave and rupture propagation velocities are fixed to 3.5 and 2.8 km/sec respectively. Waveforms and response spectra present larger amplitudes when the rupture starting point is located vertically at the middle part and horizontally near the common edge of the two fault planes. Synthetic displacement time histories that present the largest amplitudes are shown in Fig. 4 for each record used as Green's functions. In every case the waveforms of the synthetic signals are similar to their Green's function, and maximum displacement peak values of about 20 cm are observed. Fig. 5 shows the horizontal (NS) and the vertical (UD) component acceleration response spectra of these synthetic signals for 2% critical damping, compared with the design spectra for the Akashi Kaikyo bridge. The design spectra reasonably envelopes the synthetic ones.

Parameter	A Model	B Model	C Model	D Model
Length (km)	150.0	100.0	56.0	300.0
Width (km)	70.0	150.0	32.0	100.0
Strike (°)	250.0	246.0	207.0	250.0
Dip (°)	25.0	20.0	17.0	10.0
Slip(°)	116.6	128.0	90.0	116.6
Magnitude	8.2	8.0	7.5	8.2
Seismic Moment	1.5×10^{28}	2.8×10^{28}	1.5×10^{28}	1.5×10^{28}
Rise Time (sec)	9.3	11.2	3.9	9.3

Table 3 Fault parameters of source mechanisms assumed on the Nankaido Trough

Seismogenic Source on the Nankaido Trough

Another geological structure considered in this study is the Nankaido Trough, which can generate large earthquakes with magnitude as large as M 8.4 according to historical records. Huge earthquakes are assumed to be generated by this structure around the epicentral 1946 Nankaido Earthquake, for which,

four single fault plane source mechanisms of past large earthquakes are analyzed. A-Model is the M 8.0 Nankaido earthquake's source mechanism, B-Model is the M 8.2 Tokachi Oki earthquake's one, C-Model is that of the M 7.5 Hyuga-Nada earthquake, and D-Model is a modified (M 8.2)area of the source mechanism of the Nankaido earthquake. Table 3 lists the fault parameters of each model, and Fig. 3 shows the location of A-Model source mechanism.

A parametric study to analyze the influence of the rupture starting point location on the synthetic signals is done for the four source mechanisms. As could be expected, the large size of the fault planes and the different wave incidence angles render the synthetic sensitive to this parameter. Maximum peak displacement values of about 50 cm are obtained for B and C models, for the case in which the event N038 is used as Green's function (Fig. 6). As can be observed in Fig. 6, the waveform of the synthetic signals are similar to that of the observed one (Fig. 2), showing that the source mechanism has little effect on the signal's waveform.

Fig. 7 shows the acceleration response spectra of the synthetic signals obtained for the four records used as Green's functions, using B Model as source mechanism. The upper part of this figure shows the response spectra of NS component, and the vertical one is shown at the bottom. In this case also the design spectra for the bridge envelopes the synthetic ones quite well, especially those for the horizontal components.

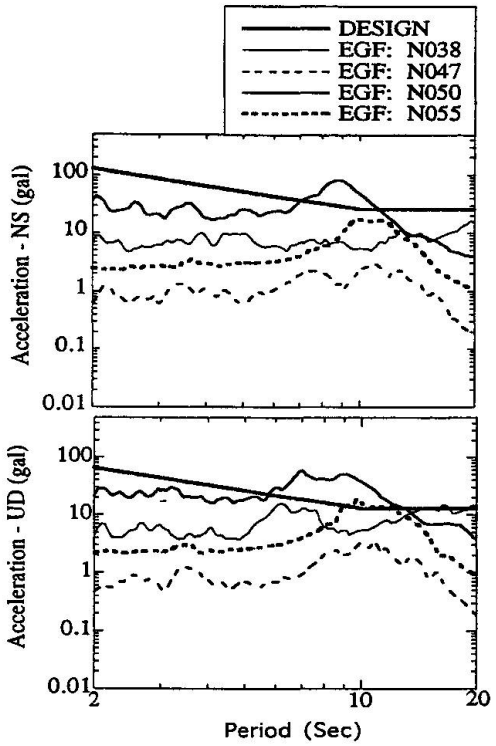

Fig. 5 Comparison of the acceleration response spectra of synthetic signals induced by the MTL (h=2%) with the design spectra for the Akashi Kaikyo Bridge. Components NS (top), and UD (bottom)

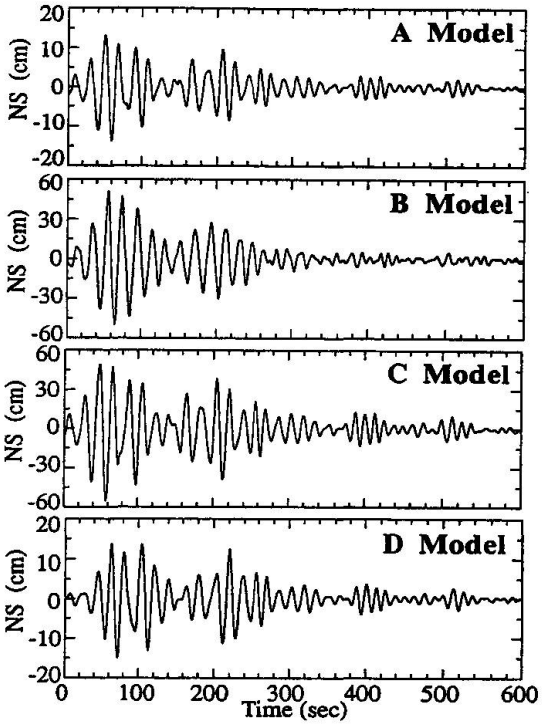

Fig. 6 Synthetic displacement time histories at Akashi Station induced by the Nankaido Trough. Event N038 is used as Green's function for each source model.

4. Discussion of Results

The results found in this study show that a hypothetical M 8.0 earthquake, that could occur on the Median Tectonic Line, would generate long-period ground motion with maximum peak displacement values of about 20 cm at the Akashi Kaikyo Bridge construction site. Synthetic acceleration response spectra obtained in this analysis show amplitudes lower or equal to the design spectra for the bridge. In this case, only when the Notohanto Oki Earthquake (N050) is

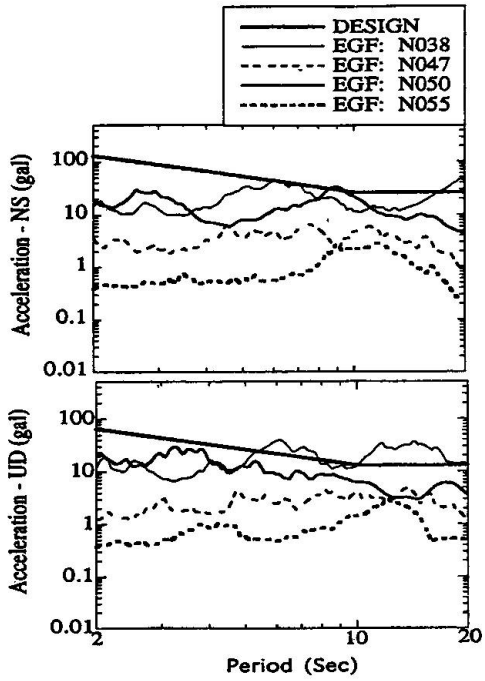

Fig. 7 Acceleration response spectra of synthetic signals induced by B model on the Nankaido Trough (h=2%) compared with the design spectra for the Akashi Kaikyo Bridge. Components NS (top), and UD (bottom)

used as Green's function, the synthetic response spectra becomes larger than the design spectra at periods around 9 sec. Therefore, considering that the design spectra was calculated for a 150 years return period, and the low probability of the occurrence of a M 8.0 earthquake along the MTL (about 1000 years return period), it can be concluded that the hazard this tectonic structure represents to the bridge is acceptably included in its design spectra.

On the other hand, the synthetic signals obtained at the bridge construction site, assuming a magnitude M 8.2 earthquake on the Nankaido Trough, present larger displacement amplitudes, with peak values of about 50 cm. However, most of their acceleration response spectra are enveloped by the design spectra for the bridge. In this case, only the response spectra of the signal obtained using event N038 as Green's function are larger than the design spectra, especially in its vertical component for periods longer than 10 sec. Therefore, for the worst earthquake case scenario the bridge's vertical vibration mode is the most critical one.

5. Conclusions

1. Earthquake records obtained at the Akashi Kaikyo Array Observation System are used to synthesize long-period strong ground motions around the bridge construction site. Huge earthquakes are assumed to be generated by two of the most hazardous geological structure in this area, namely, the Median Tectonic Line and the Nankaido Trough.

2. Synthetic ground motions generated by an assumed M8.0 earthquake in the MTL present peak displacements of about 20 cm; however their response spectra are reasonably enveloped by the design spectra for the Akashi Kaikyo Bridge.

3. Hypothetical huge earthquakes in the Nankaido Trough generate long-period ground motions whose peak displacement are about 50 cm in the bridge construction site. Most of the synthetic response spectra present lower or equal amplitudes than the design spectra for the bridge; however, for the worst earthquake case scenario the bridge's vertical vibration mode becomes the most critical one.

References

- Iemura, H., K. Izuno, M. Yasuda, S. Nakanishi, & T. Shiromoto, (1994). "Array Observation of Long-Period Earthquake Ground Motion for the Aseismic Design of Akashi Kaikyo Bridge". Proc. of the 9th Japan Earthquake Engineering Symposium, pp. E049-E054.
- Irikura, K. (1986). "Prediction of Strong Ground Motions using Empirical Green's Function". Proc. of the 7th Japan Earthquake Engineering Symposium, pp. 151-156.
- Kanaori, Y., S. Kawakami, & K. Yairi, (1994). "Seismotectonics of the Median Tectonic Line in Southwest Japan: Implications for Coupling among Major Fault Systems". Pure and Applied Geoph.,V-142, pp. 589-607
- Shiono, K., (1980). "Seimological Study on the Median Tectonic Line of Southwest Japan". Memoirs of the Geological Society of Japan, No. 18, pp. 155-174.
- Takeo, M., & H. Kanamori, (1997) "Simulation of Long-Period Ground Motion Near a Large Earthquake", BSSA, 87, pp. 140-156.

Earthquake Protective Design for Super-Long-Span Bridges

Koichi YOKOYAMA
Dir., Earthquake Disaster Prevention
Ministry of Construction
Tsukuba City, Japan

Keiichi TAMURA
Head, Ground Vibration Div.
Ministry of Construction
Tsukuba City, Japan

Shigeki UNJOH
Head, Earthquake Eng. Div.
Ministry of Construction
Tsukuba City, Japan

Toshimi MORITANI
Mgr, Third Design Div.
Honshu-Shikoku Bridge Authority
Kobe City, Japan

Summary

Japan is one of the most seismically disastrous countries in the world and has often suffered significant damage from large earthquakes. Therefore, the effect of earthquakes is one of the most critical issues in the design of civil infrastructures. We have studied the feasibility of a super-long-span suspension bridge with a center span length over 2,000m that is to be constructed on the fault zone which may cause large earthquakes with Magnitude 8. This paper presents the research and development on the earthquake protective design and technology for the super-long-span bridge, including seismic design ground motions, innovative seismic design methods for foundations and earthquake response control technology for superstructures.

1. Introduction

The tower-pier foundations and anchorage foundations of a super-long-span suspension bridge with a center span length over 2,000m becomes extreme large and heavy rigid foundations to support the weight of long-span superstructures. When the foundations are subjected to strong ground motions during large earthquakes, the inertia force of the foundation itself is the most critical for the stability of the foundations. It is important to decrease the mass and then the inertia force to improve the seismic performance of the foundations and to develop the stability evaluation methods for the foundations considering the nonlinear effect of surrounding soils. To solve these subjects, research and development on new types of foundation as well as the seismic design methods against large earthquake has been conducted [1].

On the other hand, since superstructures with longer spans over 2,000m becomes relatively flexible and have smaller damping characteristics, therefore, the vibration of the superstructures such as towers and stiffening girders is easily developed by external excitations such as wind and earthquakes. In the design of the superstructures, the effect of wind is generally the most critical design conditions. However, when the bridge with low damping characteristics is subjected to extremely strong earthquakes, the effect of earthquakes also becomes a critical issue to determine the member design. To improve the safety of superstructures against earthquake ground motions, one solution is an application of earthquake protective systems such as installation of damping augmentation devices.

To protect the super-long-span bridges from earthquakes and to achieve economical and practical design, the new design concept is being introduced in the seismic design methods for the super-long-span bridges. Two stage design concept considering moderate earthquake ground motion with high provability to occur and extreme earthquake ground motion with low probability to occur. Against such two types of earthquake ground motions, the acceptable design limit state of the bridge is being studied and proposed.

This paper presents the earthquake protective design and technology for the super-long-span bridges, including seismic design ground motions, innovative design methods for foundations and earthquake response control technology for superstructures.

2. Seismic Design Ground Motions

2.1 Basic Concept of Seismic Design Ground Motions

In Japan we have threat of destructive ground motions caused by both inter-plate earthquakes in the ocean such as the 1923 Kanto Earthquake and inland intra-plate earthquakes such as the 1995 Kobe Earthquake. These earthquakes are very rare to occur, however ground motions generated by them are extremely strong. In addition to these earthquakes, we also have many earthquakes which occur more frequently. Considering the occurrence ratio and influence of various earthquakes, it is rational to classify ground motions into two groups for seismic design of structures as follows:

(1) L1 Ground Motion
L1 Ground Motions represent those generated by earthquakes which have relatively high probability to occur during design life time of structure. This ground motion may be determined as ground motion with return period of 150 years. A bridges shall be designed so that it is not damaged against this ground motion.

(2) L2 Ground Motion
L2 Ground Motions correspond to those generated by earthquakes which unlikely to strike a structure during its life time. Ground motions due to huge inter-plate earthquakes which have their hypocenters in the ocean and earthquakes by inland faults should be incorporated into L2 Ground Motions. A bridge shall be designed so that it is not fatally damaged when this ground motion strikes.

2.2 Establishment of Seismic Design Motions

(1) L1 Ground Motion
This ground motion can be determined by risk analysis [2]. The relationship between earthquake magnitude and occurrence ratio, e.g., Gutenberg-Richter equation, and the attenuation equation of ground motions may be incorporated into this analysis. The deviation associated with attenuation equation and so forth should be carefully considered in this process.

(2) L2 Ground Motion
In case of developing L2 Ground Motion, it is necessary to consider the spread of fault plane and location of fault, because near field ground motions should be incorporated into this seismic design ground motion. As an example, fault plane models proposed for the 1923 Kanto Earthquake are illustrated in **Fig.1**. The following methods are employed to establish L2 ground motion. Note that each method has its own characteristics and obtained result should be compared each other when a seismic design ground motion is proposed.

Attenuation Equation
Estimate the peak ground motion and response spectra from earthquake magnitude and distance from epicenter or fault by attenuation equations. This method has been widely used in engineering practice. Note that the near field ground motion data are usually limited and this equation gives average ground motion, therefore suitable correction for near filed and the deviation from inferred result should be considered.

Fault Rupture Process Model
Divide a fault into subfaults, simulate the rupture process and generate a ground motion.

Vigorous studies have been made in this area mainly from a viewpoint to reproduce ground motions of past events [3-5]. This method requires various information about a fault and its rupture, however, note that available information is generally limited and the estimated result strongly depends on assumed conditions.

Recorded Strong Ground Motion

Use ground motions recorded at near field of large earthquakes as design ground motions. Ground motions reflect various conditions including earthquake magnitude, distance from fault and ground condition, and these conditions should be carefully considered when they are employed as seismic design ground motions. With deployment of strong motion monitoring networks, near field ground motions have been accumulated, and these ground motions can be effectively used with results inferred by other methods.

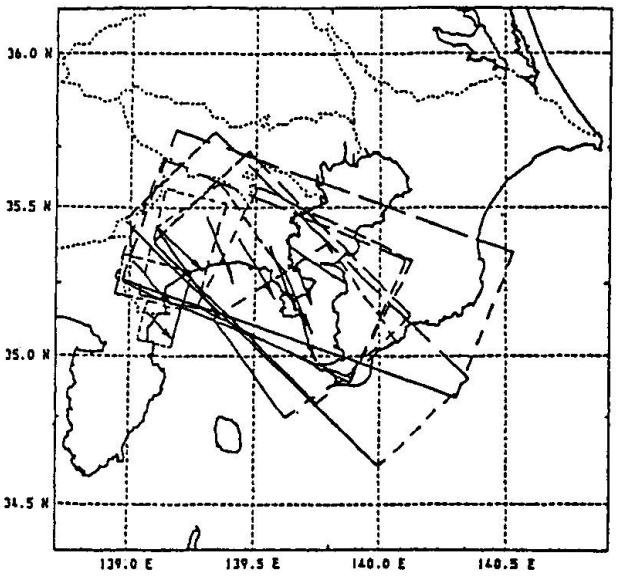

Fig.1 Fault Plane Models Proposed for 1923 Kanto Earthquake

3. Seismic Design Methods for Foundations

3.1 Design Methods against L1 Ground Motion

Fig.2 shows an analytical idealization of a rigid foundation using a two-degree-of-freedom model. The earthquake response against Ll Ground Motion is analyzed by the response spectrum analysis method considering the effects of soil-foundation-interaction and the strain dependence of soil stiffness. Acceleration response spectrum for the seismic design is given for each foundation obtained based on the fundamental acceleration spectrum which was given as L1 Ground Motion in the preceding section and the ground condition. To determine the design acceleration response spectrum, the effect of soil-foundation-interaction is included in the effective earthquake ground motion.

Analytical model of the rigid foundation is two-degree-of-freedom system with a horizontal mass consisted of the weight of foundation itself and additional mass including dynamic water pressure, and rotational inertia mass. Soil stiffness is obtained based on the soil-foundation-interaction. Dynamic soil stiffness is a reaction force to develop unit displacement to the foundation. The complex soil stiffness, which gives soil stiffness by a real part and damping by an imaginary part, is used in the analysis. Complex soil stiffness is given as Eq.(1) which is depending on a frequency.

$$K(\omega) = k(\omega) + i\,\omega\, c(\omega) \quad (1)$$

where, $K(\omega)$: dynamic soil stiffness, $k(\omega)$: spring function, $c(\omega)$: damping function, ω : circular frequency, and i : imaginary number.

Complex soil stiffness, K*, considering material damping, D, is approximately given by Eq.(2).

$$K^* = k(a_0) + i\,\{a_0 c(a_0) + 2\,Dk(a_0)\} \quad (2)$$

where, $a_0 = \omega\, a/\, Vs$, a : diameter of foundation, and Vs : shear velocity of soil.

Separation between the ground and the bottom of the foundation is considered by the Eq.(3). **Fig.3** shows the relation between the moment and rotation angle of the foundation. The energy equal concept is used to estimate the nonlinear response of the foundation.

$$\left.\begin{aligned} &\theta_N = \theta_L \quad (M_L/M_0<1.5)\\ &\theta_L/\theta_0 = \{6(\theta_N/\theta_0) - 40/3(\theta_N/\theta_0)^{3/10} + 25/3)\}^{1/2} \quad (M_L/M_0 \geqq 1.5)\\ &\theta_0 = M_0/k_R \end{aligned}\right\} \quad (3)$$

where, θ_N : nonlinear rotation angle of foundation, θ_L : rotation angle obtained from linear analysis, M_N : moment at the bottom of foundation considering separation between foundation and ground, M_L : moment obtained from linear analysis, M_0 : moment when separation between foundation and ground is initiated, and k_R : rotation stiffness.

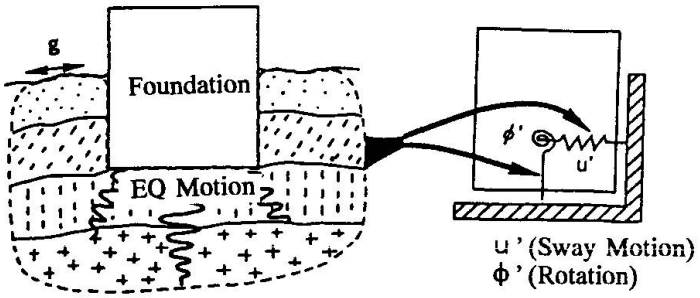

Fig.2 Analytical Idealization of Rigid Foundations

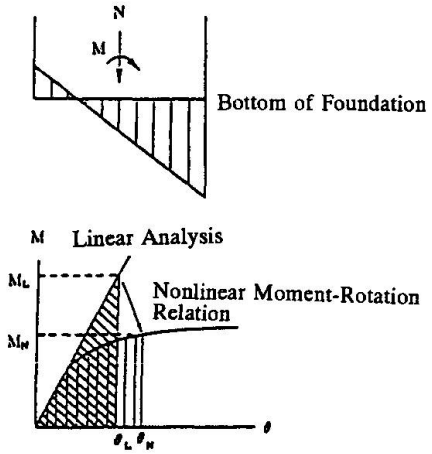

Fig.3 Evaluation of Nonlinear Response of Foundation considering the Separation between Foundation and Ground

Strain dependence of the soil stiffness is also considered in the design. The shear strain is obtained based on the horizontal response displacement and rotation angle of the foundation.

$$\gamma = \alpha \cdot \theta + \beta \cdot u_B/B \quad (4)$$

where, γ : shear strain, u_B and θ : response displacement and rotation angle of foundation, B : width of foundation, and α, β : coefficients. In the response analysis, the shear strain is given based on the relation between the shear strain and shear stiffness, G, or material damping, D, obtained by the material tests. The iteration analysis is made to achieve enough convergence of the shear strain.

The stability of the foundations is checked by :

1) Foundations should be supported by the stable stiff ground. Safety on bearing capacity and sliding capacity of ground should be checked and the displacement developed at the foundations should be within an acceptable limit so that the displacement of the foundations does not affect the superstructures.
2) Vertical soil reaction at the bottom of foundations should be within an acceptable limit of vertical bearing capacity.
3) Horizontal force at the bottom of foundation should be within an acceptable shear strength.

3.2 Design Methods against L2 Ground Motion

The check of the stability of the foundations against L2 Ground Motion is made by the elasto-plastic finite element analysis methods (FEM). The soil-foundation system is idealized as two dimensional finite element model and the foundation is modeled as the rigid mass with the concentrated mass at the center of the foundation or the elastic body with the distributed mass. The boundary condition of the FEM model of the ground is assumed as a viscous boundary at the bottom and the both sides. The nonlinearity of the soil is modeled as the modified model of the Ramberg-Osgood model. Integration for the response analysis is made in the time domain to consider the separation between foundation and ground and the nonlinear stress-strain relation of the soil. Through the nonlinear response analyses, the strain distribution and the stability of the soil element considering the failure criteria and the residual displacement are obtained. The stability of the foundation is checked for the most critical condition as follows:

1) Vertical soil reaction at the bottom of foundations should be within an acceptable limit of vertical bearing capacity.
2) Horizontal force at the bottom of foundation should be within an acceptable shear strength.

Proposed design methods in the above is based on the in-situ tests on the dynamic characteristics of soils and the field loading tests using large soil specimens. The analysis methods was used to check the safety of the Akashi Strait Bridge against the Hyogo-ken Nanbu Earthquake of 1995 [6].

5. Earthquake Response Control for Superstructures

5.1 Effect of Earthquakes on Member Forces

In the design of the superstructures, the effect of wind is generally the most critical design conditions. However, when the bridge with low damping characteristics are subjected to extremely strong earthquakes, the effect of earthquakes also becomes a critical issue to determine the structural member.

The effect of earthquakes on the member forces is studied through the dynamic analysis of a long-span suspension bridge with a center span length of about 2,000m. The analytical model is made based on the Akashi Strait Bridge. The earthquake response is computed by the response spectrum analysis using a linear three dimensional beam-mass model. The member forces obtained through the analysis is compared with those against wind loads. The damping ratio is assumed as 0.005 and the L2 Ground Motion which was given for the trial analysis in our study is used [1]. Wind velocity is assumed as 46m/s as a fundamental design wind velocity based on the Wind Resistant Design Manual for Akashi Strait Bridge.

Computed member forces and displacement is shown in **Table 1**. In the longitudinal direction, displacement of the stiffening girder developed during earthquakes is almost the same or slightly greater than that against the wind load. The member forces developed at the bottom of tower and mid-height section of tower during earthquakes is about two to three times those developed by the wind load. Therefore, they can be decreased by applying the damping augmentation devices. The member forces developed at the stiffening girder and the cable during earthquakes is enough small comparing these developed against the dead load and live load.

5.2 Effect of Damping Augmentation Devices

In the analysis above mentioned, the damping ratio is assumed as 0.005. The damping ratio for predominant modes is increased by the damping augmentation devices and the effectiveness to decrease the member forces is analyzed. The increased damping ratio is assumed as 0.055 and **Table 1** shows the effectiveness to decrease the member forces and displacement. If the damping ratio is increased form 0.005 to 0.055, the response can be decreased up to about half. The damping augmentation devices are designed so that the damping ratio is increased from 0.005 to 0.055. The damping coefficient is assumed as about 29,400kN·s/m and **Fig.4** shows the design examples of the devices using elasto-plastic effect of lead.

5. Conclusions

This paper presents the earthquake protective design and technology for the super-long-span bridges, including seismic design ground motions, innovative seismic design methods for foundations and earthquake response control technology for superstructures. These are our on-going study and the further study is being made including the development on evaluation methods of earthquake ground motions based on the active fault model, the feasibility of reinforced concrete tower against strong earthquake ground motions.

Table 1 Comparison of Member Forces between Earthquake and Wind Loads and the Effectivenss of Damping Augmentation Devices

	Location	Wind Load	Earthquake Load without Damper (A)	Earthquake Load with Damper (B) (B/A)
Displacement of Stiffening Girder	Side Span (Anchorage)	2.16 m	2.03 m	1.20 m (B/A=0.56)
	Center of Center Span	1.00 m	0.88 m	0.60 m (B/A=0.60)
Bending Moment of Tower	Bottom	1.89×10^{6} kN•m	1.03×10^{6} kN•m	1.23×10^{6} kN•m (B/A=0.65)
	Mid-Height	7.25×10^{5} kN•m	2.40×10^{5} kN•m	not Analyzed

Acknowledgements

This study has been conducted under the guidance of the Investigation Committee on Strait Crossing Highway Projects in Japan (Chairman : Iwao YOSHIDA, President of Honshu-Shikoku Bridge Engineering Co. Ltd.). We sincerely thank Dr. Yoshida and all of the committee members for their encouraging guidance.

References

[1] Public Works Research Institute : Report of the Investigation Committee on Strait Crossing Highway Projects in Japan, Technical Memorandum of PWRI, No.3479, March 1986 (in Japanese)

[2] Arakawa, T. et al. : Determination of Input Ground Motions for Dynamic Analysis Based on Probabilistic Methods, Technical Memorandum of PWRI, No.1992, 1983 (in Japanese)

[3] Hartzell, S. H. : Earthquake Aftershocks as Green's Function, Geophysical Research Letters, Vol.5, No.1, 1978

[4] Irikura, K. : Semi-Empirical Estimation of Strong Ground Motions during Large Earthquakes, Bulletin of Disaster Prevention Research Institute, Kyoto University, Vol.33, Part 2, No.298, 1983

[5] Midorikawa, S. and Kobayashi H., A : Semi-Empirical Method for Estimating Response Spectra of Near-Filed Ground Motions with Regard to Fault Rupture, Proc. of Seventh European Conference on Earthquake Engineering, 1982

[6] Honshu-shikoku Bridge Authority : Report of Committee on Seismic Design and Foundation Design, March 1997 (in Japanese)

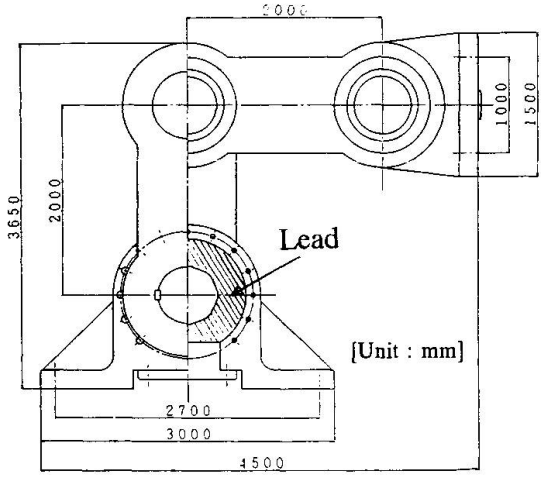

(a) Rotational Lead Extrusion Damper

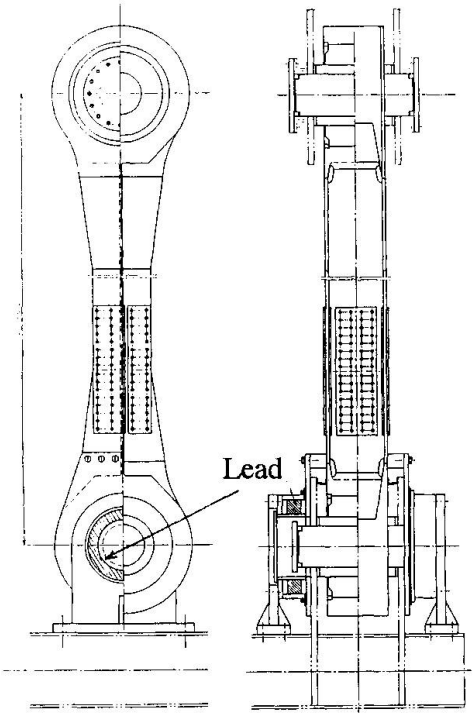

(2) Tower Link Rotational Lead Damper

Fig.4 Design Examples of Damping Augmentation Devices at Tower and Pier Connection

Noise and Vibration Induced by Train: The Case of the Messina Bridge

Giorgio DIANA
Professor
Politecnico di Milano
Milano, Italy

Federico CHELI
Professor
Politecnico di Milano
Milano, Italy

Francesco NATONI
Head Eng.
Italferr
Rome, Italy

Stefano BRUNI
Researcher
Politecnico di Milano
Milano, Italy

Andrea COLLINA
Researcher
Politecnico di Milano
Milano, Italy

Giuseppe TRAINI
Head Eng.
Italferr
Rome, Italy

Summary

The paper reports the main results of researches aimed at designing the railway box and the superstructure of the 3300m span bridge proposed for the crossing of Messina straight.
To this end, besides experimental experiences described in previous work, a mathematical model of train-track-structure interaction has been used to evaluate the performances of the alternative solutions proposed. In particular, to kinds of track are considered, a traditional direct fastening one and a slab track; the latter shows considerably better performances in terms of noise and vibration attenuations, making attractive its adoption, despite its greater weight.
The paper also points out the role in the design activities of a mathematical model of train-track interaction, in order to assess the efficiency of the different alternatives considered.

1. Introduction

Railway box girders of long span suspension bridges are relatively light and flexible structures, which can be subjected to high dynamic effects induced by the passage of the trains. These effects must be carefully analysed in order to verify that no structural damage will be caused by repeated train passages and that the generation of noise and vibrations is kept under control. Moreover, the structure must satisfy restrictive requirements regarding global and local deformations under train passage, in order to ensure the safety of ride of the train and passengers' comfort.
An overview of railway runnability problems is given in [1], where an important distinction is established between global train-structure interaction, involving deformations of the whole structure, and local interaction, due to components of deformation of the deck with wavelengths equal to the longitudinal separation of the hangers. Other local effects are related with deformations of the upper side of the deck, having wavelengths of the same order of magnitude of the sleeper bay (distance between two consecutive sleepers).
The present paper focuses on the problems of local interaction, which is particularly critical for box girder decks, due to the presence of local resonances of the upper plate of the deck which can be excited by the passage of the trains. In this regard, the design of the superstructure, that is a set of devices (generally including sleepers, rubber pads, fastenings) connecting the rails to the deck, is of paramount importance, as this component performs as a low-pass filter in the transmission of forces and vibrations from the wheelsets to the structure.
Within the design activities regarding the Messina bridge project, extensive experimental and theoretical researches were carried out , with the aim of defining a suitable typology of superstructure to be employed for the definitive setup of the bridge. As a first step of the work, several tests on a full-scale section of the railway box girder of the bridge were performed: different typologies of superstructure were tested, including direct fastening systems and slab track. The measure of the transfer function between a vertical force applied to the rail and the acceleration of the upper plate of the railway allowed the evaluation of the filtering effect

introduced by the different when connected to the railway box [2]. Moreover, the results of numerical simulations allowed to evaluate the dynamic forces transmitted to the deck [3]. Recently, an improved version of slab track was proposed, on the basis of field experiences acquired for metro and urban railway lines, which were carried in 1996 [4]. The problem of optimising the design of the superstructure is therefore still open, and the present work aims at contributing to this matter by comparing traditional and innovative solutions, the target being to ensure low levels of structural noise, good dynamic performances of the vehicle, low weights and low maintenance costs.
To this end, the passage of the train on the deck has been simulated by means of mathematical model of train-track-structure interaction developed at the Department of Mechanical Engineering of Politecnico di Milano and implemented in a computer code called A.D.Tre.S. [5].

2. Key factors affecting local train-structure interaction

As discussed above, the local interaction is mainly governed by the structural properties of the superstructure. Nevertheless, for box girder bridges, also the design of the deck assumes great importance: in fact its local deformations must be kept as small as possible, and the excitation of local resonances of the upper plate by the forces transmitted by the superstructure should be kept as small as possible.
Therefore, different strategies have been considered in order to increase the local stiffness of the upper side of the railway deck: figure 1 shows a section of the railway box, where longitudinal ribs are recognisable, moreover, diaphragms have been inserted each 2.65 meters along the deck in order to connect the upper and lower sides of the box.

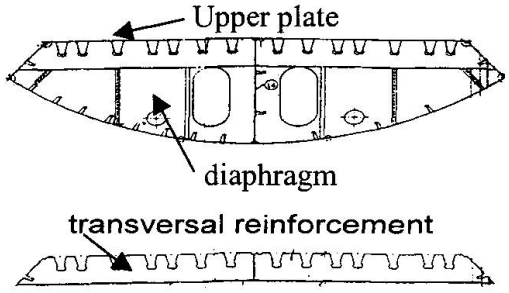

Fig. 1 Section of the railway deck and transversal reinforcement

Finally, the use of two supplementary reinforcements per each 2.65 m sub-span of the deck has been considered as a way to further reduce local deformations. A first question this paper is concerned with is whether or not the use of these reinforcements is necessary.
The second problem addressed in the paper, which is strictly related to the first, is what kind of superstructure can reach the best performances in reducing the effects of local interaction between the train and the deck. To this end two kinds of superstructure have been compared, a direct fastening track (D.F.T.) and a slab track (S. T.), where a concrete slab acts as a foundation elastically suspending the rail from the deck.
The direct fastening system is shown in figure 2: the rails are connected to separate steel plates, fastened by means of bolts to the upper plate of the deck. This kind of track is widely adopted, especially for subway lines, its main advantages are low maintenance costs and low weight while, from the point of view of its dynamic properties, a fundamental role is played by the rubber pad interposed between the deck and the steel plates: previous experiences showed that low values of the stiffness of this pad improve the performances of the superstructure in terms of isolation of vibrations but, conversely, an excessively low stiffness makes difficult to control the geometry of the track, causing problems to vehicles' safety of ride.
The improved version of the slab track considered in the project is shown in figure 3: the rails are fastened to steel plates connected through rubber pads to a concrete floating slab. The slab is then laid on a continuous layer of resilient material, in order to create an elastic foundation insulating the deck from the rails.
For each of the two solutions, an optimization of stiffness and damping parameters has been performed based on the knowledge acquired in previous experiences on both prototypes for the Messina bridge and in-line applications for high speed and underground railways, so that the two

solutions which will be compared can be considered as optimised versions of the two kinds of superstructure. Slab track is expected to show a better behaviour than direct fastening track [6], but a quantitative evaluation of the advantages of this solution are mandatory in order to judge if they can justify the important increase in the weight of the structure introduced by this solution.

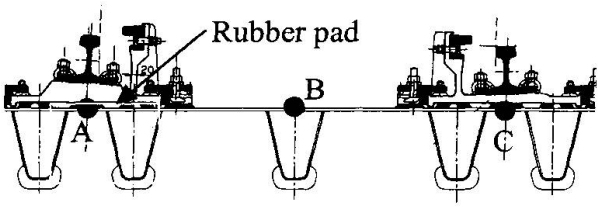

Fig. 2 Direct fastening track

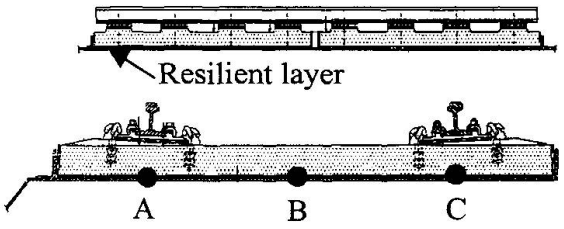

Fig. 3 Slab track

3. Track and structure modelling

The deck and the superstructure are modelled by means of a three-dimensional finite element scheme; since the attention is focused on the local track-structure interaction, only the upper plate of the railway box girder is modelled. To this end, plate elements are used, while the diaphragms are introduced in the model as rigid supports constraining the vertical motion of the plate. The presence of the reinforcing ribs is kept into account by considering an appropriate equivalent thickness for the plate elements, the value of this parameter has been adjusted on the basis of a more sophisticated f.e.m. model of the railway box girder. Upper-plate reinforcements have been also included in the model as beam elements, in order to evaluate their efficiency in reducing the local deformability of the deck and improve upper plate dynamic response.
As far as the scheme of the track and superstructure is concerned, the rails are modelled by means of Euler-Bernoulli beam elements, while the fastening devices and rubber pads are reproduced by means of concentrated or distributed stiffness and damping elements. Finally, the slab carrying the rails in the slab track is modelled by four nodes plate elements.
The stiffness and damping values of the rubber elements are reported in Tables I and II. It is worth mentioning that for rubber elements those parameters are frequency dependent [7]: the values adopted in the finite element model refer to the frequency of the first vertical resonance of the track coupled to the wheelset.

	Rail fasteners	Rubber pads under the steel plate	Rubber layer under the slab
Direct fastening	200	27	---
Slab Track	200	27	4.04

Table I Stiffness values of the fastenings [MN/m]

	Rail fasteners	Rubber pads under the steel plate	Rubber layer under the slab
Direct fastening	15	3.5	---
Slab Track	15	3.5	2.08

Table II Damping values of the fastenings [kNs/m]

4. Simulation of train passage

Simulations of train-track-structure interaction were performed by means of the package ADTRES [5], developed in co-operation between the Department of Mechanical Engineering of Politecnico di Milano, and Italferr, which is part of the Italian Railway Authority. This model is thoroughly described in previous pubblications from the same authors [2], [5].
The conditions of simulation are as follows: an ETR500 train (Italian high speed train) running on the deck at the design speed of 130km/h; the presence of track and wheel thread irregularities

has been considered. To this end, the spatial distribution of track irregularity was generated according to ORE low level standards [9], while for wheel threads reasonable levels of irregularity were estimated from previous work [4].
A first result, shown in figure 4, regards the vertical component of the contact force between the left wheel of the leading wheelset of a passenger car and the rail. The time history of the signals is shown in the lower side of the figures, while spectra are represented in the upper side.
The dynamic component of contact forces is produced by the interaction between the track and the vehicle, where track irregularity plays an important role. As far as the behaviour of the structure is concerned, a high dynamic component of the contact force will produce important vibrations of the track, which will be partially transmitted to the deck producing noise, vibrations and dynamic over-stresses. From the vehicle's point of view, high variations of contact forces affect the safety of ride and cause vibrations in the wheelsets and in the bogies.

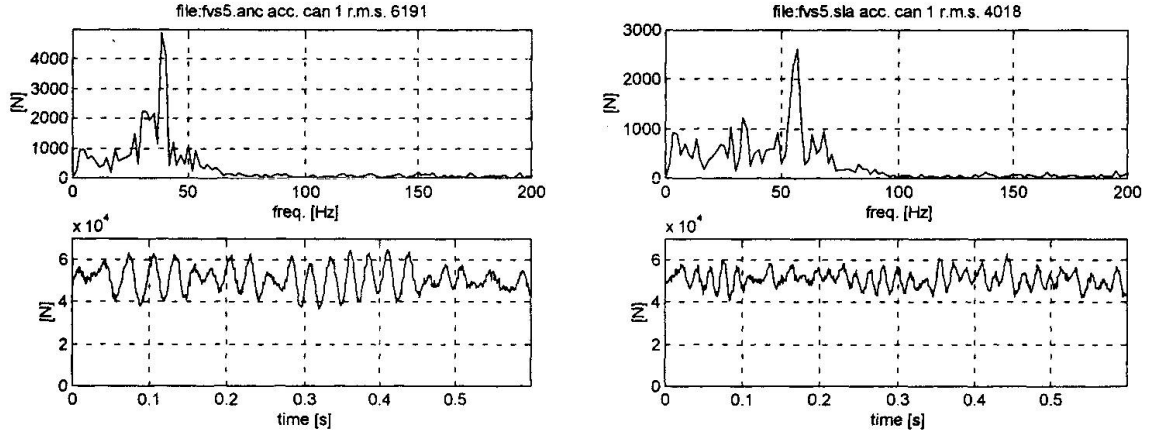

Fig. 4 Vertical contact force between left wheel of the leading axle of a passenger car and the rails (left direct fastening track, right slab track)

Both results show a prevailing frequency in the dynamic component of contact force (around 40Hz for D.F.T. and 60Hz for S.T.): this frequency corresponds for each kind of track to the first resonance of the wheelset coupled to the track. Slab track shows a lower level of amplitude of the dynamic component, as indicated also by the r.m.s. values.
The behaviour of the structure is affected not only by the dynamic forces between the wheels and the rails, but also by the filtering properties of the superstructure: in order to judge the vibratory behaviour of the deck Figure 5 shows the vertical accelerations of the deck under the inner rail (position "C" in figure 2); more precisely, the results obtained for D.F.T. without reinforcements are shown at left side, while those for S.T. without reinforcements are shown at right side.
These quantities are a measure of the transmitted vibrations, and are strictly related to the generation of structural noise in the deck.
The maximum level of vibration is one order of magnitude lower for the slab track, and the comparison of the two spectra shows that for frequencies above 60Hz slab track filters almost completely the vibrations coming from the rails. For the direct fastening track on the contrary, important contributions to the vibration of the deck are present at high frequencies: these components are expected to produce significant levels of noise.
The advantage introduced by slab track can be appreciated in figure 6, where the third octave band of the two signals are compared: in the frequency range above 100Hz the level of acceleration is two decades higher for D.F.T. (continuous line) than for S.T (dashed line).
More complete conclusions can be drawn from table III, where the r.m.s. values of the accelerations on the rails and in different locations on the deck are compared for the two kinds of track, considering or not the presence of reinforcements. While the accelerations at the rail reach similar values for the two superstructure solutions, the slab track produces much lower accelerations of the deck.
Moreover, as far as direct fastening is considered, the reinforcement can improve the vibrational behavior of the deck: in fact the levels of acceleration under the two rails are significantly reduced, while in point "B" are almost the same. On the contrary, for slab track the adoption of the reinforcements does not provide any significant improvement.

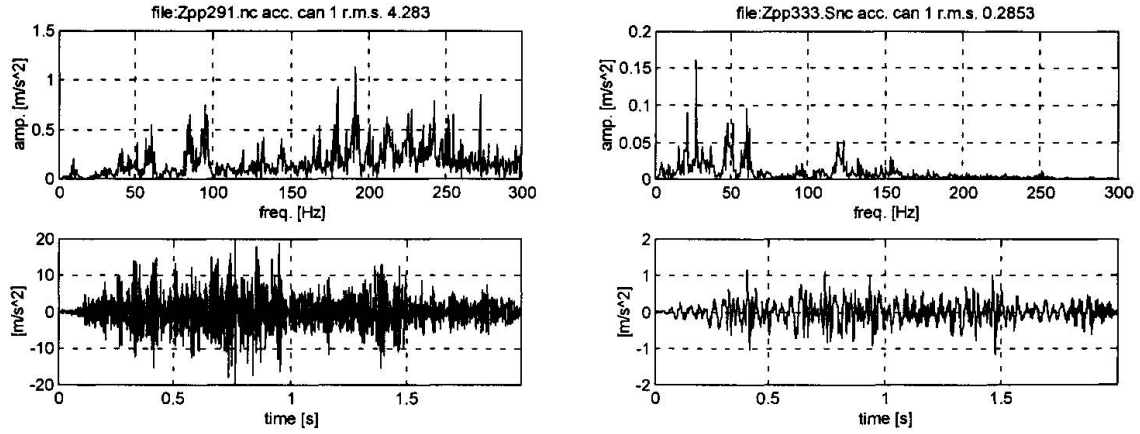

Fig. 5 Vertical acceleration of the upper side of the deck in point "C" (left direct fastening track, right slab track)

	Direct fastening No reinforcement	Direct fastening with reinforcement	Slab track No reinforcement	Slab track With reinforcement
Rail	8.88	9.43	8.43	8.44
Deck pos. A	4.65	2.31	0.21	0.14
Deck pos. B	3.90	3.69	0.24	0.27
Deck pos. C	4.20	3.29	0.28	0.26

Tab. III r.m.s. values of acceleration in different locations of the structure ([m/s^2])

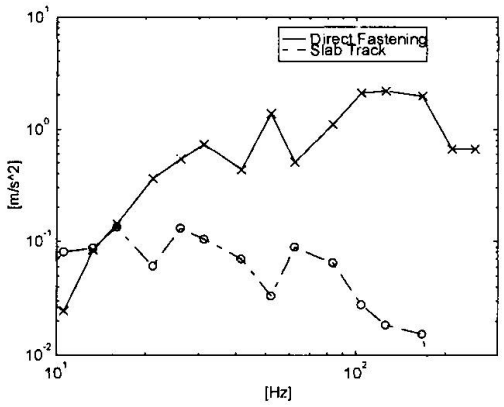

Fig. 6 Third octave band representation of vertical accelerations of the deck.

Besides the levels of vibration of the deck, it is important to evaluate the over-stresses induced in the deck by the passage of the train: in fact these quantities affect the fatigue resistance of the structure. As an example, Figure 7 shows for D.F.T. (left) the time history of the vertical force transmitted to the deck by a single rubber pad (continuous line) and the history of the same force when static train loads are applied (dashed line). The figure shows the passage of the front bogie of a passenger car (total weight 420kN approximately): a strong amplification (about 25%) of the first peak of force corresponds to the passage of the first wheelset.

Similar results are shown for slab track in the same figure (right), in this case the force transmitted by a portion of the elastic layer placed under the track has been reported. In order to make this result comparable to those for D.F.T., a portion with length equal to one sleeper has been considered. Figure 7 shows that the use of slab track can keep dynamic effects on the structure at very low levels.

A common way to represent the influence of dynamic effects on the stresses is to define suitable impact factor parameters as the ratio between the dynamic stress induced by the train and the corresponding value produced by the static application of train axle loads on the structure. These quantitites can be defined for different stress components and for different locations in the structure: Table IV reports the values of impact factors for the vertical force transmitted by the superstructure to the deck and for the stress in longitudinal direction in a point of the upper side of the deck placed under the inner rail.

The impact factors obtained with the slab track are very low (around 3%), while much higher values are obtained for D.F.T: in this latter case, a small reduction of the impact factors corresponds to the introduction of the reinforcements on the deck.

Figure 7 also shows that the static value of the force transmitted to the deck is lower for S.T. than for D.F.T.: this is due to the fact that the flexural stiffness of the slab allows the re-distribution of the axle loads on a wider portion of the deck than for D.F.T. All these circumstances show that the adoption of slab track can significantly improve the fatigue resistance of the deck.

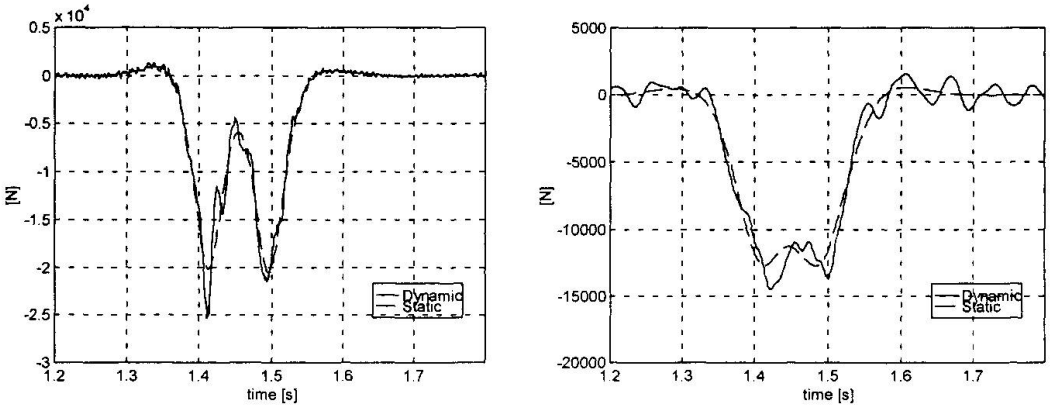

Fig. 7 Vertical force transmitted to the deck (left direct fastening track, right slab track)

	Direct fastening No reinforcement	Direct fastening with reinforcement	Slab track No reinforcement	Slab track With reinforcement
Vertical force on the deck	1.25	1.24	1.14	1.14
Longitudinal stress in the deck	1.14	1.12	1.03	1.03

Tab. IV Values of local impact factors

5. Concluding remarks

A comparison of two alternative superstructure typologies proposed for the railway box of Messina bridge has been presented. Direct fastening track is simple, light and economic, but even if its stiffness and damping values are correctly tuned, its performances with respect to the transmission of vibrations and noise cannot considered completely satisfactory. Slab track instead, though introducing a significant increase of weight (about 1 t/m), shows a very attractive dynamic behaviour, producing very low levels of vibration of the deck, low dynamic over-stresses, and good quality of ride of the vehicle.

References

[1] Diana G., Cheli F., Bruni S., Collina A., *Super long suspension bridges, railway runnability* 15th IABSE Congress, Copenhagen, Denmark, June 16-20 1996

[2] Diana G., Cheli F., Bruni S., Collina A., *Interaction between railroad superstructure and railway vehicles* 13th IAVSD Symp., Chengdu, P. R. China, August 23-27 1993

[3] Diana G., Cheli F., Bruni S., Collina A., *Train-track interaction: a comparison between a numerical model and full scale experiments*, IV to appear on Heavy haul transit, part of Int. Jour. Of Vehicle Design

[4] Diana G et al., *A.D.Tre.S., a software for railway runnability analysis* WCRR '97 Congr., Florence, Italy, 16-19 November 1997

[5] Eisenmann, J., *Vibration and structure borne sound by underground railways* Symp. on Vibro-acoustic and env. impact of underground railways, Bergamo, Italy, 2-3 June 1994

[6] Grassie S. L., *Resilient railpads: their dynamic behaviour in the laboratory and on track* Proc. Inst. Mech. Eng.rs, Part F, 1989, Vol. 203, 25-35

[7] ORE, Question B176, Utrecht, Belgium, July 1992.

Acknowledgements

This work received financial support from C.N.R., as part of P.F.T.2 researches.

New Conceptual Design for a Cable-Stayed Bridge in Poland

Grazyna LAGODA
Assist. Prof.
Warsaw Technical Univ.
Warsaw, Poland

Marek LAGODA
Assist. Prof.
Road & Bridge Res. Inst.
Warsaw, Poland

Tomasz WIERBICKI
Assistant
Road & Bridge Res. Inst.
Warsaw, Poland

Summary

The conceptual design of cable stayed bridge design was presented as a contribution to a competition for a new crossing over the Vistula river near Plock in Poland, Europe. The primary idea of the bridge was, that the main, stream span is laid over the Vistula river and it reaches 450 m. length. The bridge has just one pylon, and that is why the span belongs almost entirely to the (as far as the length span concerns) longest ones in the world. The original and unrepeatable view is given to the bridge by the "V" shaped pylon.

1. Brief foredesign

The new bridge crossing, which has been designed across the Vistula river is an element of the Plock town new orbital. The suggested segmentation of the crossing is an outcome of terrain configuration, hydrological and geological conditions analysis and it consists of three general components:

- left bank valley bridge at flooding area
- cable stayed stream section
- right bank valley bridge.

The river is not only a traffic obstacle, but also a technological one. Moreover, the Vistula is an obstacle that brings many troubles connected with supports placed in a midstream setting. Spring drifting of ice as well as frequent floods make Vistula river very difficult area for erecting and maintenance of midstream supports.
Avoiding many hydrological and geotechnical problems connected with that unstable river might be the compensation of slightly higher cost of cable stayed span as compared with traditional one. That is because at present possibilities of new materials and technologies applying, the difficulties of erecting cable-stayed and traditional spans are rather comparable.
Cable stayed bridges are always a sign of strong human activity outstanding in a country

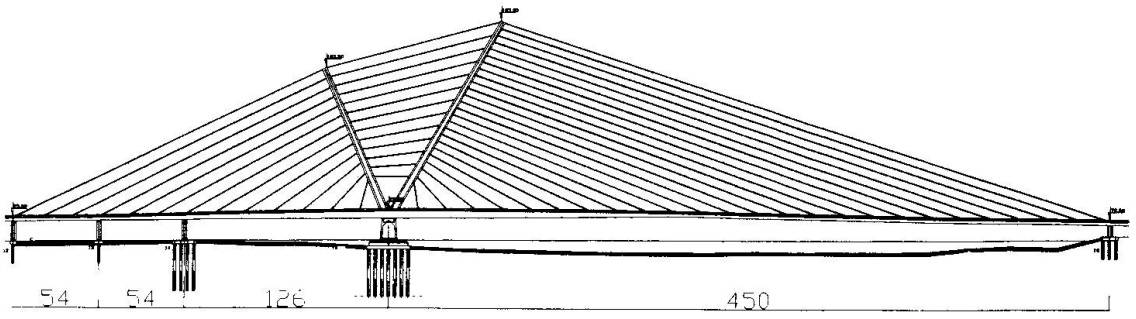

Fig 1. General view of midstream span.

landscape and an evidence of bravery and novelty of engineers' creativity. The bridges of all type, and the cable-stayed ones in particular, play a role of a symbol and of an architectural culture object. As a result of taking all above mentioned facts, the team of our bridge engineers had prepared, as a suggestion to the competition for the new bridge crossing across the Vistula river near Plock, the design of the bridge, which overlays the river with just one cable-stayed span. The aim of the team was to present the structure which differs from the other Vistula river bridges, as a more modern and esthetical appearance one.

2. Bridge structure description

The main part of the bridge (midstream one) consists of four spans 2x54+126+450 m and freely overlaps the river with one, 450 m long span, only. The pylon support is placed at left bank and is being flooded only during the high water levels. On the right side of the pylon, there is a span 450 m long, which overlays the water. The span is constructed as a orthotropic box girder beam made of 18G2A steel, with inconstant height from 5,0 m at pylon section to 2,5 m at the end of the span. On the left side of the pylon there are inundate cable stayed spans, which are concrete (B45) box girder structures. The pylon, placed centrally (in lateral crossing) is designed in a shape of two inclined steel (box section) poles. The split as well as the inclination of the pylon let to minimise its height, preserving big angle of shroud inclination, so the relevant big vertical forces acting on the bridge deck were obtained. Two arms of the pylon are fixed together with the additional ropes of similar to the shrouds structure, to balance the weight of the steel and concrete bridge spans. The concrete cable-stayed spans are placed on three supports (at flooding area) which are used as a shrouds anchorage in addition. Load-carrying structure is stayed with shrouds anchored in pylon and in the cantilevers placed at both sides of spans. This solution was accepted due to the torsional rigidity and as well as, to side wind acting. All shrouds are made of 75 H 15 ropes produced by PPC Freyssinet Company.
Every support was designed as a concrete one, made of B-30 concrete and founded on high diameter boring piles. Two different kinds of them were worked out. Due to big load of pylon support, which carries serious horizontal and vertical forces, and in addition great bending moment, it was founded on 180-cm diameter, 30-m long piles. In non-cohesive soils, which thickness of strata is about 5,0 m here, the piles bore-holes are made under the cover of steel tube, sunk in a clay roof with vibration casinghead. Further on drilling is executed with no cover tube, and the bore-hole is flooded with water, or, in case of water-bearing interbedding at high piezzometric pressure, with bentonite slurry. To increase the load capacity of about 20% - according to existing research- after embedding pile in concrete, the cement injection under the foot and at side surface of pile is performed. The remaining supports are designed as drilled in withdrawn steel 150-cm diameter tube holder with no cement injection.

3. Conclusion.

The analysis performed during the designing process proved that:

- the enlargement of span length causes elimination of midstream supports, which is connected with serious economical savings,
- the heavy concrete span structure placed at one side of pylon causes positive counterweight to the other much longer steel one,
- the "V" shape pylon is an original, not practised in bridge engineering yet, and it allows to reach bigger angles between shrouds and bridge deck and in addition shows an interesting architectural accent.

Composite Suspension Bridge Tower with Concrete Filled Double Steel Walls

Shunichi NAKAMURA
Prof. Dr
Tokai Univ.
Hiratuka, Japan

Kenji NISHIUMI
Civil Eng.
Nippon Steel Corp., Steel Struct. Dev.
Futtu, Japan

Summary

A new composite tower is developed and applied to the suspension bridge towers. The new tower consists of corner columns and side walls with double steel plate elements, and concrete is poured inside the columns and the steel elements. The columns and steel elements are connected by the composite joints which are usually used for steel sheet piles. An alternative design is performed for the Akashi Kaikyo Bridge Tower, which shows that the steel weight of this composite tower becomes half of the original steel tower.

1. Structural forms of new composite tower

Two types of towers have been used for suspension bridge towers: steel and concrete towers. Steel towers enable quick site erection but are relatively expensive mainly because of facing machine work on the plate ends. Concrete towers are advantageous in resisting compressive forces but careful quality control is required to avoid cracks due to bending moments, and mold works are inevitable for concrete work. A new type of composite towers are developed for suspension bridge towers as shown in fig.1. Columns consisting of steel box or pipes are arranged at the corners, double wall steel elements connect these columns, and concrete are filled inside the columns and the steel elements. Adjacent steel elements are jointed by the composite joints with claws which are used for steel sheet piles. The filled concrete mainly resists compressive forces and steel plates resist bending moments. This type of composite towers have been already used for bridge piers of Meiko Center Bridge with about 50m high, as shown in picture 1.

2. An alternative design of the Akashi Kaikyo Tower using composite tower

This new composite tower is designed as an alternative for the tower on the Akashi Kaikyo Bridge with spans 960+1990+960m. Dimensions of the assumed cross sections for steel and composite towers are shown in fig.2. The design loads on a cable plane are the dead load of suspended girders and cables of 200kN/m, live loads of 21kN/m, and cable temperature change of 30deg. Table 1 shows the main calculation results. Horizontal tower displacements of both towers are not very much different instead of the large difference of the bending stiffness of towers, but bending moment of the composite tower is 2.5 times large that of the steel tower. Strength is checked by the following equations.

$$\gamma = \nu P/Pcr + \nu M/My \leqq 1.0 \qquad \text{for steel tower}$$

$$\gamma = \nu^2(1+\beta)(P/Pu)^2 - \nu\beta(P/Pu) + \nu M/Mu \leqq 1.0 \qquad \text{for composite tower}$$

where ν: safety factor 1.7 for steel towers and 1.5 for concrete towers, P: axial forces, Pcr: critical axial strength, Pu: ultimate axial strength, M: bending moment, My: yield bending moments, Mu: ultimate bending moments and β: coefficients proposed by Nakai (Proc. JSCE, I-6, 1986). The steel towers are checked by the yield strength but composite towers by the ultimate strength. The compressive strength reduction due to buckling is included in Pcr and Pu. Structural detail for the Akashi Kaikyo Bridge Tower is shown in fig.3. Six square box columns with width of 1.2m are arranged at the corners. Double wall steel elements with width of 0.9m connect the columns with the composite joints. Concrete is poured inside the columns and the steel elements,

and no mold is required for concrete works. The steel weight of the composite tower is 50% of the steel tower but the total weight is 3.4 times large as shown in table 1.

Table 1 Calculation results

Calculation results (per column)	Composite Tower	Steel Tower
Cable tension due to dead load (kN)	497,500	497,500
Cable tension due to live and temperature loads (kN)	38,130	37,610
Vertical force at tower top (kN)	467,500	465,200
Vertical force at tower bottom (kN)	776,200	583,900
Maximum tower bending moment (kN.m)	2,285,000	911,800
Moment of inertia of tower (m^4)	197.0	56.80
Horizontal tower displacement (m)	1.48	1.61
Safety factor : ν	1.50	1.70
Value of capacity check equation : γ	0.98	0.95
Total weight of steel (ton)	4,710	9,325
Total weight of concrete (ton)	27,600	0
Total weight (ton)	32,310	9,325

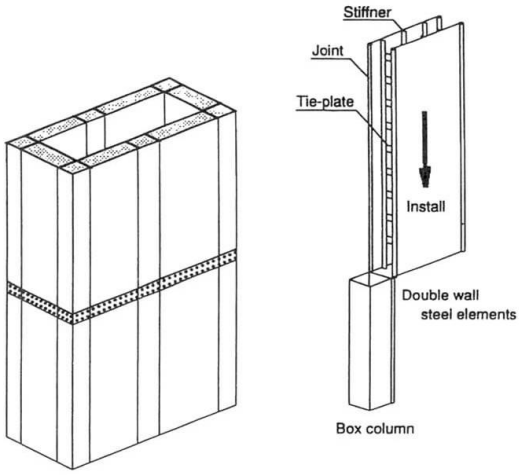

Fig.1 A new composite tower

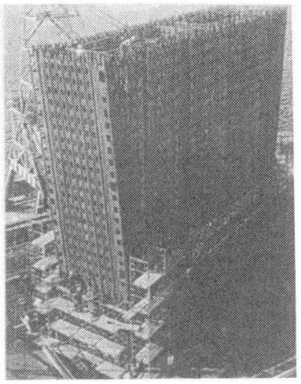

Picture 1 Meiko Center Bridge Tower

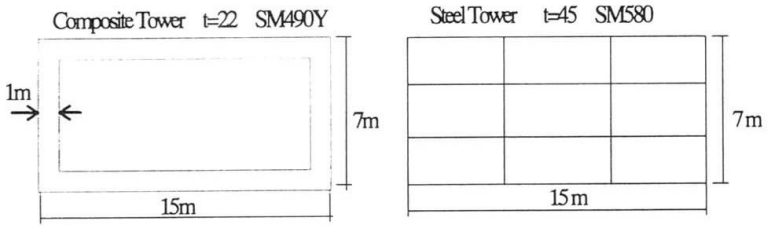

Fig.2 Cross sections of composite and steel towers

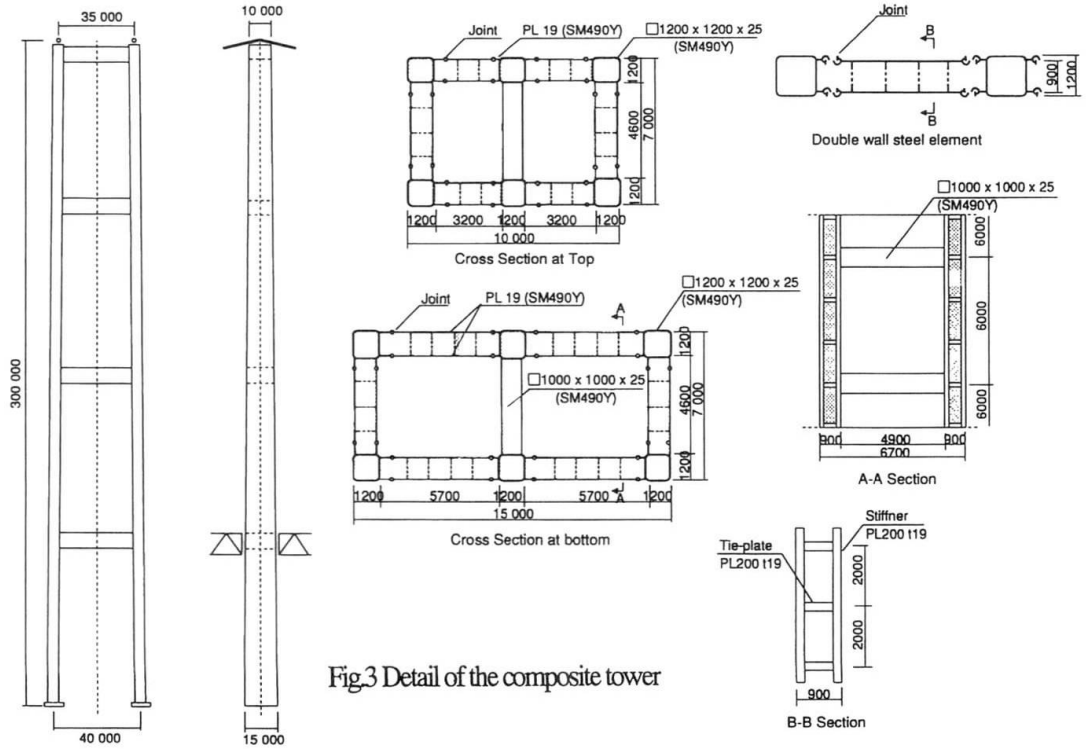

Fig.3 Detail of the composite tower

Application of Gravity Base Structure Technology to Bridge Substructures

Naoki MASUI
Design Mgr
Obayashi Corporation
Tokyo, Japan

Naoki Masui has conducted design and analysis of large concrete structures including bridges and offshore structures.

Iwao YOSHIDA
President
Honshu-Shikoku Bridge Eng.
Tokyo, Japan

Iwao Yoshida, formerly director of Honshu-Shikoku Bridge Authority, is currently the chairman of the committee on the future strait crossing projects in Japan.

Kjell RUSTAD
President
Aker Norwegian Contractors
Oslo, Norway

Kjell Rustad has quite a lot of experience of construction of large offshore concrete structures in the North Sea and Canada.

Summary

In Japan there is ongoing preliminary design on several ultra-long span bridges for strait crossings in deep open waters. This paper mainly discusses the performance of the proposed substructure subject to earthquake effects for these bridge projects.

1. GBS Technology for bridge foundation

The large offshore concrete structures, so called GBS (Gravity Base Structures), have successfully been applied to the oil and gas developments in the North Sea for the last 25 years. Later also in Canada and Australia. Through these experiences the typical features of GBS technology are characterised as follows.

① Construction completely in dry dock or on land and afloat inshore
② Installation in deep open water on the seabed without any preparation prior to installation
③ Applicability to various soil condition from hard to soft by utilising skirt foundation
④ Utilisation of cell and shaft structures with durable high strength concrete

Although previous GBS has been installed in waters without significant seismic action, the concept of the GBS is found applicable to a bridge foundation in a highly seismic area.

① The typical structural configuration of existing GBS consists of shafts above cells, as shown in Fig.1, which minimise the hydro-dynamic force and the overburden pressure on subsoil because of reduction in displacement and selfweight.
② The skirt foundation frequently employed in concrete GBS is also applicable to bridge substructures installed on a thick sedimentary soil.

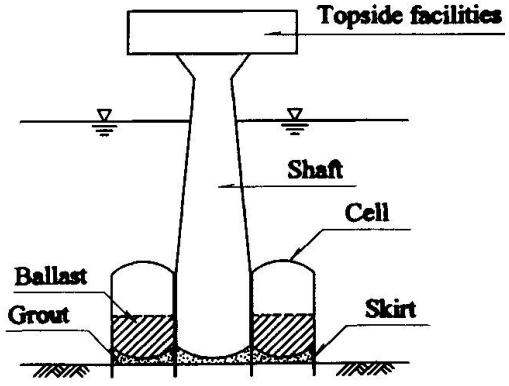

Fig.1 Schematics of GBS

2. Outline of bridge substructure with GBS technology

The conceptual design of bridge substructure for ultra-long span bridge crossing deep strait has been conducted with due consideration to seismic effects. The substructure installed in a water of 70m depth supports the main tower for suspension bridge with 2,400m center span. The soil profile at the site is shown in Fig.2, where the tip of the skirt is penetrated into the mid-depth of the Upper Diluvium.
Two levels of earthquake, L1 and L2, have been considered. L1 is the design earthquake of 150 year return period, and L2 is the ductility level earthquake which means the maximum credible earthquake at the site.

Fig.3 illustrates the dynamic analysis models including the structure-soil interaction to evaluate the earthquake effect. Model for L1 uses soil springs devived from the elastic half space theory. On the other hand model for L2 includes non-tension soil springs allowing the redistribution of subgrode reaction.
The analysis shows that due to allowance of some displacement of soil the medium dense sand considerably reduces the response, because the overall stability of the structure at L2 has the safety margin of 1.1 for both sliding and bearing capacity. This means that the critical area for stability appears at the interface between them. This is due to a large eccentricity and inclination in resultant loads caused by the earthquake.

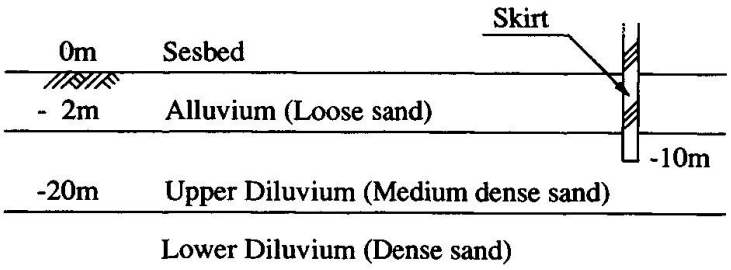

Fig.2 Soil profile

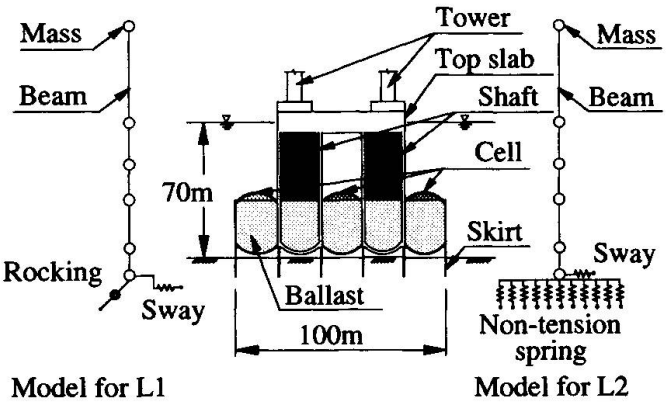

Fig.3 Lumped mass model for dynamic analysis

The structural analysis for the concrete cells subject to seismic effects demonstrates in-plane shear forces together with thrusts rather than flexures dominate the amount of reinforcement as well as concrete section properties and strength, as shown in Fig.4.

The above analysis illustrates the excellent seismic performance of skirt foundation, because only moderate response takes place at even L2 earthquake due to large damping effect of loose soil and flexible structure and soon.

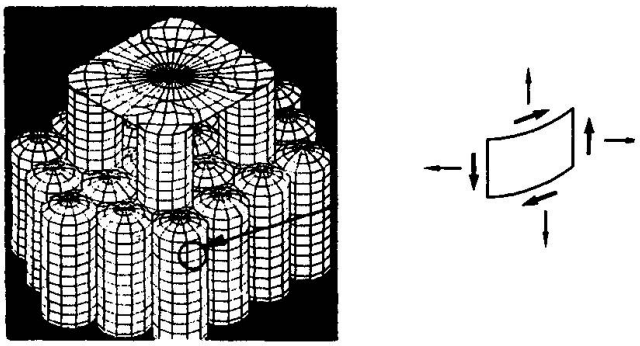

Fig.4 Structural behavior under seismic effects

Toward more rational design detailed engineering will be incorporated with attention to site specifics and construction method.

Ultimate Strength and Ductility of PC Beams with External Tendons

Thiru ARAVINTHAN
Doctoral Student
Saitama Univ.
Urawa, Japan

Hiroshi MUTSUYOSHI
Prof.
Saitama Univ.
Urawa, Japan

Yoshihiro HISHIKI
Section Chief
Kajima Corp.
Tokyo, Japan

Summary

Precast segmental concrete bridges with external prestressing have become popular in the current construction trend due to their advantages such as reduced web thickness and possibility of repairs. The use of continuous beams could be a remedy for reducing the number of expansion joints, thus providing a better driving conditions. However, the inherent structural behavior of such beams is not well understood especially at the ultimate limit state. This paper describes the experimental investigation conducted to examine the flexural behavior of two spans continuous beams with external and combined prestressing, under unsymmetrical loading.

1. Introduction

One of the latest developments in the construction technology has been the use of external prestressing with precast segmental construction which lead to considerable economical and time saving. The use of continuous span structures is gaining popularity since the number of expansion joints are reduced, resulting in better driving conditions. Concern has been expressed that adequate ultimate behavior and sufficient strength could not be obtained. Moreover, lack of ductility of precast segmental bridge girders is another big issue that had to be addressed when such bridges are built as frame structures in earthquake areas. To obtain an insight of the ultimate flexural behavior of such beams, an experimental program was conducted on precast segmental two span continuous beams. In a previous investigation, the flexural behavior of such beams was studied with symmetrical loading conditions, whereas in the present study, the loading pattern was unsymmetrical to increase the moment ratio at critical sections [1]. The results of this investigation are presented in this paper, with emphasis on the influence of confinement reinforcement and combined prestressing on strength and ductility.

2. Experimental Methodology

Three specimens with equal span length of 4.05 m having a T-shaped section were cast. The layout of the specimens is shown in Fig. 1. The specimens No.1 and No.2 are with external prestressing while No.3 is prestressed with combination of internal and external prestressing. The difference between No.1 and No.2 is the provision of confinement in the compressive zone of concrete at critical locations. This was provided in view of increasing the rotational capacity at critical sections, thus improving the ductility of the structure, as shown in a previous study [2]. The confinement reinforcement is of D10 at 50 mm spaced rectangular hoops. This was provided in the top flanges in segments Nos. 5-7, and in the bottom of web in blocks Nos. 12-14. The segments are of 300 mm in length, provided with multiple shear keys. The specimens were concreted by long line match cast technique to have a good fit at the joints. These blocks were assembled and joined by epoxy resin. In specimens No.1 and No.2, two steel cables of type SWPR7A (12.4 mm dia.) were used as external tendons. In No.3, three cables of the same type with 10.8 mm diameter were used, two as external tendons and one as internal. The total design prestress of 180 kN was introduced to all the specimens, which was about 50-55% of the ultimate tensile strength of the tendons. Two point static monotonic loading was applied in each span, as shown in Fig.1. However, the left span was heavily loaded compared to the right span, thus having an unsymmetrical loading arrangement. The load ratio of right to left span was 0.3 to 1. Measurements were taken at regular intervals of loading.

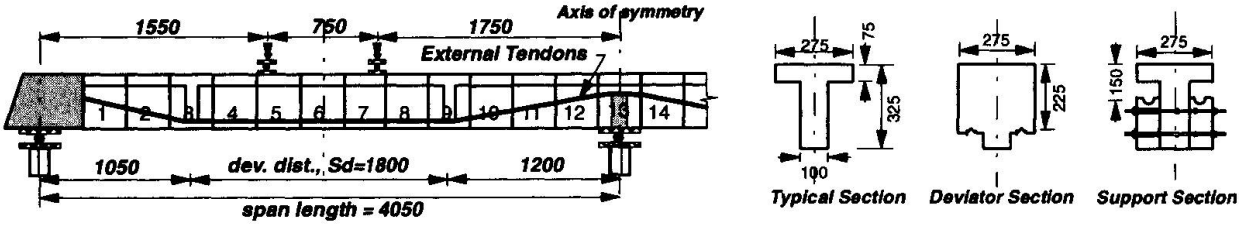

Fig. 1 Layout diagram of test specimens

Table 1. Summary of test results

No.	Description of specimens	Cracking load (kN)		Max. load (kN)	Ultimate deflection (mm)	Stress increase in ext. tendon (MPa)	failure mode
		span	support				
1	External PS, not confined	39.2	56.7	70.2	47.1	232	crushing of concrete
2	External PS, confined	44.9	56.9	71.9	80.1	323	crushing of concrete
3	Combined PS, not confined	44.1	60.9	79.6	80.1	341	crushing, yielding of int. tendon

3. Test Results and Discussion

The test results are summarized in Table 1. The load-displacement characteristics are given in Fig. 2. The maximum load of the specimen No.3 with combined prestressing is the highest, 13% higher than that of No.1. The maximum load on specimen No.1 and No.2 are nearly the same. Considering the final displacement which gives an indication of the ductility, it can be seen that both the specimens No.2 and No.3 show 70% larger than No.1. In addition, the displacement characteristics of No.2 and No.3 are similar except that No.3 has a higher load carrying capacity. From the above observations, it can be expected that a mixture of combined prestressing and confinement reinforcements provide the best solution in view of strength and ductility.

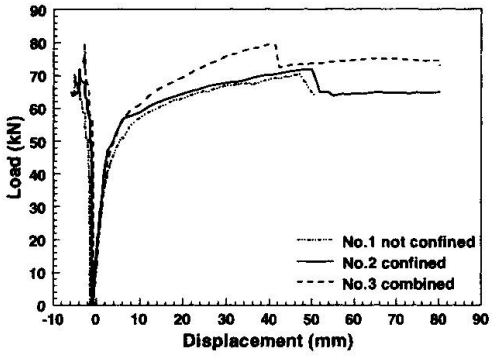

Fig. 2 Load-displacement

Increase in external tendon stress with midspan displacement is given in Fig.3. It could be seen that the stress increased in a nearly linear manner following almost the same path for all the specimens. In the specimens No.2 and No.3, there was a slight drop in the stress after crushing occurred. However, this increase is substantially lower than the symmetrically loaded specimens of similar layout.

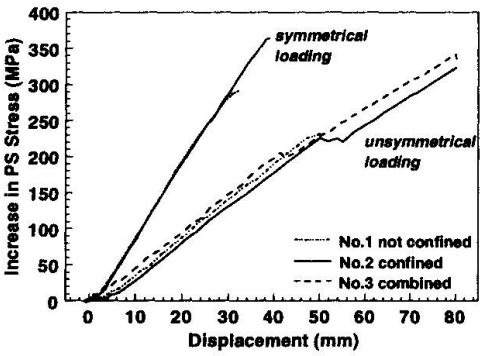

Fig. 3 Variation of tendon stress

4. Conclusions

From the experimental investigation the followings can be concluded.

- The ultimate flexural strength can be enhanced by providing combined prestressing, compared to fully externally prestresing.
- The ductility of precast segmental beams could be improved further by providing confinement reinforcement. It could be also improved by having some internal bonded tendon together with external tendons.

5. References

1. Aravinthan, T., et.al., "Moment Redistribution in Prestressed Concrete Continuous Beams With External Tendons," Proceedings of JCI, Vol. 17, No.2, June 1995, pp. 761-766.

Aerial Spinning for Intermediate Span Narrow Suspension Bridges

Jan LARSEN
Principal Eng.
Aas-Jakobsen
Oslo, Norway

Jan Larsen, born 1947, received his civil eng. degree from the Univ. of Trondheim. He is Project Mgr for the design of the suspension bridges at the Triangle Link Project.

Liv R. ELTVIK
Principal Eng.
Aas-Jakobsen
Oslo, Norway

Liv R. Eltvik, born 1951, received her civil eng. degree from the Univ. of Trondheim. She is Eng. Mgr for the design of the suspension bridges at the Triangle Link Project.

Asbjorn VALEN
Project Mgr
Public Roads Administration
Bergen, Norway

Asbjorn Valen, born 1948, received his eng. degree from the Technical College of Bergen. He is Project Mgr for the bridges and viaducts at the Triangle Link Project.

Summary

Over the past 60 years, 20 two-lane suspension bridges have been built in Norway with main spans ranging from 225 m to 850 m. These bridges all have cables of the prefabricated locked coil type, arranged in one, two or three layers. In other countries use of aerial spinning techniques for main cables have been extensively used for large span suspension bridges and smaller span bridges with large traffic volumes. In recent years the aerial spinning approach has been greatly improved in terms of cost-effectiveness. This has lead to the thinking that this technology would also have a potential of being competitive for narrow intermediate span suspension bridges. Hence, in conjunction with two such bridges for the Triangle Link Project, currently being designed, it was decided to develop both cable alternatives for bid. The design tasks related to developing technical solutions for areas such as saddles, splay chamber and anchorage which for reasons of rationality were to be as similar as possible for the two cable alternatives, yet maintaining the favourable aspects of each alternative, gave rise to particular design challenges. Generally feasible solutions were found in this respect and the outcome of the bidding for the construction contracts will determine whether the aerial spinning approach will have moved into a lower cable tonnage market or not.

1. The Triangle Link Project

The Triangle Link Project, located south of Bergen at the west-coast of Norway, consists of one rock-driven sub-sea tunnel and 2 suspension bridges, i.e. Digernessundet and Spissøysundet with main spans of 677 m and 577 m respectively. The bridges are of a design traditional to Norway, i.e. concrete towers, a narrow aerodynamic steel box girder in the main span with two traffic lanes and one pedestrian lane. Side spans are in the form of concrete or composite steel viaducts and main cables are anchored in rock.

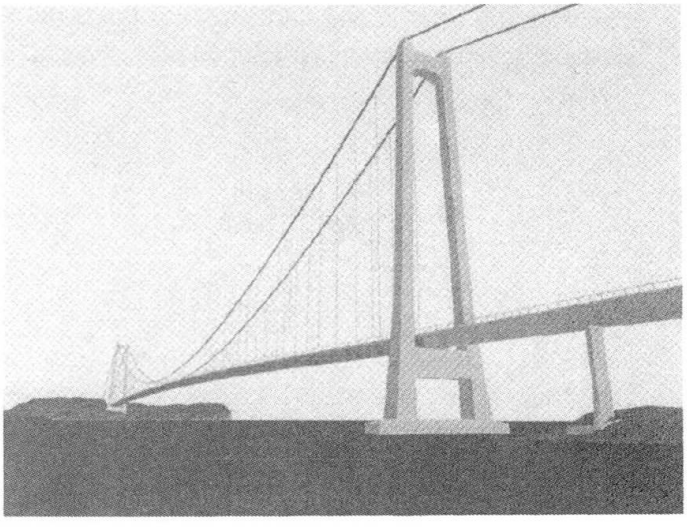

Fig. 1 Digernessundet Bridge

2. Cable Configurations

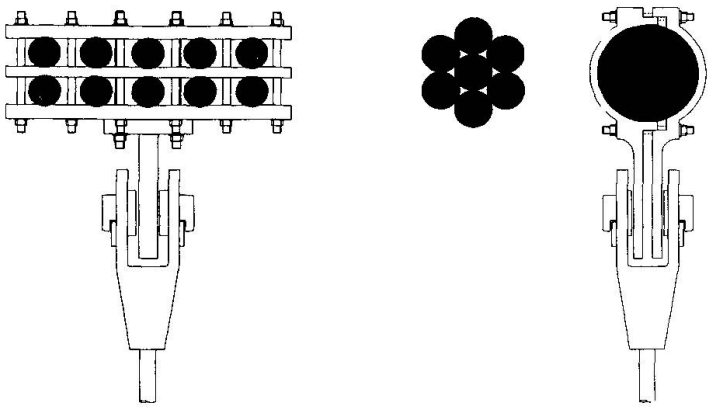

Fig. 2 Cable Configurations

The two bridges are of similar size, e.g. diameter of the aerial spun cable is 317 mm and 297 mm respectively. For the prefabricated alternative five cables in two layers on either side of the bridge with diameters of 102 mm and 95 mm was chosen. For the aerial spun cable, a major decision relates to selecting number of strands. The choice was between 7, 10 or 19, where both 7 and 19 are optimal in terms of compacting. 19 was eliminated as the strands became rather small whilst 10 was, albeit attractive due to likeness with the prefab alternative and a good handling size of strand, eliminated for lack of optimal shape prior to compacting. The chosen 7 strands, which has a diameter of 120 mm (112 mm) is attractive also from the aspect of resulting in a minimum number of anchors. Diameter of thread was chosen at the design stage to be 5.27 mm, which has no other foundation than being the same as used on one other recently built Nordic bridge. This results in totally 2940 (2576) threads per cable and 420 (368) per strand. The actual diameter of thread may be revised subject to contractor proposal. Total cable weight is 1236 + 897 tonnes for the two bridges. Corresponding prefabricated cable weights are 1535 + 1101 tonnes.

3. Saddles and Splay Chamber

Typical splay chamber lay-out is shown in Fig. 3, comprising splay saddle and anchor shoes located inside a concrete house deeply embedded in rock mainly for aesthetic reasons and prestress cables extending between the splay chamber and the anchorage chamber. The concrete house is identical for the two cable alternatives, the need for more space between the anchor shoes for the aerial spun alternative is largely off-set by less anchor points. The steel splay saddles are identical for the two cable alternatives except for the structural elements directly embracing the cables. The traditional Norwegian tower saddle for prefabricated cables is a combination of steel and concrete. For the aerial spun alternative an entire plated solution (no cast steel elements) was developed thus recognising the more concentrated nature of load transfer.

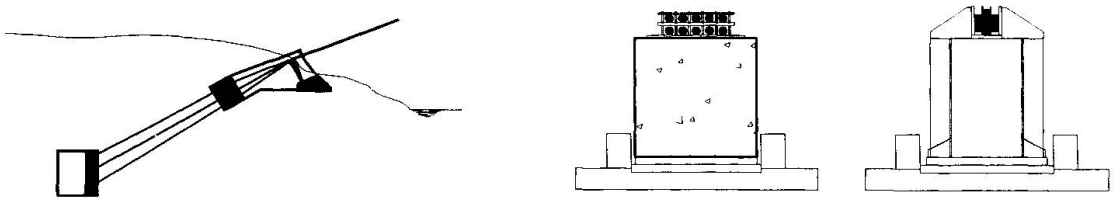

Fig. 3 Splay Chamber and Tower Saddle Concepts

Prestressed Concrete Bridge with Tendons of Large Eccentricities

Jun YAMAZAKI
Professor
Nihon Univ.
Tokyo, Japan

Born in 1942, received his degrees at Univ. of Tokyo and Univ. of Washington.

Kosei IDO
Graduate Student
Nihon Univ
Tokyo, Japan

Born in 1973, graduate from Nihon Univ., College of Science and Technology.

Hiroki KONO
Graduate Student
Nihon Univ.
Tokyo, Japan

Born in 1973, graduate from Nihon Univ., College of Science and Technology.

Summary

A model favorable in structural behavior and ease of construction was created based on a design rationale selected for prestressed concrete (PC) girder bridge with external tendon of large eccentricity. For a self anchored suspension PC bridge, possible minimum values were derived for girder depth, area, section modulus, tendon sag and prestressing force. For this type of structure a span length of about 180 m was found to be favorable. A finite deflection analysis suggested that ultimate state of 1.7 times (Dead load+ Live load) is not attained for span lengths larger than 180 m. Load test results for reduced scale specimen were satisfactory for preliminary plans and tests are being continued.

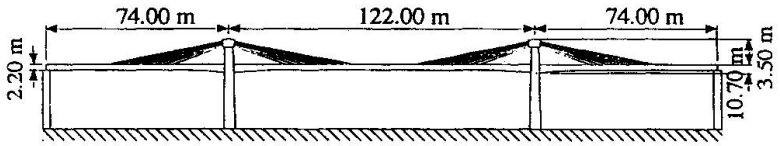

a. Extradosed PC bridge (Odawara 122 m,1995)

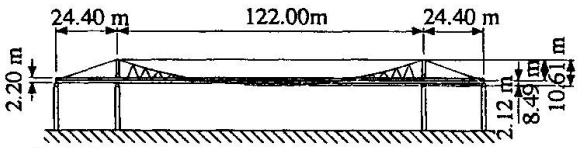

b. Self anchored suspension PC bridge (Model)

Fig.1 Prestressed concrete (PC) bridges with tendons of large eccentricity

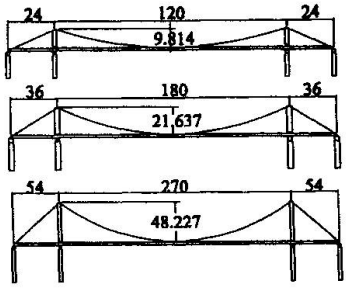

Fig.2 Structure profile shapes derived by stated rationale for varying span lengths

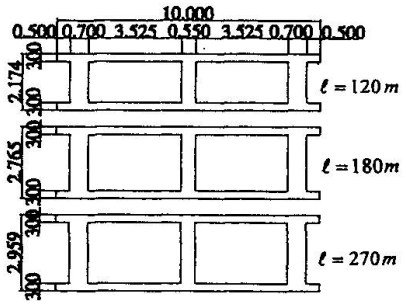

Fig.3 Cross section shapes

1. Proportioning the structure for service load

A model chosen was mono-cable self-anchored PC suspension bridge (Fig.1,b). For an assumed live load of 4 kN/m^2, requirements set for proportioning were; (1) deflection due to live load is 1/1000 of span, (2) maximum fiber stress in concrete beam under extreme moments is 10MPa, (3) ultimate tendon strength is 1900MPa. In a simplified response model the assumptions were; (1) cable profile shape is parabola and remains as parabola after deflection, (2) cable and beam deflection is same at span center only and compatibility is ignored elsewhere, (3) and thus the beam is loaded downward by uniform design load and upward by uniform load from cable.

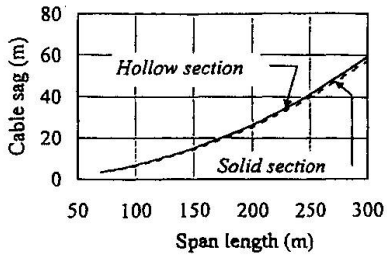

Fig.4 Cable sag

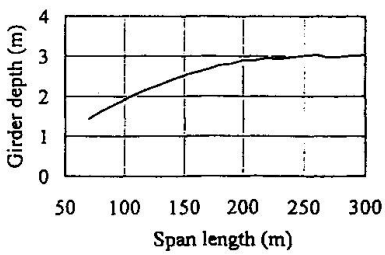

Fig.5 Girder depth

2. Structural characteristic obtained

In view of results shown in Figs.2 through 7, a proportion for a span length of 180m is found to be favorable in terms of response to service load and construction method. A stress increase due to live load in tendon was 7% of initial tension (Fig.6). Tendon is composed of 335 of 15.2mm strands and initial tension is 51,100kN (0.6 times the ultimate). A girder depth of 2.765m (Fig.3) and a height of deviator tower of 21.6m (Fig.2, span-sag ratio is 8.32) are favorable for current state of practice of construction method.

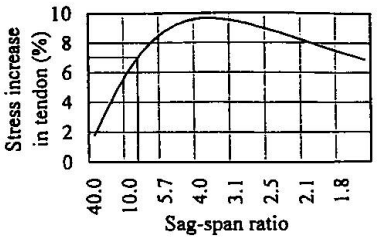

Fig.6 Stress increse in cable due to live load

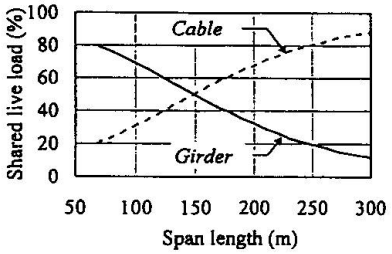

Fig.7 Load shared by girder and cable

3. Finite deflection analysis for ultimate

An assumption of load sharing between cable and beam is same as stated before in Section 1.
An analysis model is as shown in Fig.8. Load carrying capacity of the beam is reduced by axial force component of prestress as deflection increases. However, ultimate strength of 1.7 times (D+L) is attained for span length of 180m as seen in Fig.9.

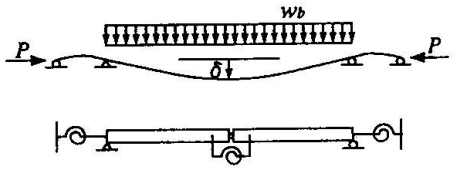

Fig.8 Mechanics model for deflection analysis

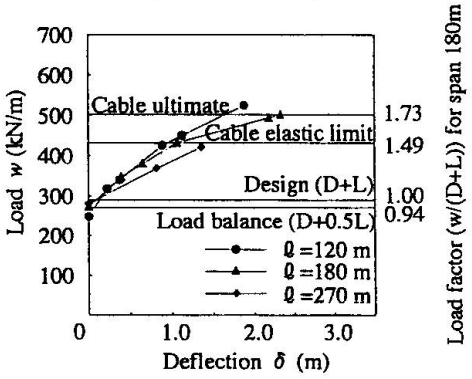

Fig.9 Load vs deflection by finite deflection analysis

4. Load testing model

Similitude of 1/24 scale model (Fig.10) was true for sag-span ratio and girder depth, but it was violated for girder cross section area and section modulus (by factors not exceeding 2) and prestress. For elastic range of tendon, response to load was satisfactory to prediction including deflection (Fig.11) for preliminary stage of test plan.

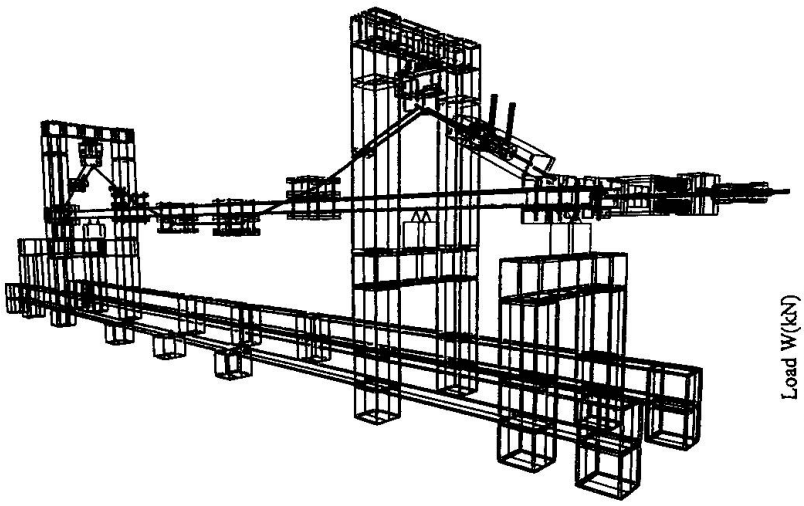

Fig.10 Scheme of load test apparatus (scale 1: 24)

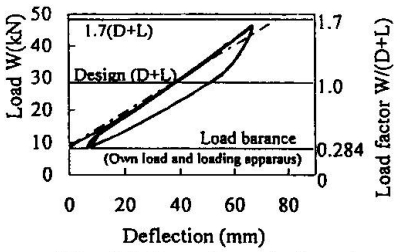

Fig.11 Load vs deflection